Development of the Synthesis of Thiophene and Thiazole Based Conjugated Polymers Through Direct Arylation and The Separation of Carbon Nanotubes Using Degradable Conjugated Polymers

by

Javan Alexander Buratynski

A thesis

presented to the University of Waterloo

in fulfillment of the

thesis requirement for the degree of

Masters of Science

in

Chemistry

Waterloo, Ontario, Canada, 2023

Author's Declaration

I hereby declare that I am the sole author of this thesis. This is a true copy of the thesis including any required final revisions, as accepted by my examiners.

I understand that this thesis may be made electronically available to the public.

Abstract

Conjugated polymers are an ever-growing field due to their ability to be used for a variety of purposes such as photovoltaics, field-effect transistors, light emitting diodes, and organic sensors. To further this field, research must constantly be performed to develop novel methods of synthesis and test a variety of substrates to determine potential applications. Of particular interest is direct-arylation polymerization which allows for the synthesis of conductive polymers without the production of quantitative amounts of metal-halogen waste.

Firstly, one of the primary drawbacks of direct arylation polymerization is the potential for defects during polymerization. This is due to the low difference in energy required to react with protons on the substrate. The solution proposed is to develop a catalyst system that alleviates this issue while maintaining good yields, high molecular weights, and low catalyst loadings.

Secondly, although it has been reported on for over two decades, the amount of research done on bithiazole polymers is relatively low when considering their unique properties. In this work, a facile method was developed to generate a variety of bithiazole based polymers. These polymers displayed a wide variety of electrical properties while eliminating some of the issues seen in more common conductive polymers.

Finally, a novel application was investigated for conjugated polymers: the separation of carbon nanotubes. Through the use of degradable conductive polymers, a method was developed to separate and isolate desired types of carbon nanotubes. This would allow for much simpler and cheaper access to one of the most desirable materials in materials science

Acknowledgements

Nearing the end of my educational career there are so many people to thank. First and foremost are my family. My parents Karen and Mike, my brother Quinn, my Grandmother Betty, and my partner Hannah. You have all been pillars of strength in, what were often, trying times. I truly could not have made it to where I am today without each and every one of you. The love and support I have received from you all cannot be overstated, and I am thankful for it every day.

I would also like to thank Dr. Derek Schipper for the opportunities he gave me in pursuing chemistry both in my undergraduate and graduate careers. Without his guidance I would not be the scientist I am today.

I would also like to thank all of the members of the Schipper group both past and present. The community fostered and the friends gained in my time here will not soon be forgotten. In particular: Wayne, you gave me my first real taste of organic chemistry and for that I will never forget, nor forgive, you; Sarah and Sara, you are both such compassionate and caring people and made up an integral part of the amazing environment that was fostered in the lab; Serxho, although our time working in the lab together was short the D&D sessions and the lab conversations will never be forgotten; Boris, thank you for your council throughout our time here it has been invaluable, I know you are destined for great things and I can't wait to see where you end up; Mila, the rate that I saw you grow as a chemist has been wonderful and I hope your passion for science continues; Gigi, you are such a kind person and a true light in the lab and I am thankful for the time we were able to spend together; Jianan, although sometimes thought of as the more silent member of the lab you are one of the kindest people I have ever met, I appreciate all of the time we have been able to spend together and hopefully we can hit the gym

together again once our defences are finished ;Geoff, thank you for all of your guidance during our time together from your time as my TA to our time working on chemistry together I truly never stopped learning; Raf, as the person I probably spent the most time with in the lab you had a huge impact on my growth as a chemist, although you could be harsh I truly believe you are a kind person who had everyone's best interests at heart, we will get the band back together one day.

I would also like to thank many of the undergrads that have come through the lab during my time here. In particular I would like to thank Lucas, Jack, Scott, Emily, Danny, and Josh. You are all amazing people with a lot of potential, I hope you can fulfil it.

Finally, I would like to thank those friends that were indispensable outside the lab: Andy, Kyle, Dimitri, Rob, and Khalid you have all added important parts to my life. I would also like to particularly thank Mike and Fabio for their constant friendship and support all throughout our undergraduate and graduate careers, I hope that I was as valuable to you as you were both to me through all our years together.

Table of Contents

List of Figures

List Of Schemes

List of Tables

List of Abbreviations

Abbreviation	Definition
Abs	Absorbance
Ac	Acetate
Ar	Aromatic group
cat	Catalytic
CMD	Concerted Metalation-Deprotonation
CNTs	Carbon Nanotubes
CV	Cyclic Voltammetry
CVD	Chemical Vapour Deposition
DArP	Direct Arylation Polymerization
dba	Dibenzylideneacetone
DCE	1,2-Dichloroethane
Dec	Decyl
DFT	Density Functional Theory
DMSO	Dimethyl Sulfoxide
DNA	Deoxyribonucleic acid
E_{Dist}	Energy of Distortion
Eg	Band Gap
E_{Int}	Energy of Interaction
equiv	Equivalent
Et	Ethyl
eV	Electron Volt
FDOF-TP	poly[(9,9-dioctylfluorene-2,7-diyl)-alt-(2,3,5,6-tetrafluoro-1,4-phenylene)]
ΔG	Change in Gibbs Free Energy
GC-MS	Gas Chromatography Mass Spectroscopy
GPC	Gel Permeation Chromatography
h	hour
Hex	Hexyl
HOMO	Highest Occupied Molecular Orbital
HPLC	High Pressure Liquid Chromatography
IR	Infrared
L_n	Ligand
LUMO	Lowest Occupied Molecular Orbitals
[M]	Monomer concentration in mol/L
M	Metal
mCPBA	Meta-Chloroperoxybenzoic Acid
Me	Methyl
MMPP	Magnesium Monoperoxyphthalate
M_n	Number Average Molecular Weight
Ms	Mesylate
MTBE	Methyl Tert-Butyl Ether
M_w	Weight Average Molecular Weight
MWCNT	Multi Walled Carbon Nanotube

NBS	N-Bromosuccinimide
NHC	N-Heterocyclic Carbene
nm	Nanometer
NMR	Nuclear magnetic resonance
Non	Nonyl
[O]	Concentration of Oxidizing Agent
o	Ortho
o-anisyl	Ortho-anisyl
Oct	Octyl
OFETs	Organic Field-Effect Transistors
OLEDs	Organic Light Emitting Diodes
Opt	Optical
OPVs	Organic Photovoltaics
P3HT	Poly(3-hexylthiophene)
PDI	Polydispersity Index
PEDOT	Poly(3,4-ethylenedioxythiophene)
PF	Polyfluorene
pH	Potential of Hydrogen
PivOH	Pivalic Acid
ppm	Parts Per Million
PPP	Polyparaphenylene
PPV	Polyparaphenylenevinylene
Precat	Precatalyst
PT	Polythiophene
PTFE	Polytetrafluoroethylene
quant.	Quantitative
RAFT	Reversible Addition–Fragmentation Chain Transfer
rt	Room Temperature
SWCNT	Single Walled Carbon Nanotube
^{t}Bu	Tert-Butyl
TCE	Trichloroethylene
TFA	Trifluoroacetic Acid
TGA	Thermogravimetric Analysis
THF	Tetrahydrofuran
TIPS	Triisopropylsilyl
TMEDA	Tetramethylethylenediamine
Tol	Toluene
TON	Turn Over Number
USD	United States dollar
UV	Ultraviolet
UV-vis	Ultraviolet-Visible

Chapter 1: Conjugated polymers

Conductive organic polymers have been a topic of interest since the 1940s.[1] This is due to their unique properties including: durability, tunability, and flexibility. This makes them qualified for a variety of applications such as photovoltaics (OPVs)[2,3], organic field-effect transistors (OFETs)[4,5], organic light emitting diodes (OLEDs), and chemical sensors.[4] All of these purposes take advantage of the processability, large area coverage, flexibility, and comparatively low cost of the polymers. These beneficial properties are particularly relevant when compared to existing inorganic materials that see use for these purposes such as silicon, germanium, and germanium arsenide. Although the field is relatively young, seeing that most of its development started in the 1980s, a significant amount of progress has been made towards the usage of these materials.[4]

1.0: Conductive Polymers

The synthesis of organic conductive polymers is an ever-expanding field because of their myriad of uses. This category of compounds is defined by the backbone of the polymers: namely the fact that the π electrons on the backbone can be delocalized throughout the polymer, meaning that their p orbitals overlap, in other words, the backbone of the polymer must be conjugated.[6] This allows for the entire polymer to have charge mobility enabling the movement of electrons, or positively charged ‘holes’ across whatever surface can be coated (Fig 1).

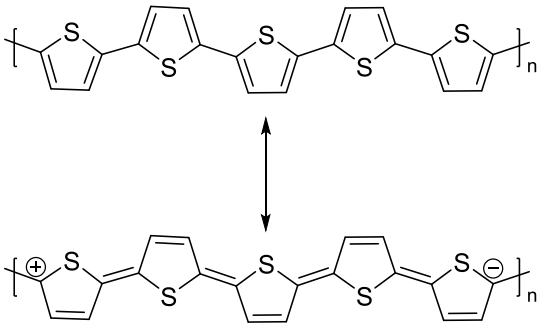

Figure 1 Conjugated Polythiophene: translation of charge along the backbone allows for the transportation of charge along the polymer.

The electrical properties of these polymers can then be influenced by multiple factors such as the electrical properties of the side chains or the backbone itself. These modifications are a large part of what allows conductive organic polymers to be applied to such a wide variety of fields. Ignoring even the potential to change the varieties of side chains, which in turn can affect the properties of the polymer and thereby the electrical properties, there lies an enormous amount of potential variability in the backbone as the only true requirement is a continuous conjugation (Fig. 2).

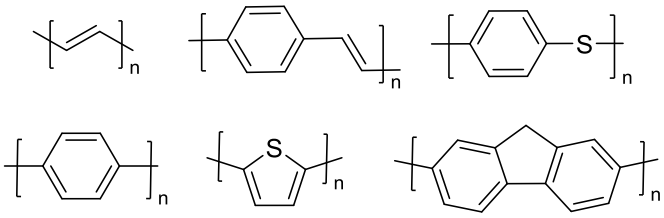

Figure 2 Polymer Examples: Various types of conjugated polymer backbones that currently see use.

Polymers used for this purpose are characterized in multiple ways to determine their usefulness. The first of these is to measure the molecular weight of the polymer. This is measured as an average as not all polymer chains will have the same length. The two most common weight measurements are the number average molecular weight (M_n) and the weight average molecular weight (M_w). The M_n of a polymer is merely the statistical average

determined by the addition of the molecular weights divided by the total number of polymer chains in the sample. M_w is much the same but lends more statistical weight to polymer strands of higher mass. For a polymer to see use in materials, certain thresholds much be achieved in both of these to promote functionality. The other measure that is based on weight that is commonly used is the polydispersity index which simply refers to the distribution of the molecular weight of a polymer. This will affect how consistent the properties of the polymer are. The closer the PDI is to one, the narrower the molecular weight distribution of the polymer is. All three of these factors affect how a given polymer can be used as they can affect many characteristics such as: solubility, aggregation, thin film morphology, and mechanical strength.

All three of these benchmarks are generally measured through the use of gel permeation chromatography (GPC). This method uses a chromatographic column with beads with various pore sizes to separate various sized polymers from each other. This functions due to the fact that the larger polymers will interact with fewer of the pores meaning that the time it takes for them to elute from the column will be reduced.[7] Combining the variation in elution times based on the size of the polymer with a set of internal standards allows for a relatively accurate approximation of the size of a polymer sample and from this the PDI of this sample can be determined.

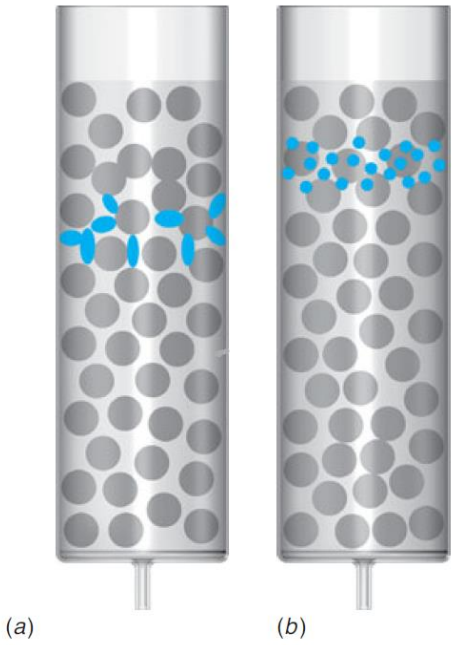

Figure 3 GPC Separation: Large molecules pass through rapidly due to their lack of interaction with the pores on the beads (a) while the small molecules take longer to pass through (b)[8]

The research into the compounds themselves breaks down into a few categories: synthesis, properties, and applications. The synthesis of conductive polymers is a rapidly growing field as new methods are developed to approach the construction of what can be challenging molecules to synthesise and extract. Furthermore, this research is linked to the discovery of new properties of the compounds as, due to the broadness of the field and the low barrier for entry for a polymer to be conductive, new potentially applicable polymers are constantly being discovered and researched. Finally, the practical applications of these polymers are constantly being investigated. This is partially due to the fact that new polymers being developed may find use in an existing field as a replacement for current technologies or be able to be applied in a way that had not been yet considered.

1.1: Organic Semiconductors

One of the most useful aspects of organic conjugated polymers is their semiconducting properties. Semiconductors are a class of electronic materials that exist between insulators, which do not conduct electricity, and conductors, which will freely allow the flow of electrical charge.[9] Semiconductors are defined most easily through the size of their band gap. A band gap is commonly referred to as the energy gap between the conduction band, which is the grouping of the unoccupied molecular orbitals, and the valence band constituted by the occupied molecular orbitals.[9] While insulators most often have band gaps too large to be bridged (generally above 3 eV) and conductors have no band gap, semiconductors exist in the range between the two (Fig. 4). This allows for a significant amount of freedom in the range of what is considered a semiconductor.

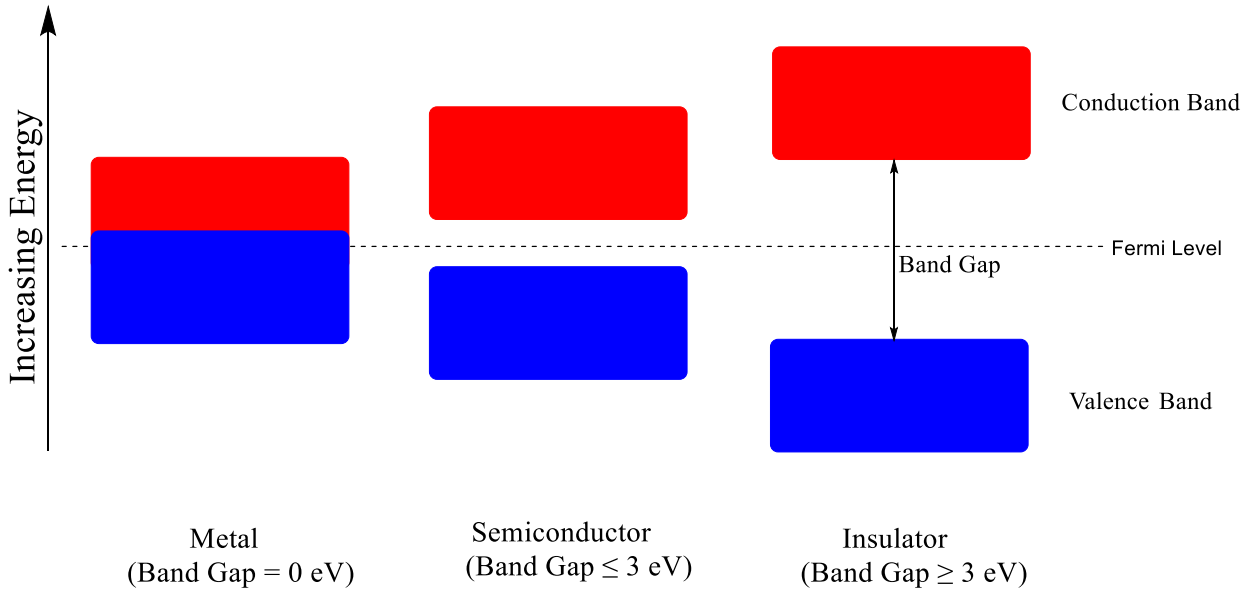

Figure 4 Comparison of Conducting Materials: Metals have overlapping conduction and valence band. Insulators by comparison have a band gap between the conduction and valence band. Semiconductors are found in the middle having a band gap between 0 and 3 eV.

There is a further divide amongst semiconductors based on the style of charge transport that the materials use. These are termed p and n-type semiconductors. P-type semiconductors use positive charges, or holes, to transport charge.[10] N-type semiconductors by comparison use a conjugated negative charge to transport charge.

To understand semiconductors specifically one must understand the Fermi level. The Fermi level refers to the energy level of an electron which has a 50% chance of being occupied at thermodynamic equilibrium.[11] The Fermi level in relation to its orbital type defines the type of charge transport used by a semiconductor.

When discussing this topic in relation to organic molecules, it is easiest to understand through molecular orbital theory. N-type semiconductors often have lowest occupied molecular orbitals (LUMO) closer to the Fermi level of the polymer. Their electron deficiency makes them easier to reduce thereby creating a negative charge that can be transported. It follows then that p-type materials are most often electron-rich with a high energy highest occupied molecular orbital (HOMO) and can thereby be easily oxidized creating the necessary positive charge.[9] While p-type materials are the most common type of polymer, there has been much recent study into the exploitation of a small number of polymers with a particularly high electron affinity as n-type materials.[10] Of note is the fact that these distinctions are not based on whether the charge can be effectively mobilized but simply which charges are most easily created within the molecule.

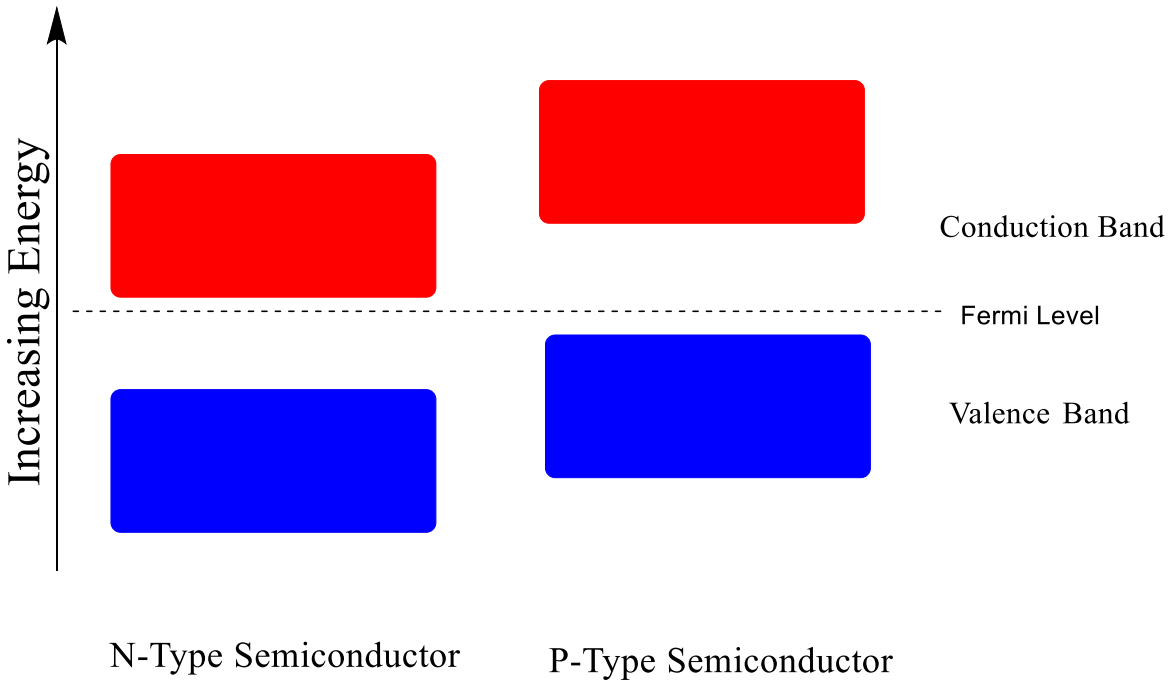

Figure 5 Semiconductor Differences: Differentiation of semiconductors based on their orbital grouping in relation to the Fermi level.

Generally, N-type materials have electron withdrawing groups attached to the backbone to guarantee low energy LUMOs and increase electron affinity. These include imides, amides, boron nitrogen complexes and cyano groups (Fig. 6). While the functional groups can divert from these four, they are often the easiest to include. As with many other large polar polymers, there are also solubilizing chains attached to enhance its solubility in a variety of solvents.

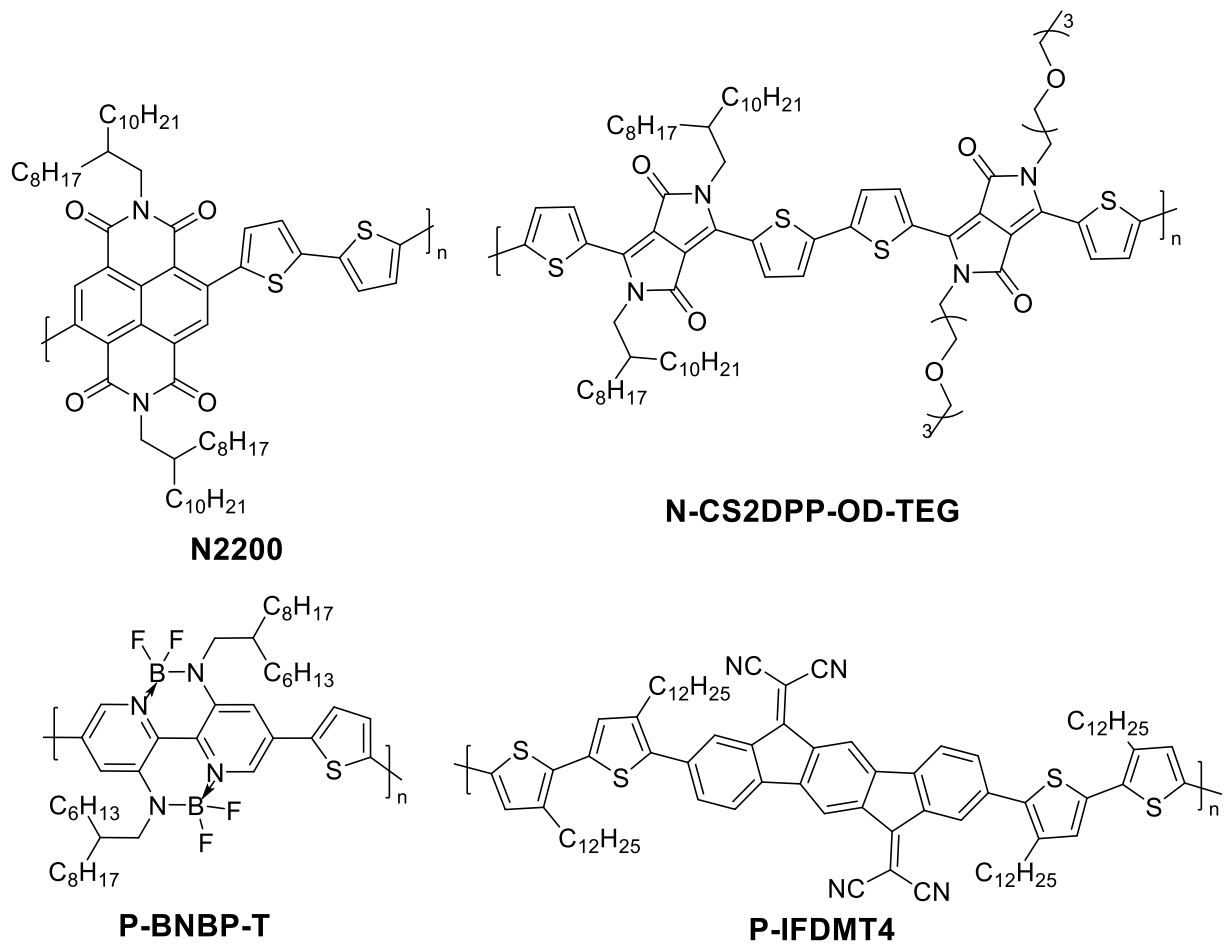

Figure 6 N-Type Polymers: Several n-type organic Polymers currently used in industry[12]

P-type polymers by comparison have been developed to a higher degree. This is due to the fact that many unfunctionalized conjugated polymers are p-type in nature. These polymers have energy levels where the HOMO is closer to the Fermi level meaning that they are easier to oxidize than reduce. This will yield a conjugated positive charge, termed a hole, which allows for conduction along the polymer.

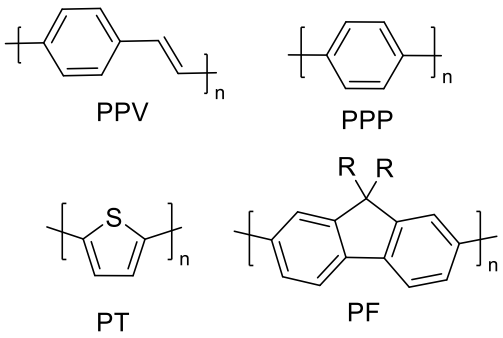

Figure 7 P-Type Conjugated Polymers: Several P-type conjugated polymers that have undergone rigorous study. Includes polyparaphenylenevinylene (PPV), Polyparaphenylene (PPP), polythiophene (PT), and polyfluorene (PF).[13–16]

Other than the electron affinity of the materials, the most important factor is the band gap of the polymer itself. Since the applications of conductive organic polymers are varied, the ability to synthesise polymers with differing band gaps is paramount to their commercial use. This fact has inspired much of the research performed in this field.

Band gaps and HOMO-LUMO gaps are primarily investigated through either cyclic voltammetry or ultraviolet-visible (UV-vis) spectroscopy. UV-vis techniques are straightforward: light at known wavelengths is passed through a sample leaving the remaining light to be collected by a detector. Through this method, it can be determined at what energy levels light is being absorbed by the polymer and thereby the energy required for an electron to transfer from the HOMO to the LUMO can be calculated.[8]

Cyclic voltammetry is a process by which the electrical properties of a material can be observed. The analyte is exposed to three electrodes in solution with strictly controlled voltage which will gradually increase and decrease. The first of these electrodes is the working electrode which will be under the control of a potentiostat to vary its voltage.[17] Different working electrodes can be chosen based on the electrical potential range of interest. A reference electrode is also included which simply acts as a reference point which the other two electrodes can be

measured against. The final electrode in the solution is the counter electrode which acts to complete the circuit as the electrical potential is applied to the working electrode.[17] Throughout the varying of the voltage in the electrochemical cell, the current is monitored to determine at what potentials the analyte is oxidized and reduced. These potentials are then most often compared to an internal standard to determine the locations of the frontier orbitals in relation to the vacuum level.

1.2: Conjugated Polymer Synthesis

Conjugated polymers can be synthesised in a variety of ways. This can range from more traditional methods such as dehydration to more complex cross couplings. Although there are a variety of potential methods used, the most common are generally cross coupling methods. This is largely due to the simplicity of the reactions, their robust scope, as well as the availability of the substrates. The most popular of the cross-coupling methods include: Suzuki, Stille, and Sonogashira.

Suzuki is one of the most well-known and widely used cross coupling reactions. It makes use of a boronic acid on one of the substrates and a halogen on the other.[18] This coupling is extremely flexible as boronic acids, based on the substrate being used, are relatively easy to come by. The other primary advantage of using this method is the mild reaction conditions as it can be performed in mildly basic conditions and at low heat.

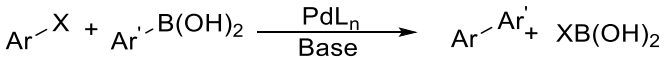

Figure 8 Suzuki Coupling: Coupling between an organohalide and aryl boronic acid

While the boronic acid group provides much of the benefit in this reaction system, they also have many drawbacks. Firstly, the list of boronic acids available commercially is not

exhaustive and the boronic acid functional group can be difficult to introduce if the substrate is not commercially available, most often requiring reaction with Grignard or organolithium reagents which is not always an option.[19] Finally, although the conditions are relatively mild the other drawback of the method is that most common reactions use potassium carbonate or a hydroxide salt as is required based on the solvent used.[19] This means that even when using the most mild possible conditions, problems can still arise if any of the substrates are base-sensitive.

Stille couplings are another option for polymer synthesis. Organo-tin compounds along with aryl halides are used to create a carbon-carbon bond.[18] There is a high tolerance for the substrate used allowing for the synthesis of any organnostannane. There is also a wide variety of viable palladium sources that can be used allowing for Stille coupling to be employed regardless of the target compound.

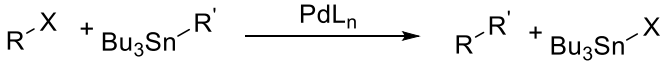

Figure 9 Stille Coupling: Coupling between an organohalide and an organostannane

Although the reaction conditions are exceedingly flexible, there are a multitude of drawbacks to Stille coupling. Not only are organo-tin reagents required to be synthesised under much the same conditions as the boronic acids, leading to limitations in the substrates that can be used, but a stoichiometric amount of tin must also be used to complete the reaction, meaning that there is a stoichiometric amount of tin waste produced. The solubility of the organo-tin compounds can also cause issues as they are nonpolar limiting the number of solvents that can be used in the synthesis.[20] Finally, there are a multitude of side reactions that can occur during the reaction itself including homocoupling and exchange of aryl groups on the palladium and phosphine ligands.[21]

Sonogashira coupling is a copper based cross coupling reaction using organo-cuprates.[22] While limited to alkynes due to the secondary copper cycle required as well as the fact that it requires base to proceed, it is useful since it can be performed at room temperature with a wide variety of aryl or alkyl halides.

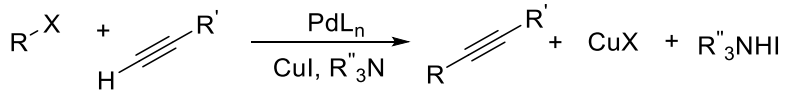

Figure 10 Sonogashira Coupling: Coupling which occurs between an organohalide and alkyne

While Sonogashira coupling is interesting, the scope of the reactions is severely limited by what can be converted into organocuprates. While the mechanism is yet unclear, it is hypothesised that there is a second catalytic cycle occurring, where the base deprotonates the alkyne leading to the formation of organocuprate. This means that the substrates, that can be used, are limited by the pKa of the target proton.

Cross couplings are an important factor in the production of polymers. They exist in a variety of forms ranging from Stille to Sonogashira to Suzuki.[23] These reactions all follow similar reaction pathways as the one shown in (Fig. 11). The type of coupling chosen to be used in a given reaction is often based off the desired reaction conditions as well as the availability of the precursors. One of the primary drawbacks of most palladium cross couplings is that additional functionalization is required such as the boronic acids or organo-tin motifs. This can lead to loss of starting material and lowered yields. Another important drawback to be considered from the general framework of cross coupling reactions is their waste products. Due to the transmetallation step present in the majority of cross coupling reactions, a stoichiometric amount of metal-halogen waste is produced which is difficult to dispose of in an environmentally friendly manner.

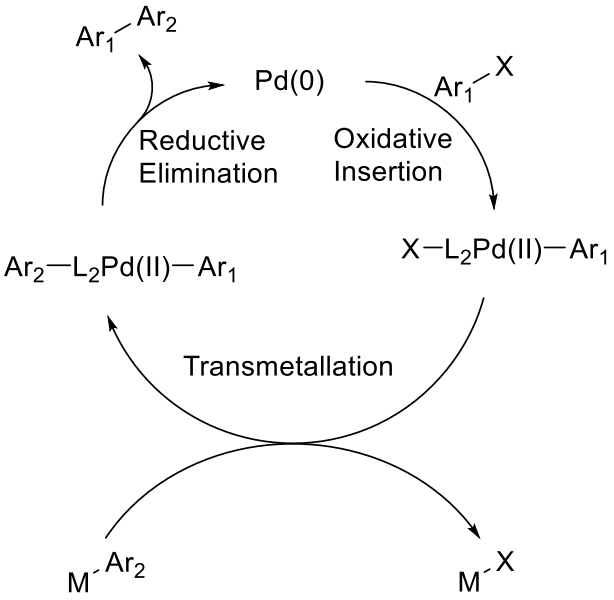

Figure 11 Cross Coupling Cycle: Palladium cross coupling beginning with a palladium (0) species undergoes oxidative insertion followed by transmetallation followed by reductive elimination to retrieve the original palladium (0) and the cross coupled product

1.3: Direct Arylation Polymerization Development

There has been growing interest in a reaction that addresses the problems caused by current cross coupling methods such as metallic waste and difficult to obtain starting materials. A cross coupling that has gained popularity after being investigated by Ozawa *et al.* in 2010 is direct arylation.[24] This reaction seeks to address these issues while having similar reaction conditions. Although more limited in its reactant scope, direct arylation eliminates the requirement for pre-functionalization of its monomers and does not produce metal halogen waste.

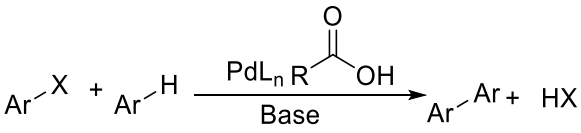

Figure 12 Direct Arylation: Aryl halide is coupled with an aryl compound with an acidic proton

This reaction takes advantage of acidic protons on substrates in a similar way to a Sonogashira coupling. Through the removal of the proton on one of the substrates the traditional transmetalation step can be circumvented. This process has been termed concerted metalation-deprotonation (CMD). This allows for the coupling of a hydrocarbon directly to the palladium complex without the need for an intermediate metal.[25]

Initially discovered in 1999 by Lemaire *et al.*, direct arylation was thought to be a novel variety of the Heck reaction.[26] The initial polymerizations using the method were not overly successful granting a polymer with an M_n of approximately 3 kDa. Ozawa *et al*. expanded on this work in their synthesis of poly(3-hexylthiophene). Initially $Pd(OAc)_2$ was used as the catalyst but, when running reactions at higher temperatures, the catalyst system was deemed to be too unstable as the polymers produced were extremely inconsistent with M_n values ranging from <3 kDa to 10 kDa. This inconsistency was one of the primary indicators of the need to change the parameters of the synthesis. The other indicator was the production of palladium black which showed that the palladium being used was degrading throughout the reaction.[27] This palladium degradation indicated to the investigators that the reaction itself was not the main issue but the palladium system. A Herrmann-Beller catalyst was then tested with a variety of ligands to attempt to remedy these issues as the catalyst has been shown to have high thermal stability.[28] The catalyst system was combined with a stoichiometric amount of cesium carbonate in THF ranging from 120-125 °C. These conditions produced the desired product consistently with M_n above 30 kDa.[24]

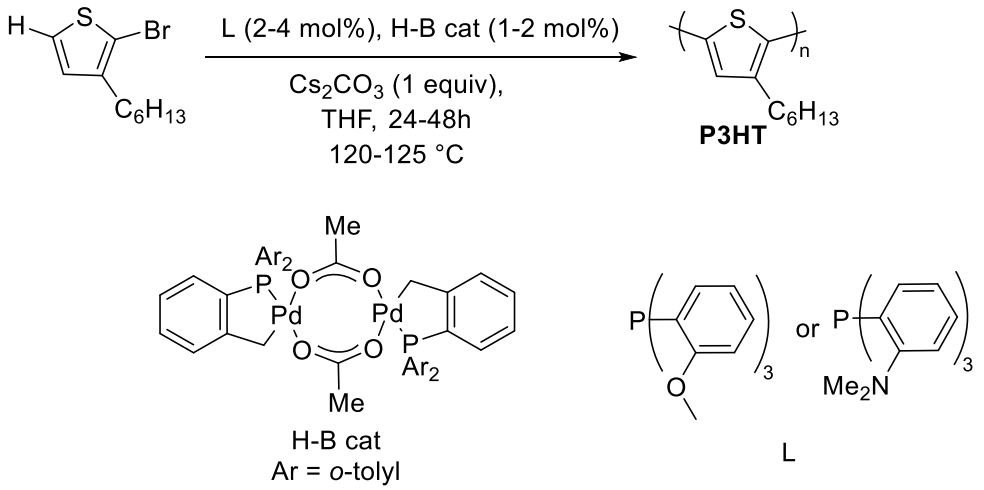

Figure 13 Direct Arylation Polymerization: Polymerization of P3HT through the usage of DArP. This reaction was tested with a variety of palladium sources and ligands, but a Hermann-Beller catalyst combined with P(o-tolyl)$_3$ was found to have the best results

Ozawa *et al.* continued investigating the polymer synthesis applications of this method and, taking inspiration from the work of Sigman *et al*., used an acetate as part of the reaction.[29] This, along with the discovery that P(*o*-tolyl)$_3$ was the most efficient ligand to be used in this synthesis allowed them to consistently synthesise high M_n polymers with more than 80% yield.[30] These projects laid the groundwork for much of what was to be done with respect to direct arylation polymerization.

1.4: Direct Arylation Reaction

The cycle of direct arylation polymerization (DArP) is similar to that of many other cross couplings. Research on the mechanism of this reaction began in the late 1990s, pioneered by both the Echarvarren and Fagnou groups.[31–36] The reaction itself starts with a Pd(0) species which will oxidatively insert into a carbon halogen bond. From this point, a ligand exchange is hypothesised to occur with an acetate. This allows for the addition of the aryl group through a process termed concerted metalation-deprotonation (CMD). As the name implies, the step allows

for a concerted step that will deprotonate the aryl substrate as well as add it to the palladium. After the CMD reductive elimination can occur leaving the final product.

The key difference between the catalytic cycles of DArP and other cross coupling methods that makes it so unique is the CMD. Most other cross coupling methods require one of the substrates to be functionalized with a metal or some equivalent so that transmetalation can occur. DArP seeks to replace this step through the use of substrates that can react without the requirement of pre-functionalization. CMD is simply the simultaneous cleavage of the C-H bond and the formation of a new C-Pd bond.[25] To enable this, an acetate or pivalate are often introduced to aid in the deprotonation step as well as a carbonate, most often cesium carbonate, is used to allow recycling of the ligand.

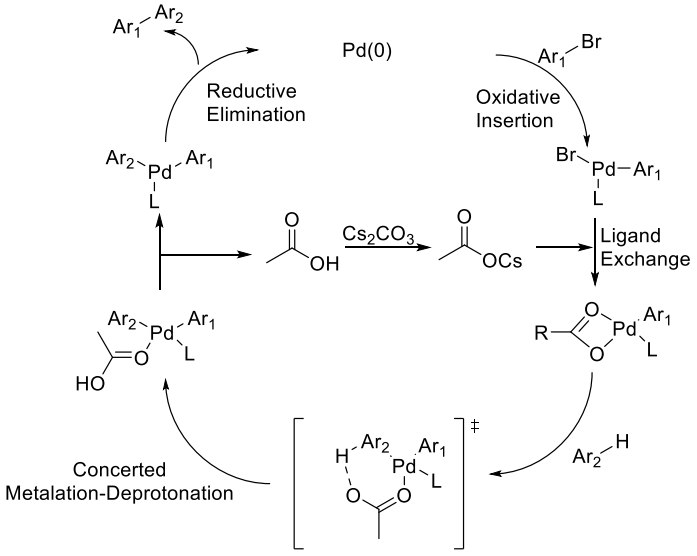

Figure 14 DArP Cycle: Catalytic cycle of DArP beginning with a Pd(0) species

The ability of a given substrate to participate in CMD and thereby direct arylation is based on two factors: the nucleophilicity of the substrate and the acidity of the proton. These factors affect one of the energies contributing to the overall activation energy.[37] The energy of

distortion (Ar-H) is affected by the acidity of the proton while the energy of initiation is changed through the nucleophilicity of the position in the substrate.[38]

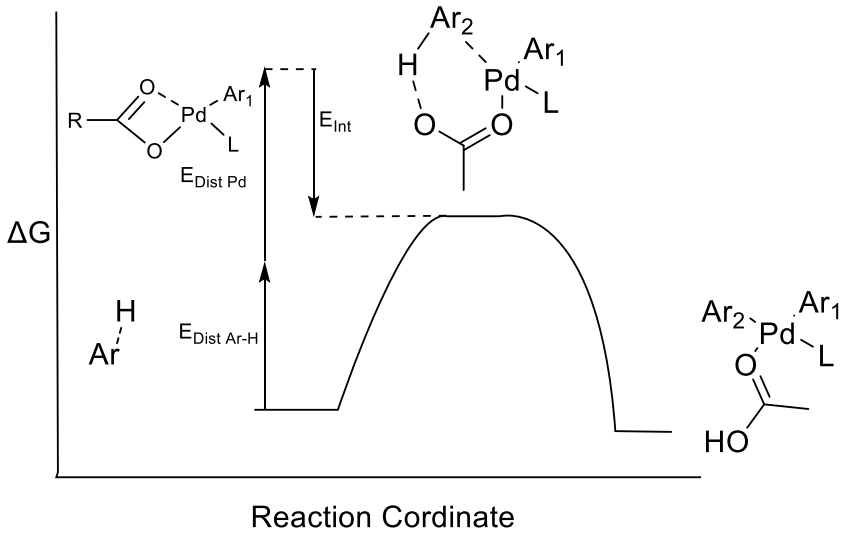

Figure 15 CMD Reaction Coordinate Diagram: Reaction coordinate diagram of CMD whereby the activation energy of the step is dictated by the energy of distortion of the Ar-H bond and the energy of interaction of the Ar-Pd bond

The differing energy barriers affecting the overall energy required to perform the reaction divides substrates into three classes that can affect both the rate and regioselectivity of the reaction. The first class of compounds, these being the substrates with a lower energy of distortion, will react with the most acidic proton. The second class of compounds, those with a higher energy of interaction, will react at the most nucleophilic site. The third category of substrates are those whose site of reaction is dictated by the energy of distortion of the Ar-H bond and the energy of initiation. These compounds exist as a class of their own due to the difficulty of predicting the regioselectivity without a computational study.[39]

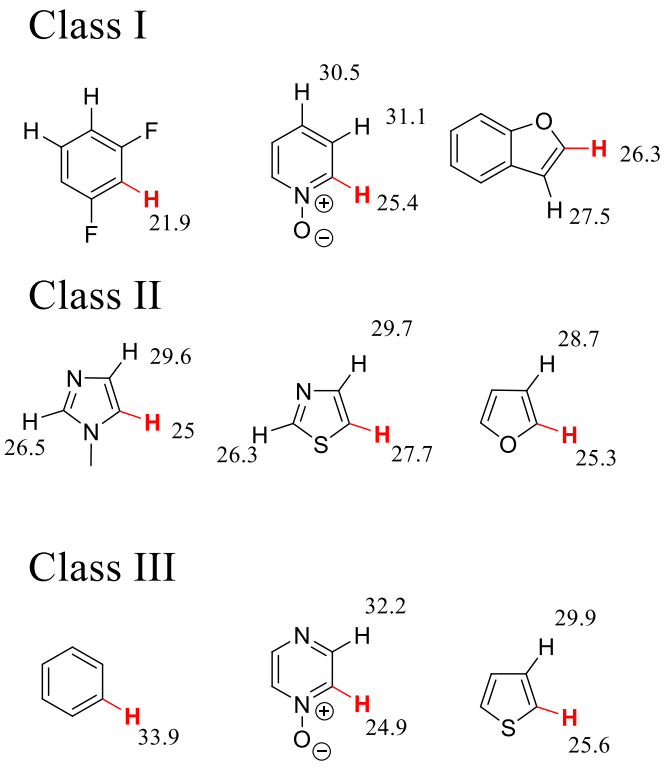

Figure 16 Direct Arylation Compound Classes: The three calsses of compounds usable for direct arylation. The reactive site is highlighted in read as well as the energy of activation measured in kcal/mol.[39]

Chapter 2: Palladium Precatalysts

Palladium as a catalyst has seen use in many fields for decades in many varieties of organic reactions. As previously discussed, there are a wide variety of possible cross-couplings based on the available substrates and potential reaction conditions. This in turn implies that a significant amount of research has been conducted into the potential palladium sources that can be used for cross couplings. Historically this included a range of Pd(II) species such as $PdCl_2$ and $Pd(OAc)_2$. Due to the inherent drawbacks of these palladium species, namely the fact that they must be converted to Pd(0) before the beginning of the reaction, research was performed to determine if more efficient methods existed to either synthesise Pd(0) or have a direct route to it from a Pd(II) species.[40–42] This led to the investigation of palladium precatalysts that could be synthesised ahead of time and stored while allowing them to be easily activated with the desired ligands whenever needed.

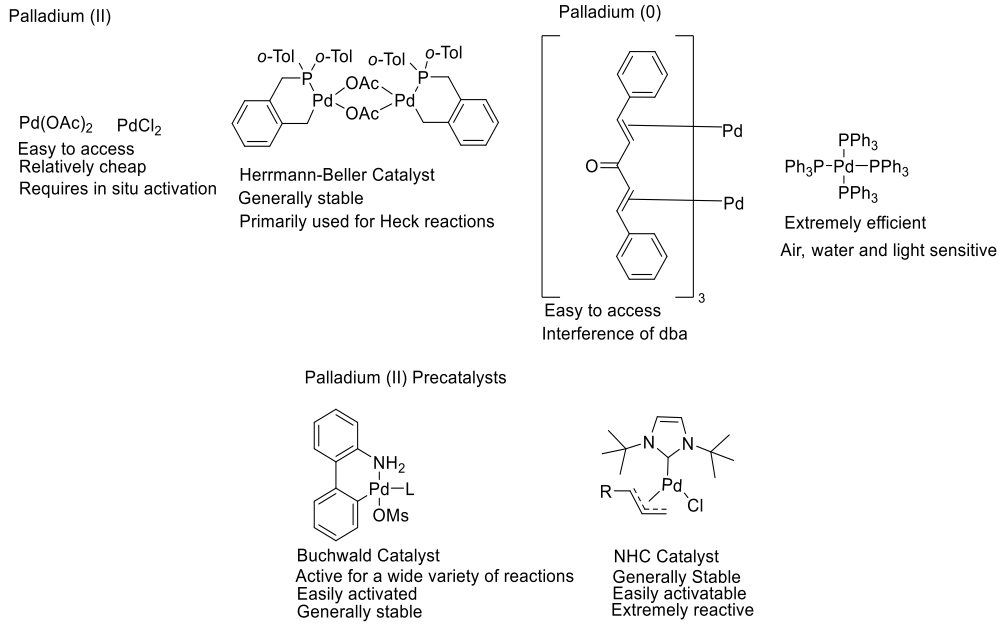

Figure 17 Available Palladium Sources: Palladium catalysts available for purchase. $Pd(OAc)_2$, $PdCl_2$, and Hermann-Beller catalysts are available as Pd(II) sources. Pd_2dba_3 and $Pd(PPh_3)_4$ are available as Pd(0) sources. Any generations of Buchwald catalysts and a variety of NHC catalysts are also available as Pd(II) when purchased and can be easily converted to Pd(0)[40–42]

In nearly all cross couplings, the first stage that must be passed is the conversion of a Pd(II) species, such as palladium acetate or palladium chloride, to a Pd(0) species so that the cycle can begin.[43,44] This generally occurs through either the introduction of ligands that participate in a redox reaction with palladium bringing it down to an oxidation state of zero or through pre-functionalization to guarantee that the species introduced is already Pd(0). There are advantages and disadvantages to both of these methods. For the conversion of Pd(II) species to Pd(0) through in-situ introduction of ligands, the primary advantage is the facility of the method. Most of these conversions are simply one pot while also guaranteeing that both the reactants remain stable until the reaction can begin. The primary disadvantages of this being the cost of adding excess phosphine ligands as well as the potential interference of the prebound ligands such as dibenzylideneacetone.[45] The other most common method is to modify the palladium species before the reaction to guarantee that there is no interference from the pre-bound ligands as well as saving time and reducing costs through efficient usage of the desired ligands. The issues with this lie either with difficult or sensitive reaction methods if a lab is producing the products themselves or large expense and unreliability if they are purchased through a third party. These issues have led to the division on what palladium sources to use in reactions with many defaulting to the less effective, but cheaper and more widely available, Pd(II) sources.

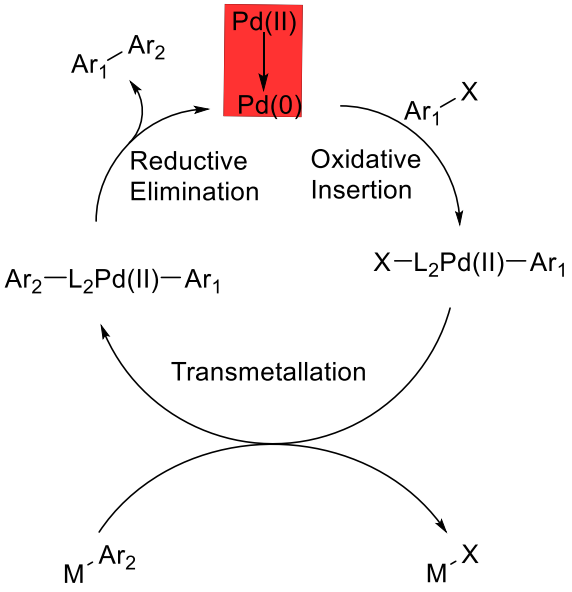

Figure 18 Palladium Cross Coupling: Before the beginning of palladium cross couplings Pd(II) must be reduced to Pd(0). This is done in a variety of ways depending on the palladium source

Catalyst selection is an important aspect of any cross-coupling reaction. Choosing the correct oxidation state of palladium and the correct ligand can affect the yield and rate of the reaction. This is not only due to the oxidation state required for the reaction to occur but also to the electron richness and sterics of the ligand.[46] For DArP to occur Pd(0) species are required. This means that, since most commercially available palladium sources, such as $Pd(OAc)_2$ and $Pd_2(dba)_3$ are either a Pd(II) source that requires in-situ reduction with the ligand or have ligands already attached that can heavily interfere with the reaction, potential defects may be observed.

2.1: Palladacycles

Palladacycles were discovered in the 1960s.[47,48] Initially, they were merely novel compounds allowing chemists to investigate the reactions of transition metals where most of the work was focused on discovering and confirming how palladium and platinum interacted with electron rich functional groups such as azo compounds.

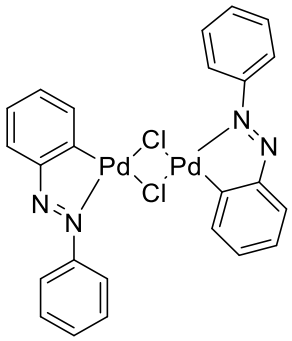

Figure 19 Cope Palladacycle: Initial palladacycles that were studied based on the affinity that palladium has for azo compounds

With the discovery and subsequent popularization of both Stille and Suzuki cross coupling reactions, the potential to use these compounds in place of commercially available palladium sources such as $Pd(OAc)_2$ and $PdCl_2$ grew in interest. Starting in the 1990s, there were investigations into palladacycles for use in cross coupling reactions.[49] This interest was stemming from the known fact that some specific configurations of palladium were more active than the traditional variants. Through the use of various palladacycles it was discovered that the efficiency, that being the amount of palladium used per mole of product produced, could be increased ten-fold over the next most efficient catalyst system.[40] These discoveries drove the investigation of palladacycles in various reactions such as hydrogenations and Heck reactions.

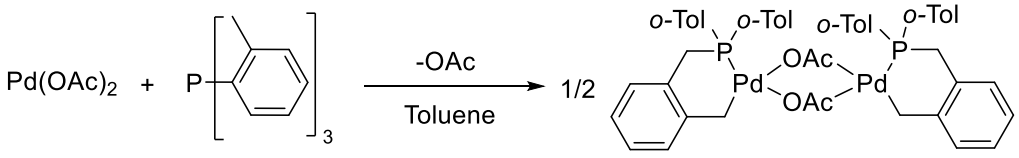

Scheme 1 Synthesis of Herman Beller Catalyst: Synthesised through the combination of $Pd(OAc)_2$ and P(o-tolyl)$_3$[49]

Past their use as catalyst systems, palladacycles have more recently begun research as precursors to other catalytic systems. Mechanistic studies were performed on immobilized palladacycles that were attached to silica. This testing was done through the performance of Suzuki reactions. A boronic acid and base were introduced to the immobilized palladacycle and

allowed a reaction period of 18 h. After this reaction period not only was palladium black observed but the framework of the palladacycle was seen through GC-MS. These results provided the hypothesis that the palladium would reductively eliminate from the palladacycle and react as Pd(0).[50] The presence of Pd(0) during the reaction was further shown through the use of a mercury drop test, in which mercury was introduced during a reaction with a palladacycle. The goal was to observe the completion of the reaction when compared to a control as mercury is supposed to only deactivate Pd(0).[51] While this evidence is not conclusive, as only certain palladacycles can be disrupted with mercury, when combined with evidence provided by the mechanistic and kinetic studies, it provides a strong case for palladacycles acting as precatalysts.

Beginning in 2008 Buchwald *et al*. were working on developing their nitrogen stabilized palladacycle precatalysts.[52] The first generation of these precatalysts saw the basis of the concept developed wherein palladium is linked to a nitrogen that, upon deprotonation would reductively eliminate to produce a Pd(0) species as well as a harmless nitrogen containing heterocycle. The issue with the first generation of these catalysts was that the conditions to activate the catalysts were too harsh, either requiring high temperatures along with a weaker base or a strong base which could interfere in the overall reaction. The first generation of catalysts also had stability issues meaning they could only exist in solution for a short period of time.

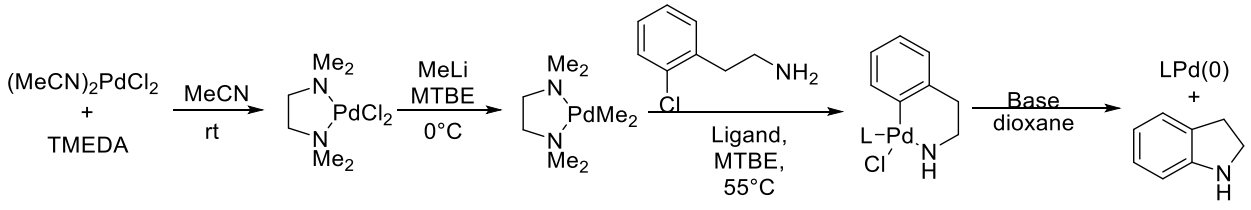

Scheme 2 1st Generation Buchwald Catalyst: Synthesis and activation of the first-generation Buchwald catalyst.

The second generation of the precatalyst built on the ideas of the first generation. The primary development of this generation was the introduction of a more acidic amine proton through the addition of another aryl group attached to the amine.[53] While this aided activation times and conditions due to the addition of the aryl group, the ligand scope was made more limited and the by-products generated were significantly more toxic. The third generation addressed the issues with the limited ligand scope by introducing a more electron withdrawing mesylate species. Due to the difference in electronics, this allowed for the ligand scope to be massively expanded. Finally in the fourth generation of catalyst the toxicity of the heterocycle product was reduced through the introduction of an alkyl group to the amine.[54]

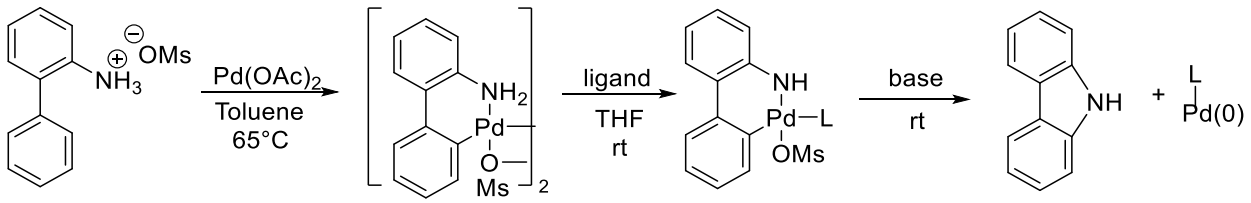

Scheme 3 3rd Generation Buchwald Catalyst: Synthesis and activation of the third generation of Buchwald catalysts

2.2: Applications to Conductive Polymers

Palladacycles are intrinsically linked to direct arylation as one of the first direct arylation products was created using a Herrmann-Beller catalyst.[49] Direct arylation polymerization also has a few aspects that make it particularly appealing to create conductive polymers on a potentially industrial scale. Without the pre-functionalization required there is a massive saving in the number of steps required and thereby the amount of time that is required to be invested in each polymerization. This same factor also offers a significant reduction in the amount of toxic waste as no tin or other metals are used in stoichiometric amounts. Finally DArP in particular

offers a similar price in reactants when compared to Stille coupling while reducing the number of steps required thereby potentially reducing the final cost of the polymer.[55,56]

While DArP provides many benefits for large scale synthesis of polymers, there are some drawbacks to using the method. Branching and other similar defects are of particular interest for these reactions as some of the most consequential polymers such as poly(3-hexylthiophene) can suffer from defects that occur during synthesis. These defects include β-defects, in which the beta proton is reacted with instead of the desired proton, cross linking, where two chains are joined by one or more substrates linked to both chains, branching wherein the same substrate is reacted with twice creating two chains growing from the same point, and homo-coupling that is the joining of two of the same monomer.[57] All of these defects can have a significant impact on the electronic performance of the resulting material.

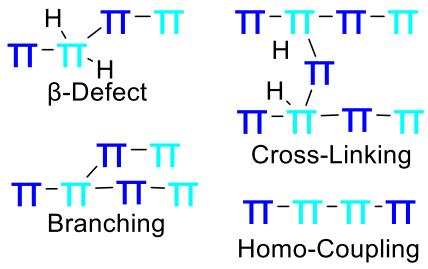

Figure 20 DArP Defects: Potential defects present in DArP due to low activation energy differences

The reason for us to attempt a new framework is to increase the turn over number (TON) as well as reduce the number of aforementioned defects. Defects are an extremely important issue for direct arylation products in particular due to the nature of the reaction where one of the substrates does not have a functional group with which to react. This can cause issues when multiple protons on the same substrate have similar activation energies.

2.3: Proposal[58]

Based on the information about palladacycles, and more specifically Buchwald catalysts, we decided to use them in conjunction with existing knowledge on conductive polymers and direct arylation. This began by finding a system that would be an analog to existing syntheses that have been shown to function in previous works. Our target polymer was based on the works by Leclerc *et al.* where, although a useful polymer was produced, a large amount of crosslinking was seen.[59] This led us to believe that we could address multiple issues with the polymerization at once. By using a palladacycle as a precatalyst, our goal was to reduce the amount of palladium needed to run the polymerization as well as reducing the amount of crosslinking seen in the final product.

Our targeted palladacycle for this purpose was X**.** It was activated to produce Y through reductive deamination via deprotonation. This reaction will yield a carbazole, a methanesulfonate salt and the desired palladium species.

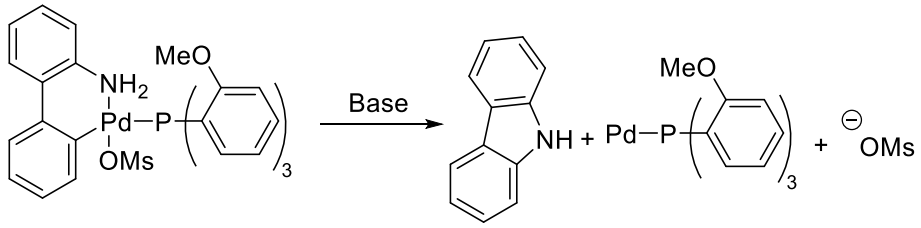

X **Y**

Scheme 4 Precatalyst Activation: Oxidative deamination of the proposed palladacycle

The reason for using this compound in particular was to attempt to create a final palladium species with identical ligands to what has already been seen in other direct arylation methods. This ligand system had already been optimized when compared to other common palladium systems that are commonly used in direct arylation such as $Pd(OAc)_2$. The usage of a similar ligand system also allowed for a more direct comparison to past research.

2.4: Synthesis

The synthesis of the palladacycle, initially conceptualized by Buchwald *et al.*, involves relatively few and high yielding steps to achieve the final catalyst.[41] Firstly, 2-aminobiphenyl is protonated with $MeSO_3H$ to form the mesylate salt. Secondly, this is followed by the introduction of $Pd(OAc)_2$ in toluene at an elevated temperature to perform a cyclopalladation. Thirdly, this reaction yields a dimer in quantitative yield. Thirdly, this palladacycle was then combined with the desired ligand to produce the Buchwald type catalyst.

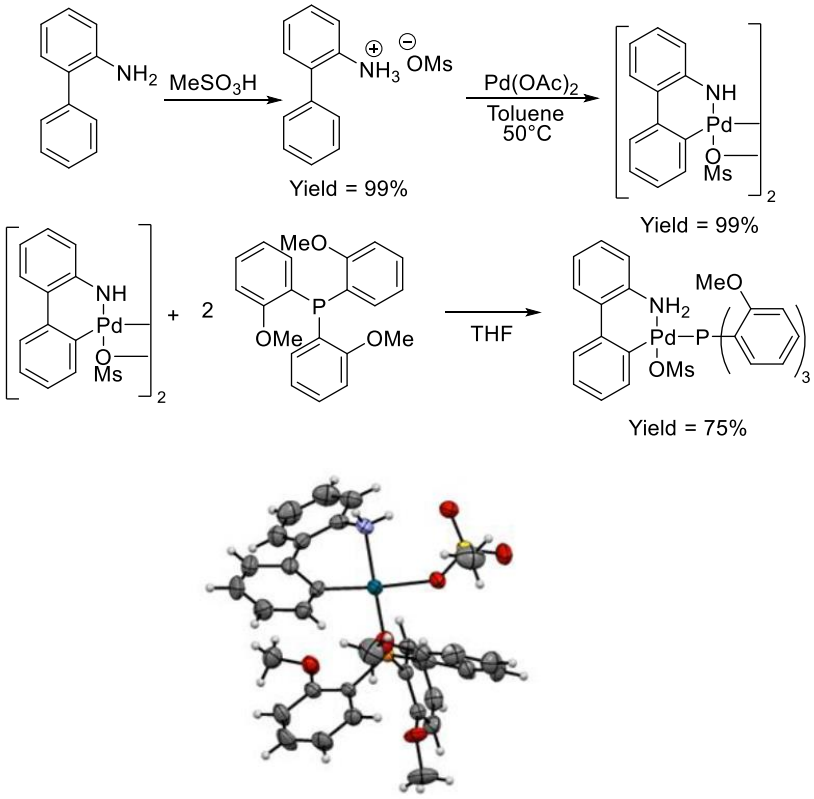

Scheme 5 Precatalyst Synthesis: Synthesis of our targeted paladacyle and the resulting crystal structure (produced by Dr. Rafael Mirabal)[58]

The polymerization methods for P1a (see chemical structure in Scheme 6) performed by Leclerc *et al.* was a suitable method for our purposes due to its past success with other catalysts. The only adjustment was the use of our precatalyst while the rest of the method remained nearly

identical.[59] This was another factor that allowed direct comparison between the branching seen as well as the palladium required and the rate of reaction between these two systems.

The polymers tested were all synthesized under similar conditions. While using the precatalyst, all solids were initially added to a sealed vial and freeze dried to reduce the amount of water present to interfere with the reaction. Toluene was then added, and the reaction mixture was heated to 100°C and allowed to react for two and a half hours. After the time period had passed, the polymer was precipitated using methanol cooled to 0°C and collected through vacuum filtration. The resulting polymer was then further purified through Soxhlet purification using methanol as the solvent. While not necessary to retrieve our final product, this allowed for a significant narrowing of the molecular weight distribution of the polymers.

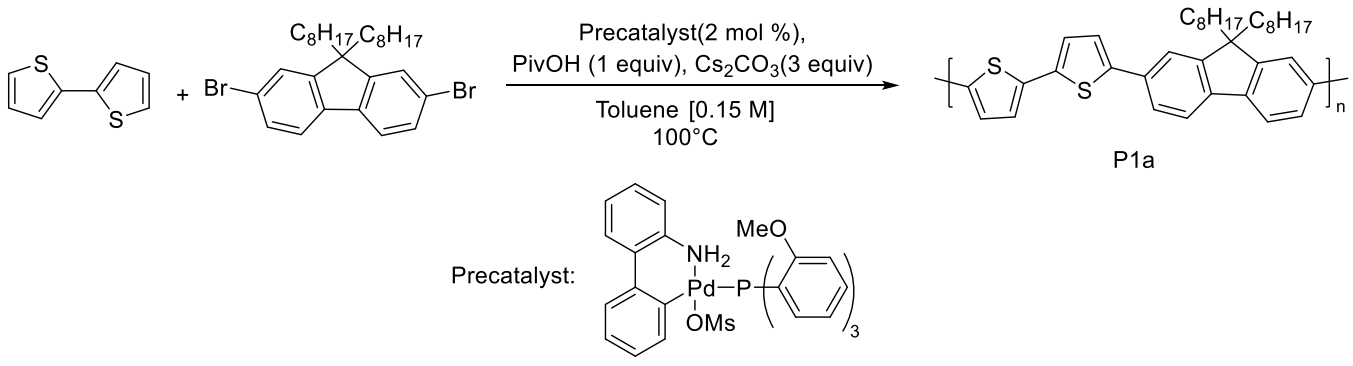

Scheme 6 synthesis of P1a: DArP using our targeted precatalyst as the palladium source

The target polymer was synthesised in two other ways to allow comparison to the effectiveness of the precatalyst. These methods were similar to those used in the synthesis of P1a with the primary difference being the palladium source. The first palladium source used was $Pd(OAc)_2$ which is one of the most common palladium sources used in direct arylation due to its experimental success.[60,61] The other palladium source compared to the precatalyst was

tris(dibenzylideneacetone)dipalladium (0). This source was used for a direct comparison of Pd(0) sources to determine how much impact the ligand had on the resulting polymer.

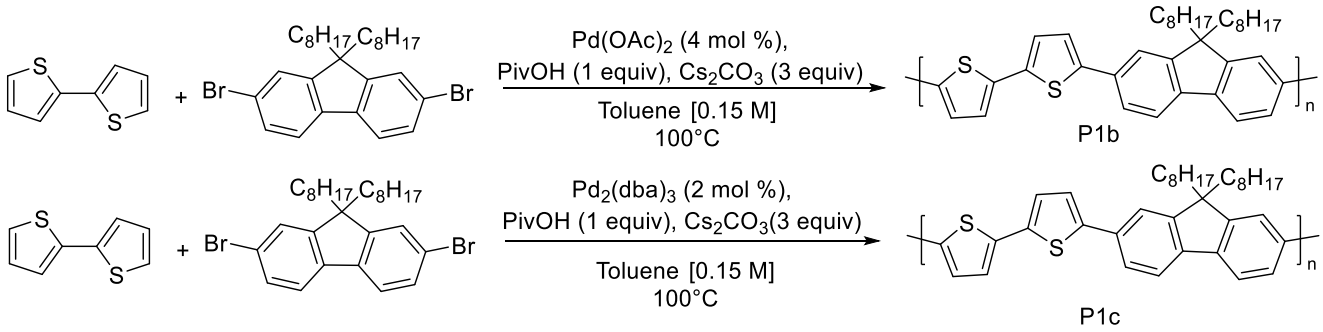

Scheme 7 Synthesis of P1b and P1c: Through DArP P1b and P1c were synthesised using $Pd(OAc)_2$ or Pd_2dba_3 respectively as the palladium sources

2.5: Kinetics

The first set of comparisons that were made were those of the rate of reaction (Fig. 21). It was observed that despite an induction period the precatalyst systems achieved higher molecular weights than the traditional $Pd(OAc)_2$ system. There is a drop off in the molecular weights seen for all systems after approximately three hours. This is due to the insolubility of the polymer. As only polymers that are soluble are observable via GPC there is a lowering of the average weights when the largest chains precipitate out of solution. The induction period seen for the first two hours of the reaction also lends credence to our hypothesis that the palladacycle is acting as a precatalyst.

Of particular interest is the high molecular weights achieved by out precatalyst. While it has been previously reported that the upper limit of the molecular weights had been achieved due to solubility or crosslinking, our precatalyst was able to surpass those molecular weights without becoming insoluble.[59] This fact points to the likelihood of cross linking being a significant

contributor to insolubility. This has likely not been reported in the past due to the difficulty of analysing insoluble materials.

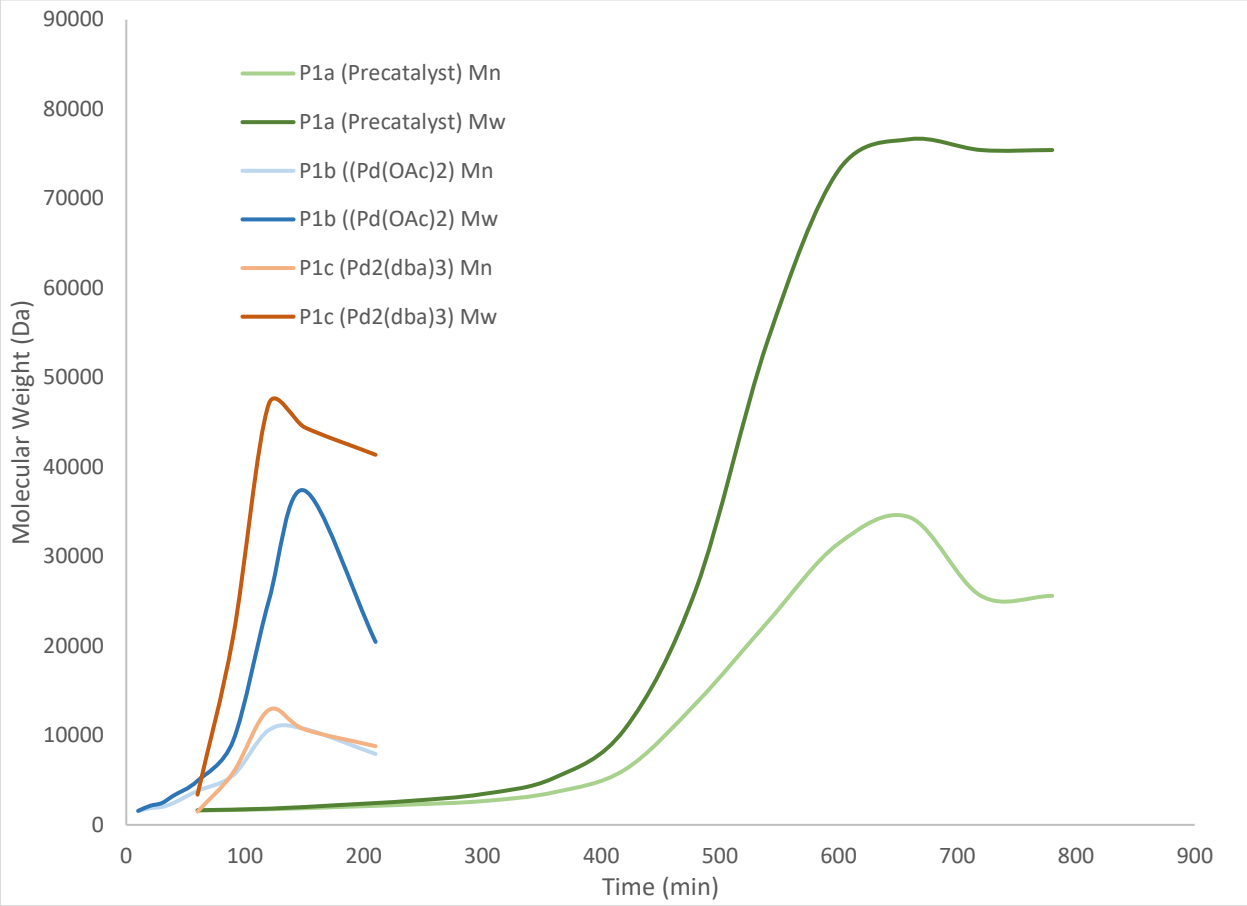

Figure 21 Kinetics Measurements: Mn and Mw growth of P1a, P1b, and P1c over time when using our precatalyst, $Pd(OAc)_2$, or Pd_2dba_3 as palladium sources

After testing multiple polymerization methods against one another to determine if our catalyst system was a viable option to produce polymers of adequate size while retaining solubility, our next step was to attempt to reduce the primary drawback seen while using the catalyst system: the activation time. We hypothesised that the rate limiting step in the activation of the catalyst was the deprotonation. Initially, due to the fact that Cs_2CO_3 was introduced as part of the reaction conditions for DArP, no base was added to the reaction. To test our hypothesis

LiO^{t}Bu was added to the solution to act as a stronger base to activate the catalyst and reduce the required reaction time.

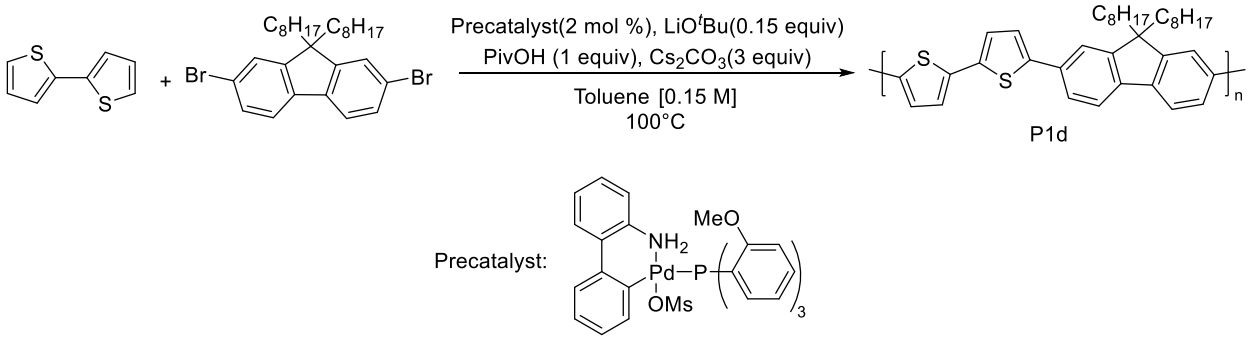

Scheme 8 Modified P1a Synthesis: Modified synthesis of PX with the addition of LiO^{t}Bu

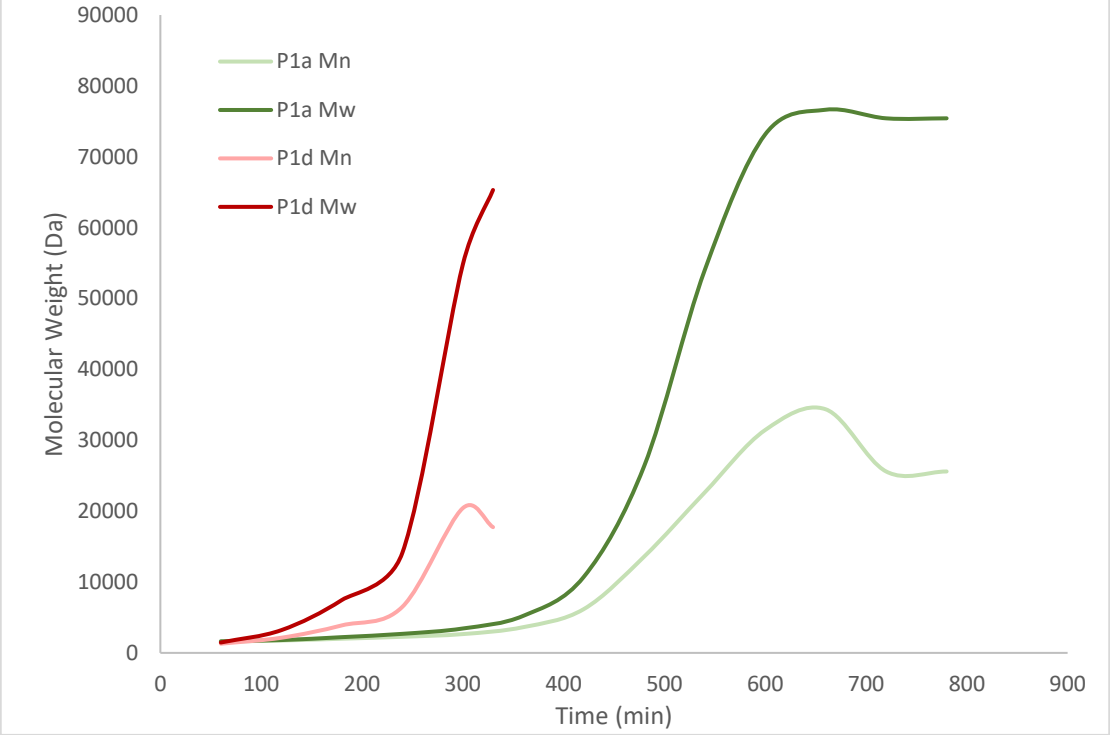

Figure 22 Modified Polymerization Kinetics Measurements: Mn and Mw growth of P1a and P1b over time while using the precatalyst as a palladium source with and without using LiO^{t}Bu as a base

As is seen in Fig 22, the rate of reaction was drastically improved when using LiO^{t}Bu to activate the palladacycle. Although the visible molecular weights were slightly reduced the reaction time was significantly closer to those seen when using $Pd(OAc)_2$ or $Pd_2(dba)_3$. This is

promising for the overall reaction as the decreased rate of reaction was the primary drawback that was initially observable. With an increased rate, the opportunities for use of the palladacycle increase. If the molecular weight of the final product is of more importance, the method without base can be employed whereas if the rate of reaction is the primary concern, a base can be used to increase it.

2.6: Polymer Analysis

Fig. 23 shows an overlay of the UV-vis spectra of the polymers created through both the precatalyst as well as traditional catalyst systems such as $Pd(OAc)_2$ and $Pd_2(dba)_3$. With the primary difference being a change in maximum absorbance with P1a and P1c being found at 450 nm and 453 nm respectively and P1b being found at 445 nm. Although there were slight differences in the UV-vis this was not enough to indicate a large shift in the properties of the P1 polymers

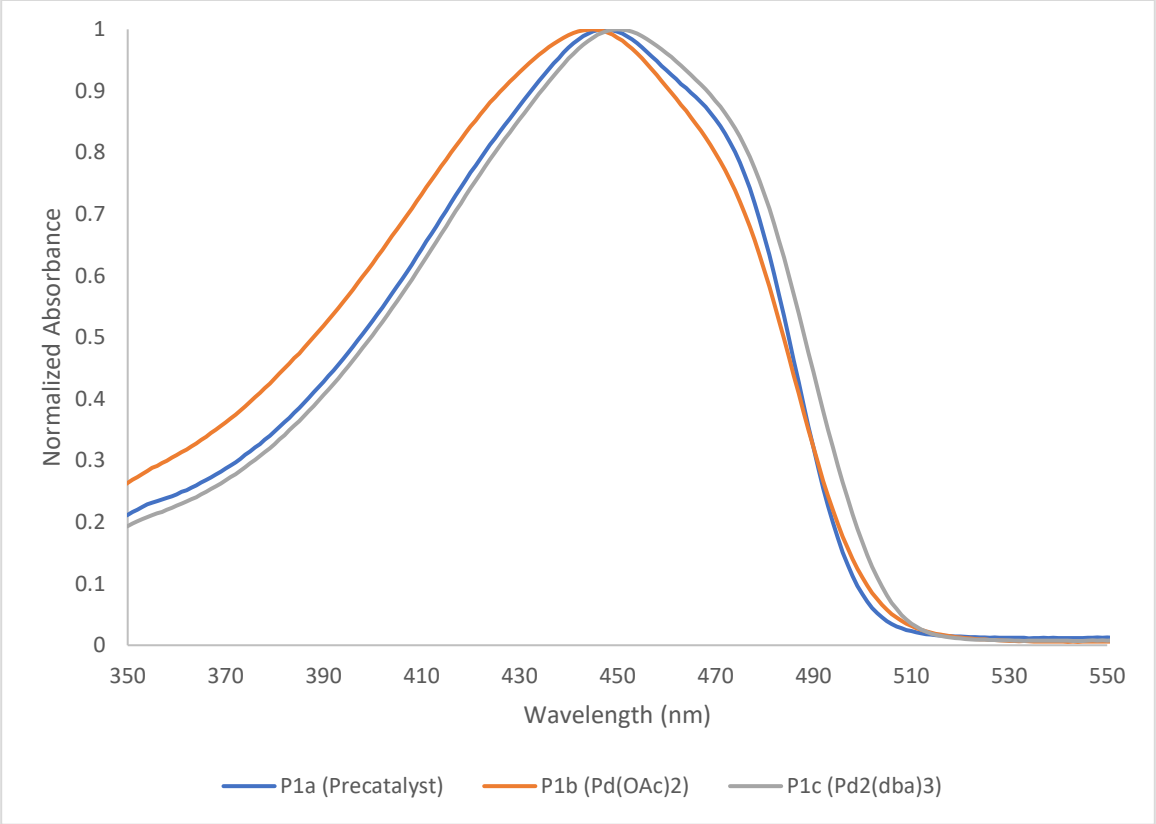

Figure 23 UV-vis Comparison: Normalized comparison on UV-vis spectra of P1a, P1b and P1c

The other method we used to measure the properties of the polymer was through NMR. The polymer was able to be analysed through NMR in TCE at 80 °C. This allowed a more concrete observation of the resulting polymer. Analysis of the NMR spectra led to the conclusion that 3 groups of protons would provide quantitative information about the degree of branching present. The doublet of doublets found at 7.69 ppm labeled A, the singlet found at 7.57 ppm labeled B and the doublet found at 7.30 ppm labeled C (Fig. 24) have been identified in past works as the protons associated with the aromatic backbone.[59]

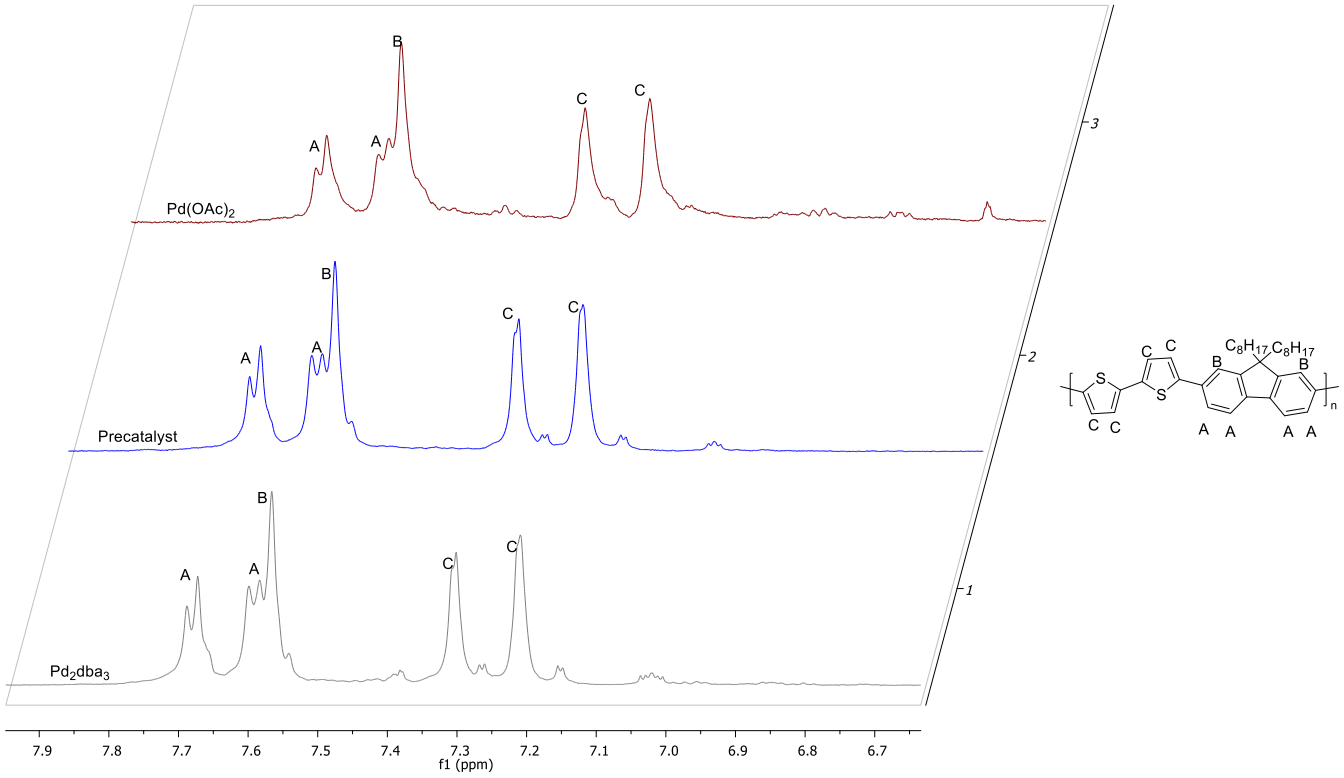

Figure 24 Polymer NMR Comparison: NMR spectra from the polymers produced with the use of each palladium source.

Following the initial observation of the peaks as well as investigation of the potential polymerization defects. There are multiple forms of potential defects. While not accounting for end group defects which, with DArP can be difficult to detect due to the lack of functional groups, the primary concerns are branching, cross linking, and homo-coupling.

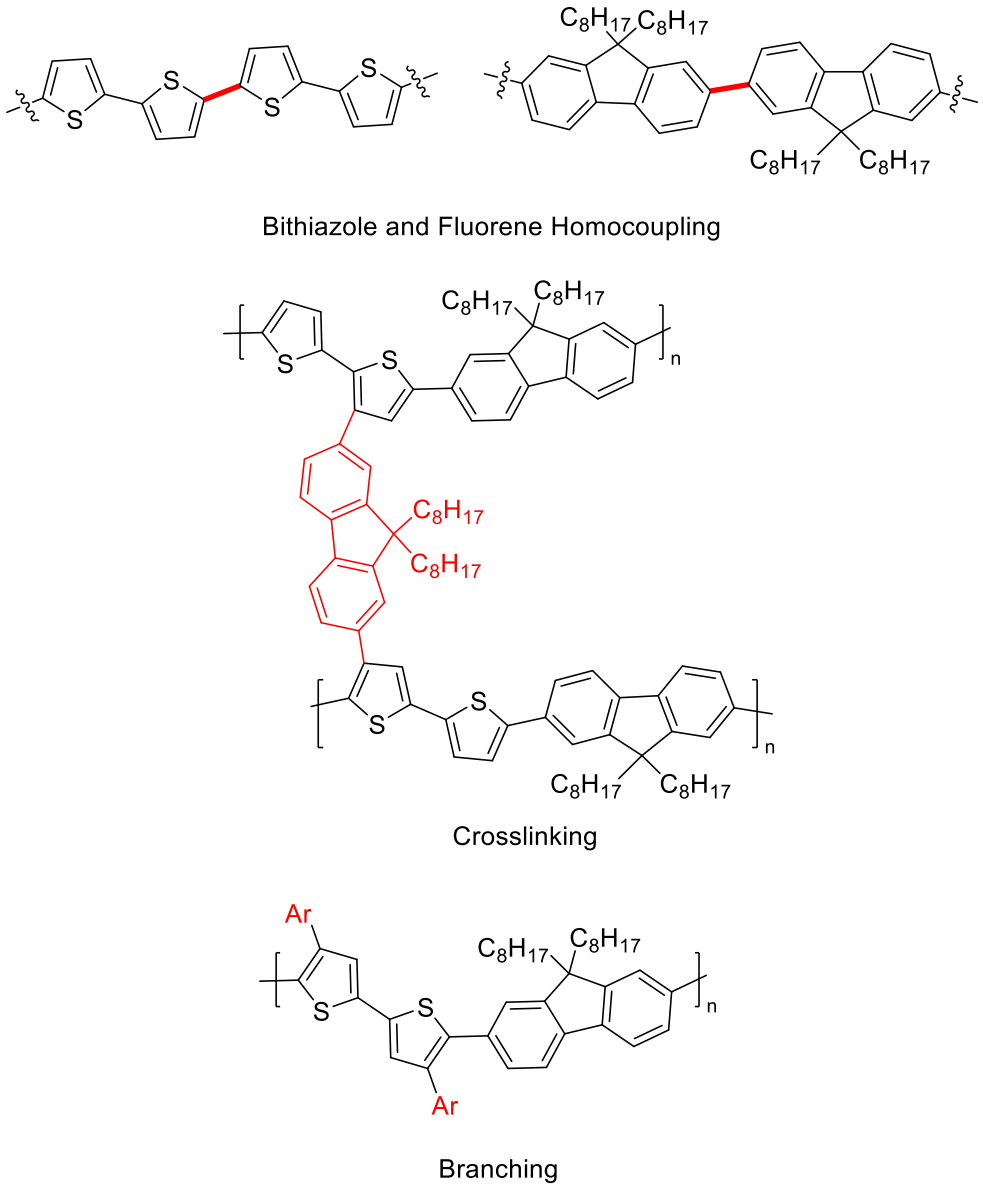

Figure 25 Potential Defects found in P1: Possible defects seen when synthesising the target polymer.

These spectra pointed to the fact that our precatalyst was allowing the synthesis of polymers with significantly less branching. This is obvious since the peaks at 7.38 ppm disappear, or at least are significantly reduced when the polymer is synthesised using our precatalyst. This result indicates that the precatalyst not only allows for lower Pd loading and more rapid reactions after activation but also allows for less branching in the resulting material.

Observing the NMR spectra of P1a, in blue, when overlayed with P1b, in red, the difference in the amount and degree of the defects found in the polymers can be clearly seen Fig 26. There are multiple regions that, when compared, indicate that the number of defects seen in the polymer is significantly effected when $Pd(OAc)_2$ is used as the catalyst, specifically at 7.36 ppm and below 7.00 ppm. Due to the fact that all of these peaks are seen in the aromatic region we hypothesize that they are a result of branching of the backbone of the polymer leading to the variation in the location of the ^1H signals.

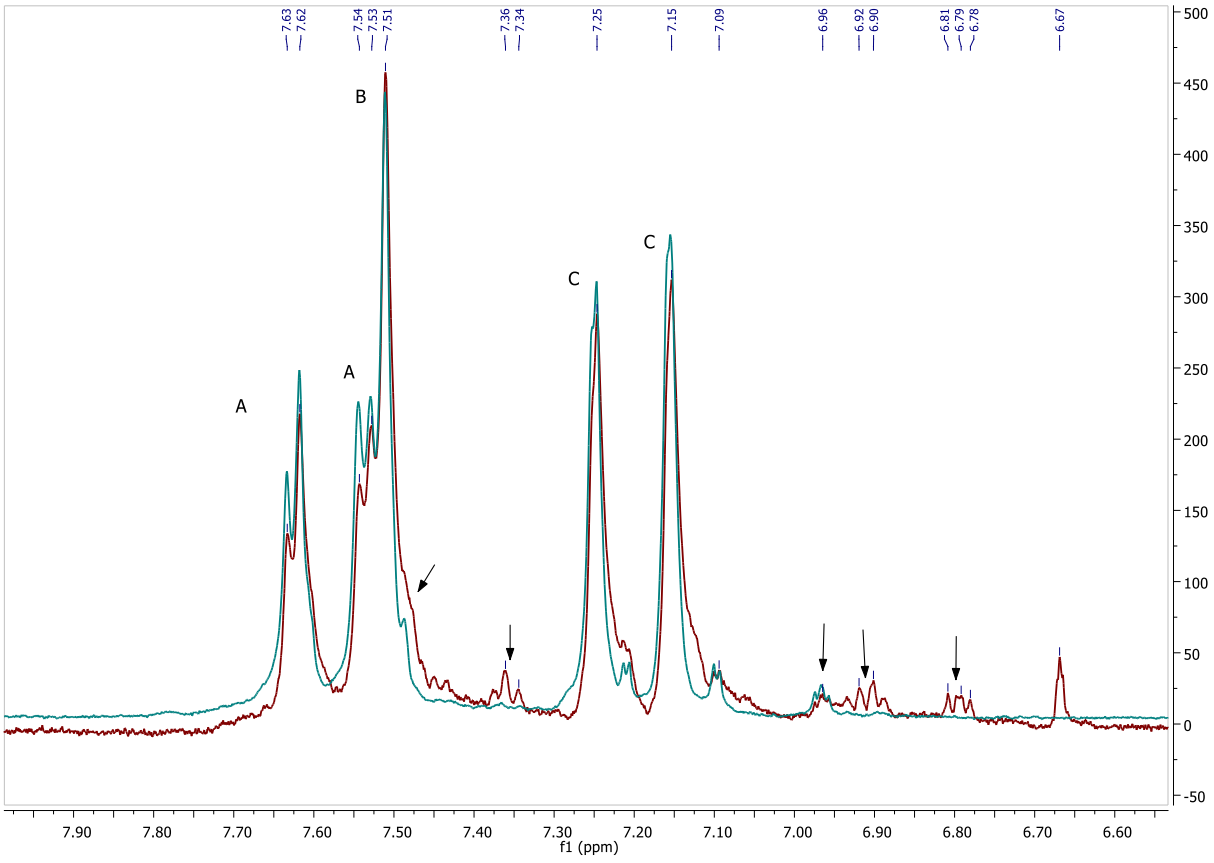

Figure 26 $Pd(OAc)_2$ NMR: Overlay of NMR spectra of P1b synthesised with $Pd(OAc)_2$ in red and P1a synthesised using the precatalyst in blue. Arrows indicate defects.

Although unclear as to the nature of the defects, there is a peak present at δ7.36 in the NMR of P1b, seen in red, that is not present in the NMR of P1a, seen in blue (Fig 27). There are

also multiple peak present at 6.95 ppm, 6.92 ppm, 6.81 ppm, and 6.67 ppm in the NMR of P1b that are undefined (Fig 27). All of these peaks along with the emphasized shoulder seen in the NMR of P1b at 7.50 ppm, 7.24 ppm, and 7.14 ppm (Fig 26) lead us to believe that our developed precatalyst has significant advantages when compared to more traditional DArP conditions. Not only is the molecular weight of the final product higher when compared to P1b (Fig 21) but, through NMR analysis, significantly less undefined peaks are seen in the aromatic region leading to the conclusion that there are fewer branching defects.

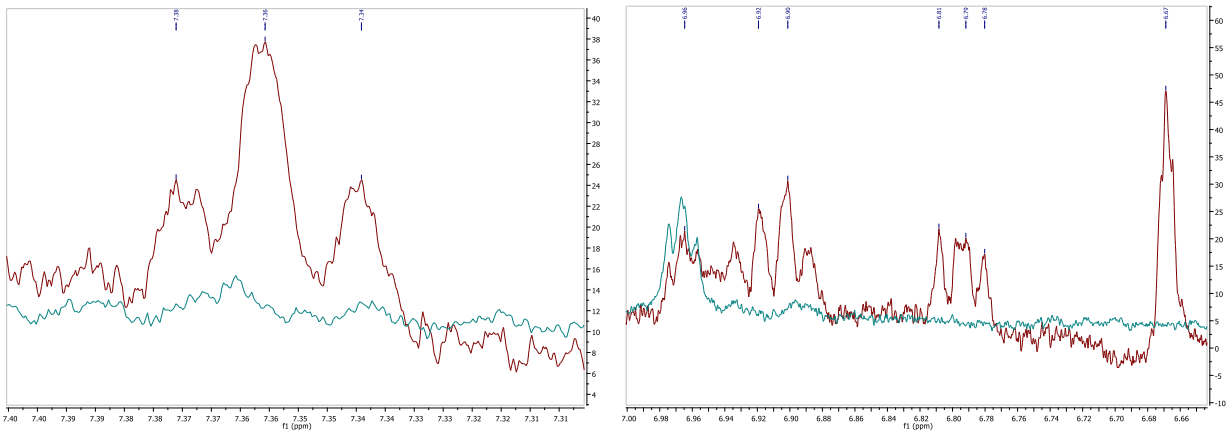

Figure 27 $Pd(OAc)_2$ NMR Defect Analysis: Overlay of NMR spectra of P1b synthesised with $Pd(OAc)_2$ in red and P1a synthesised using the precatalyst in blue from 7.40 ppm to 7.30 ppm and from 7.00 ppm to 6.67 ppm.

Considering the NMR spectrum of P1c, in grey, when compared to that of P1a, in blue, (Fig 28) it can once again be seen that there is a significant reduction in the number of defects. While this does indicate that the usage of a Pd(0) source may positively influence the synthesis of P1 there are still defects seen at 7.33 ppm and 7.02 ppm. Similarly to P1b, these defects are found in the aromatic region leading us to hypothesize that the use of Pd_2dba_3 as a catalyst can lead to branching in the backbone of the resulting polymer.

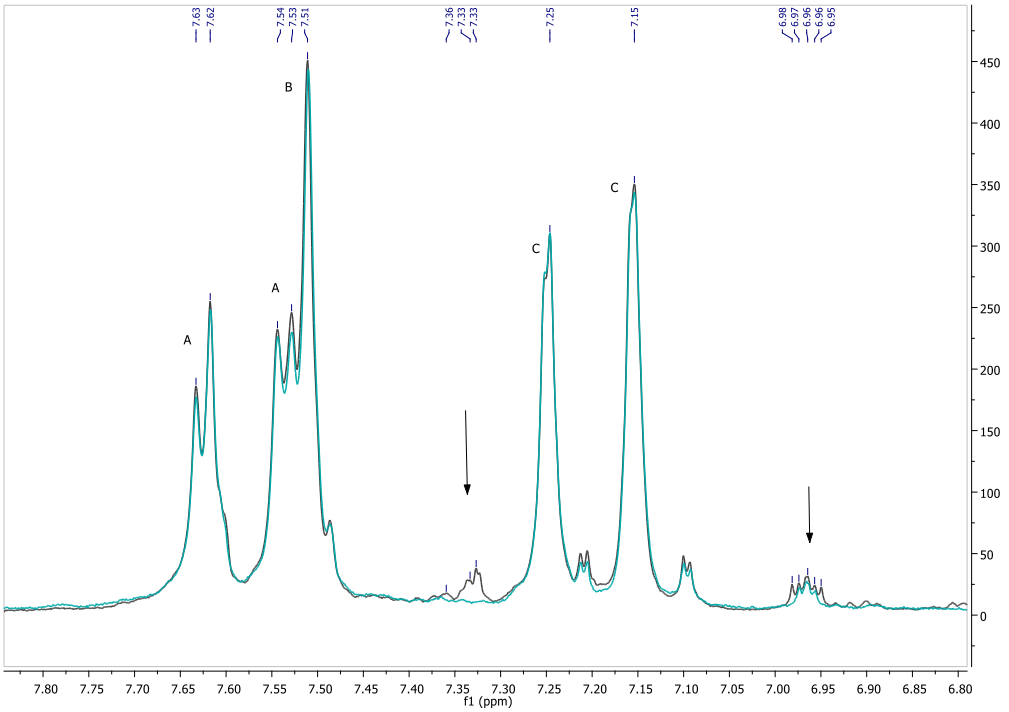

Figure 28 $Pd_2(dba)_3$ NMR: NMR spectra of P1c synthesised with $Pd_2(dba)_3$ in black and P1a synthesised using the precatalyst in blue. Arrows indicate imperfections.

Although uncertain of the type of branching caused by the palladium sources P1c, seen in grey, has a defect at approximately 7.32 ppm (Fig 29). Comparing this to the NMR of P1a in the same region, the reduction in the degree of branching is evident as there are no peaks present. From this we can hypothesize that there is a significant decrease in the number of defects observed from the polymers produced using the precatalyst even when compared to another Pd(0) source.

There is another potential defect found in the NMR of P1c at 7.02 ppm (Fig 30). It was initially believed that this was an end group. A similar peak was found in the NMR of P1a as a triplet which is expected from the proton at the 4-position of the thiophene. Upon closer investigation this same peak, when observed in the NMR of P1c, is an apparent pentet. This is

likely due to some form of branching causing end group protons to have slightly different chemical shifts further indicating the benefits of the precatalyst.

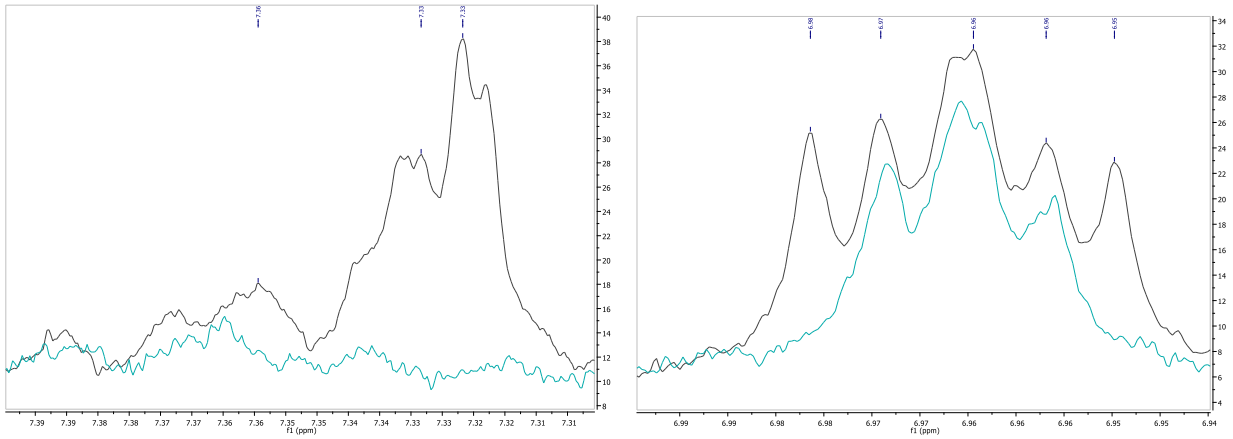

Figure 29 $Pd_2(dba)_3$ NMR Analysis: Overlay of NMR spectra of P1c synthesised with $Pd_2(dba)_3$ in grey and P1a synthesised using the precatalyst in blue from 7.40 ppm to 7.31 ppm and 7.00 ppm to 6.94 ppm.

After comparing the NMR spectra of the differing palladium sources, it becomes evident that the amount of defects seen varies greatly based on the palladium source. When using our precatalyst, the amount of defects seen in the aromatic region of the NMR spectra was significantly reduced compared to $Pd_2(dba)_3$ (Fig. 28, 29) and $Pd(OAc)_2$ (Fig 26, 27), the most common palladium source for DArP. The discernible defects seen in P1b and P1c are found in the aromatic region indicating that there is branching occurring on the bithiophene subunit. Particularly interesting are the peaks found at approximately 7.33 ppm as both P1b and P1c had a peak that was absent from P1a. Although the location and degree of the branching is yet unclear defects have been reported in these regions in past works.[59,62] These results indicate the potential to create a polymer with: fewer defects, higher solubility, and without the requirement of installing blocking groups.

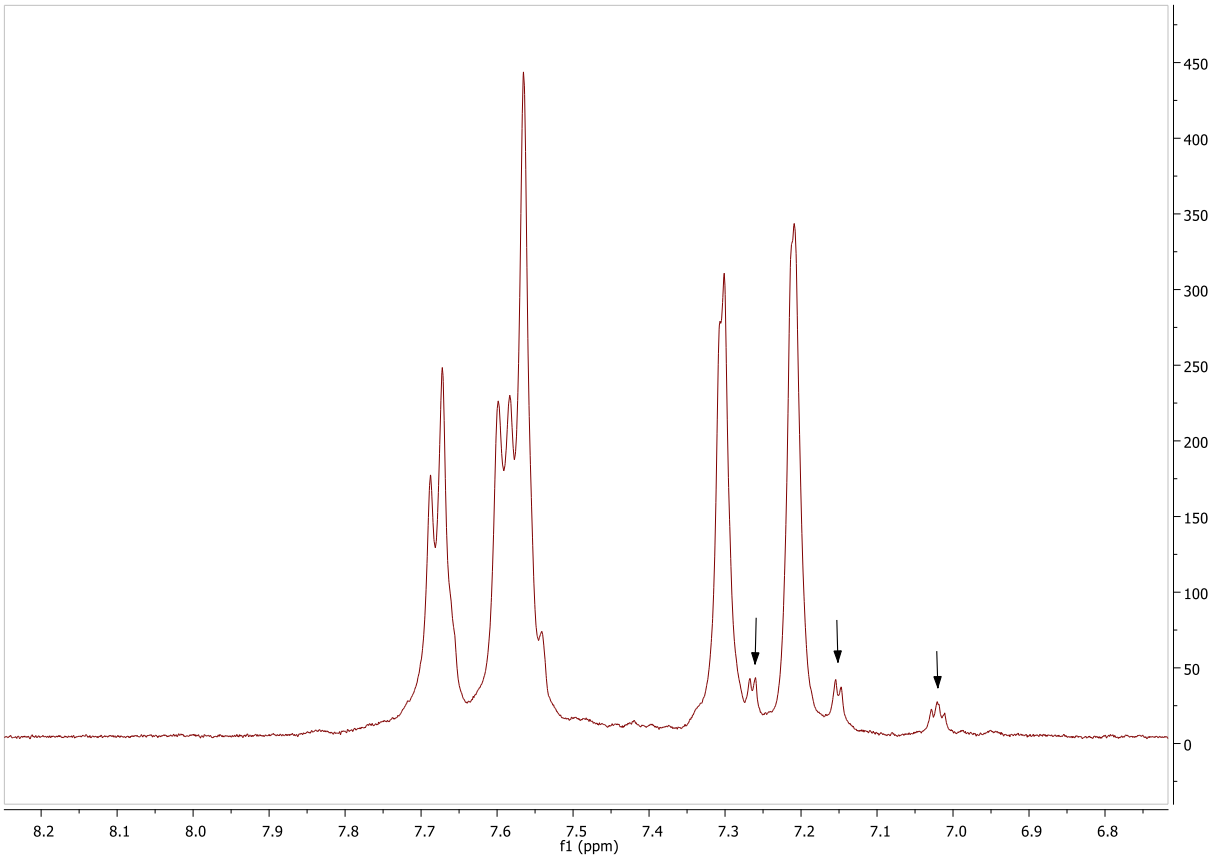

Figure 30 P1a End Groups: End group locations in the NMR of P1a

The other peaks seen in the aromatic region at 7.25 ppm and 7.16 ppm both being doublets, and δ 7.02 being a clear triplet in the NMR of P1a are end groups (Fig 30). This is based both on previous research done into this polymer as well as the reduction in peak size as the molecular weight of the polymers increases.[59] These peaks allow for end group analysis of the polymers which in turn allows for an alternate way to measure the size of the polymers produced. The polymer sizes predicted through this method are significantly smaller than those seen by GPC (Table 1). This massive discrepancy could be for one of two reasons. Firstly, the standard used in the GPC is inaccurate for predicting the size of the polymers. As GPC is based off of the hydrodynamic volume of the polymer it is never 100% accurate when measuring against a standard of a different polymer. If the hydrodynamic volume of polystyrene, the

standard most commonly used in GPC, at a given size is significantly different than our target polymer it could lead to inaccurate measurements. The other potential possibility for the discrepancy seen has to do with the solubility of the polymer in the NMR solvent used. P1 is not soluble in many common NMR solvents such as $CDCl_3$. Therefore, for the NMR spectra of the polymer to be retrieved it was required to be dissolved in TCE at 90 °C. Due to the low solubility of the polymer there is the potential that many of the polymer chains at higher masses precipitated before they could be adequately incorporated into the NMR sample. Further proof of the low solubility of the polymer affecting the mass seen through NMR is the higher molecular weight seen for P1b when compared to P1c. This is the inverse of the result seen when measured through GPC but the higher degree of defects seen in the polymer could contribute to its lower solubility and thereby the lower molecular weight.

Polymer	GPC M_n (kDa)	NMR Predicted Molecular Weight (kDA)
P1a	25.6	6.83
P1b	13.2	4.90
P1c	18.8	4.11

Table 1 NMR Molecular Weights: Molecular weights of P1 polymers measured through end group analysis via NMR

2.7: Investigation of Other Polymers

Two other polymers have been investigated for synthesis with this palladacycle. The first of these was FDOF-TP. This polymer was chosen because it has been extensively studied and also lacks a hydrogen that could cause branching. Based on the work previously done by Ozawa *et al.*, a variety of conditions were tried to surpass the molecular weights achieved in their

work.[63] The other purpose of this polymerization was to see if it was possible to eliminate soxhlet extraction as a necessary purification step. Unfortunately, the molecular weights retrieved from these experiments were not beyond what was expected and the yields retrieved from multiple experiments were above 100% indicating that further purification was required.

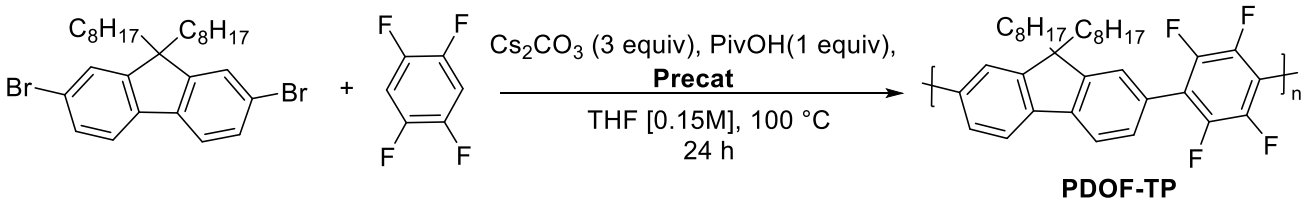

Scheme 9 DArP of PDOF-TP: Synthesis of PDOF-TP using the precatalyst as a palladium source

Reaction	Catalyst Loading (mol %)	Reaction Time (h)	Mn (kDa)	Mw (kDa)	Yield (%)
1	1	24	15.0	53.3	79
2	2	24	21.9	57.6	>100
3	2	127	12.4	21.4	74
4	0.05	24	12.9	32.4	>100

Table 2 PDOF-TP Synthesis: Summary of reaction conditions attempted to synthesize PDOF-TP through DArP using the precatalyst

The other polymer that was explored for use with this palladacycle was P3HT. This polymer was investigated for two reasons. First P3HT is one of the most researched conjugated polymers meaning that analysis of the polymer is straightforward as there are plenty of NMR spectra that are available to compare allowing for easy determination of defects. Secondly there are multiple syntheses of the polymer and a variety of conditions available to use to determine which are best suited to the catalyst system. Two sets of reaction conditions were attempted:

those performed by Leclerc *et al.* and those performed by Ozawa *et al*. with the primary difference between them being the equivalents of base and the concentration of the reaction mixture.[24] Unfortunately, neither of the conditions attempted resulted in a high yield with the molecular weights of the polymers being difficult to measure as much of it was below the calibration limit. With more exploration, conditions could be found where the precatalyst shows higher effectiveness, but more research is required.

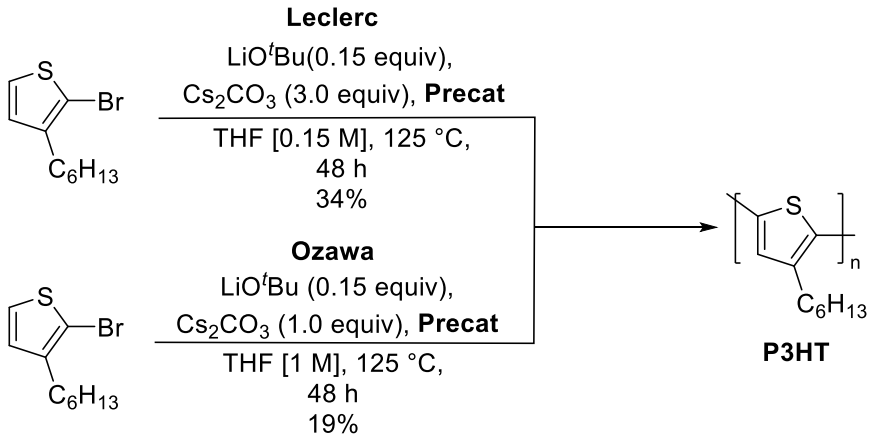

Scheme 10 P3HT Synthesis: Attempted synthesis of P3HT using DArP with our palladacycle as a palladium source. Conditions retrieved from both Ozawa et al and Leclerc et al.

2.8: Conclusions

In conclusion, we have outlined a method that uses a palladium precatalyst for DArP, which can be easily synthesised and utilized. Our experiments thus far have indicated that using this style of catalyst can reduce the amount of side reactions leading to defects. These conclusions were supported by the low PDI and high molecular weight of the polymer produced as well as their ease of processability and improved chemical purity based on the analysis of their NMR spectra. The NMR spectra are particularly significant as they display the reduction in defects seen when using the precatalyst as a palladium source leading to potentially more

regioregular polymers with enhanced solubility. The other primary advantage was the decrease in the amount of palladium required to perform the reaction thereby reducing the cost.

This concept could be further expanded on through a few methods. A wider variety of DArP friendly ligands could be tested potentially reducing the side reactions further. More polymers could also be more thoroughly tested to display the general applicability of the catalyst system. Of particular interest would be further investigation into the synthesis of P3HT as it is a commonly used polymer that could significantly benefit from higher selectivity in its synthesis.

Chapter 3: Using Direct Arylation Polymerisation to Prepare Dialkoxybithiazole Polymers

An important aspect of scientific research is the thorough exploration of possible substrates. This is particularly important in the realm of conjugated polymers as achieving unique electrical properties is the primary goal of the field. Polythiazoles are of particular interest due to their ease of synthesis and thermal and environmental stability. The primary drawback of unsubstituted polythiophenes, one of the most prolific conductive polymers, is their processability. Namely the fact that, even at relatively low molecular weights, polythiophene is insoluble in most organic solvents.[64] These issues were addressed through the addition of alkyl chains at the 4 and 4' positions. This aided in the solubility but has been shown to disrupt the planarity of the molecule negatively affecting its conductivity.[65] One of the solutions to this was to instead use an alkoxy side chain on the molecule. This addresses the planarity issue though a phenomenon termed chalcogen bonding which is a non-covalent interaction between group VI elements, or chalcogens, and electron-rich donors.[66] This allowed for S-O interactions which cause the polymers to retain their planarity while becoming soluble in a larger variety of organic solvents. While polythiophenes have been thoroughly investigated, including those with alkoxy substituents such as poly(3,4-ethylenedioxythiophene) (PEDOT), there are some issues with the polymers. One of the primary issues is that the newly introduced alkoxy side chain attached to an already electron-rich ring pushes the energy levels of both the HOMO and LUMO higher by 0.3-0.5 eV making them less generally applicable. [67]

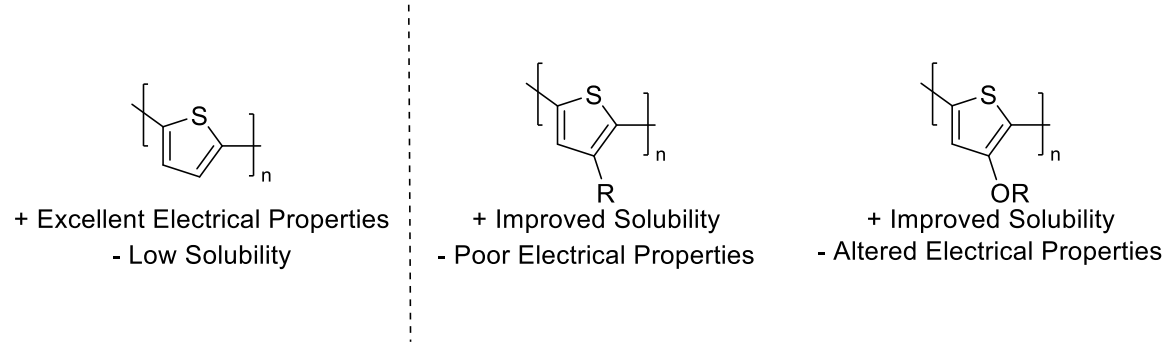

Figure 31 Thoiphene Summary: The modificaiton of the electrical properties of polythiophene by introducing alkyl or alkoxy side chains. When alkyl side chains are introduced the poor solubility of polythiophene is adressed but the electronic properties are poor due to the disruption in planarity. When an alkoxy group is introduced to the polymer the solubility is improved from the unfunctionalized version but the location of the HOMO and LUMO are shifted due to the resonance donation of the oxygen.

The high energy level frontier orbitals of the alkoxypolythiophenes indicated the need for a modification of the backbone of the polymer. Researching this, attention was drawn to one of the underexplored polymers in the realm of conductive polymers: 4,4-dialkoxybithiazoles. The benefits of the alkoxy side chain in the 4,4'-dialkoxybithiazoles are three-fold. Firstly, the inclusion of a long alkyl chain aids with the solubility issues associated with extended conjugated polymers as referred to in Chapter 2. The other two purposes of the alkoxy side chains are related to the size of the band gap and its position relative to the vacuum level. The usage of the alkoxy side chain addresses these issues. Due to the conformation of the polymer, there is a steric interaction between the bithiazole's side chain and any aromatic spacer used. This steric interaction will disrupt planarity thereby negatively affecting the conductivity of the resulting polymer. The oxygen on the alkoxy chain addresses this issue since, in a head-head linked dimer, it will maintain the planarity by coordinating with the hydrogen of the aromatic spacers. Due to the fact that a thiazole is a more electron-poor ring when compared to a thiophene, an electron-donating group can be attached without adversely affecting the desired band gap. Density functional theory (DFT) calculations reinforced this idea showing that thiophenes attached to aryl spacers with an alkyl side chain would yield a large band gap.

Changing the side chain to an alkoxy group shrunk the band gap but the HOMO was still too high for practical use. Finally changing the thiophene backbone to a thiazole lowered the energy of the HOMO in relation to the vacuum level while retaining the smaller band gap seen in the alkoxy thiophene.

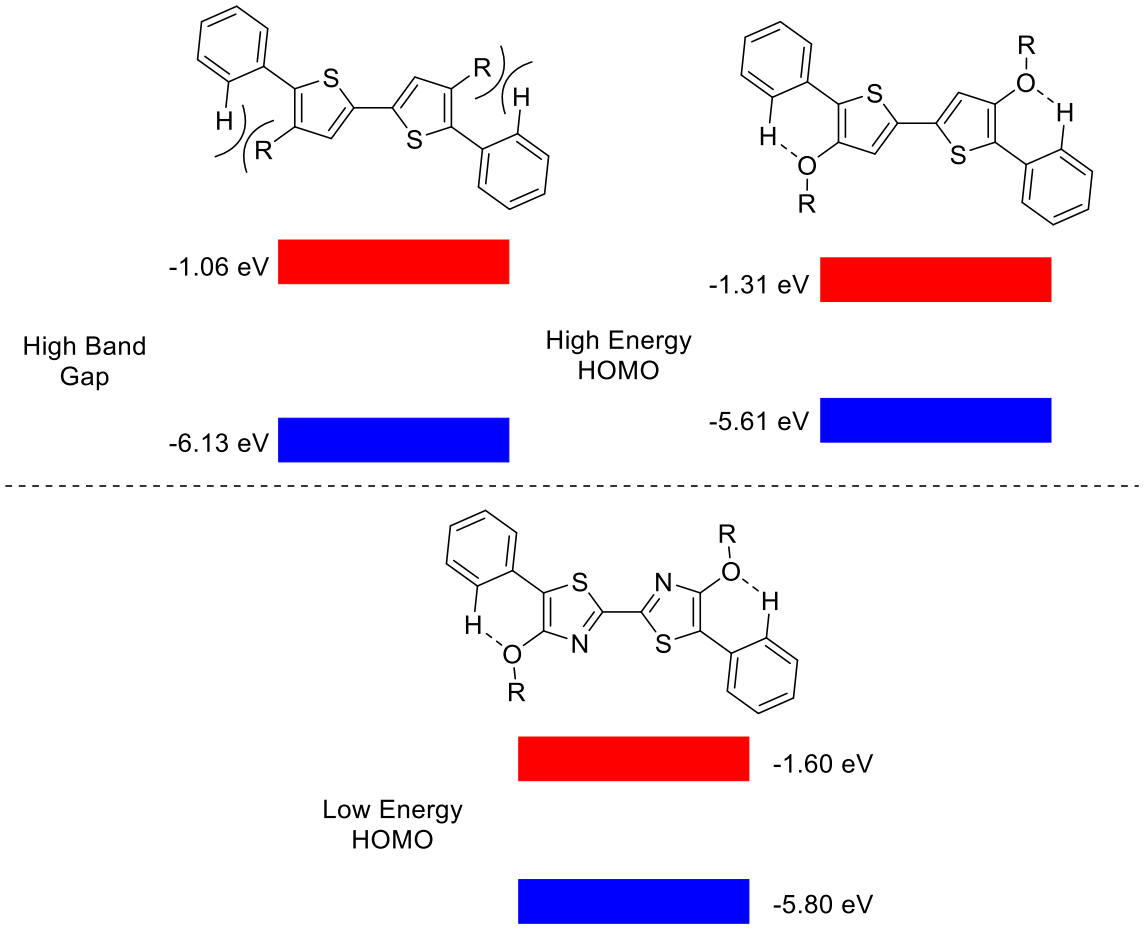

Figure 32 DFT Calculations: Performed by Dr. Sinclair showing the variation in band gap and proximity to the vaccum level of alkylbithiophenes, which have a large HOMO-LUMO gap of 5.07 eV; alkoxythiophene, whose band gap is lower at 4.3 eV, has a HOMO too close to the vacuum level; and alkoxythiozoles which have a similar HOMO-LUMO gap at 4.2 eV and a lower energy HOMO.

3.1: Past Research

Although underexplored our examination of head-to-head linked 4,4-dialkoxybithiazoles was not the first. This motif was initially investigated by Täuscher et al. in 2011 where it was

viewed as a small molecule.[68] These molecules were synthesised through a Hantzsch synthesis creating a 4,4'-bihydroxythiazole which was then alkylated with ethyl iodide.

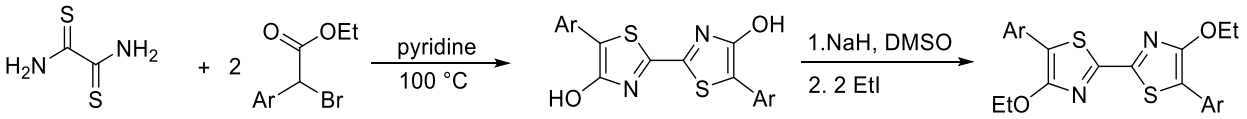

Scheme 11 Synthesis of 4,4-Alkoxythiazoles: through a Hantzsch synthesis followed by an alkylation

It was shown that the bithiazoles produced had not only a high level of fluorescence but also, upon inspection of the crystallized small molecule, a surprising level of planarity. Both the torsion angle of the thiazole units (0.2°) and the thiazole and phenol rings (6.08°) were much lower than expected when compared to that of the thiazoles when a methyl was substituted for the alkoxy functional group (32.6°).[68] This discovery led to further research of this subunit in the following years.

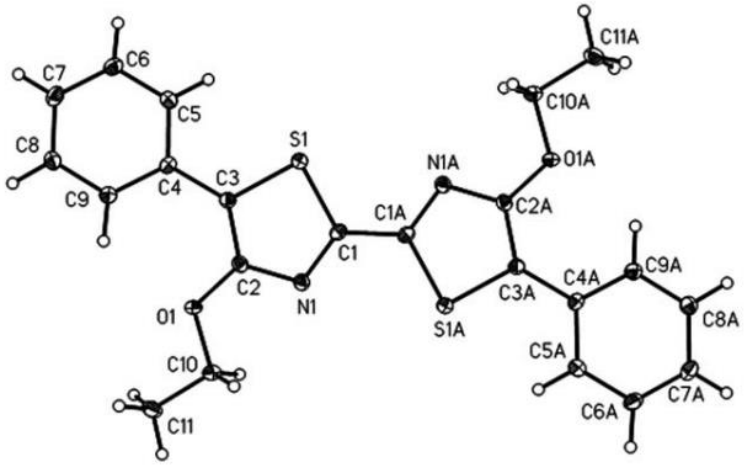

Figure 33 Crystal Structure of Alkoxybithiazole: Compound synthesized by Täuscher et al. to show the angles between the thiazole units and the thiazole and phenol rings.[68]

The next examples of studies of bithiazoles were performed by Guo *et al.* in 2013.[69] This was one of the first major investigations into using these functionalized bithiazoles as polymers after seeing their unique properties. This group pursued a tail-to-tail linkage of the bithiazole attempting to replicate the chalcogen bonding that was seen in other polymers such as PEDOT. Although differing from Täucher *et al.* the concept that was being sought after remained the same: create a bithiazole whose side chains would vary the energy level of the compound by keeping it planar through intramolecular forces. DFT calculations were performed on thiophene dimers with various side chains and compared to the thiazole dimer with the alkoxy side chain. This displayed the large difference between the two compounds: not only is the thiazole dimer further below the vacuum level even with the presence of an electron donating side chain but it also shrinks the band gap between the HOMO and LUMO (Fig. 34**)**

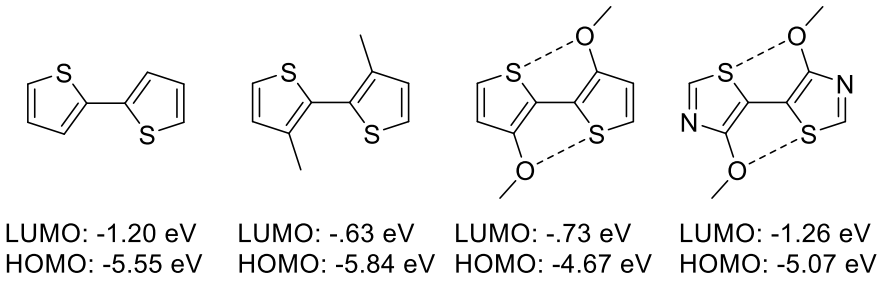

Figure 34 Bithiazole/Bithiophene DFT Calculations: Performed by Guo et al. that display the band gap difference seen between thiophenes with no substituents in the 4 and 4' positions and those with alkyl side chains and alkoxy side chains due to the difference in planarity. Also displayed was tail-tail linked thiozoles with alkoxy side chains in 4 and 4' positions.[69]

A large barrier for this particular work was the number of steps taken to reach the desired monomer. Due to the desired polymerization method being Stille coupling as well as the tail-to-tail coupling, eight steps were required to reach the monomer for polymerization. This makes the synthesis process unnecessarily long while losing starting material along the way converting under 10% of the starting material to usable monomer (Scheme 12)

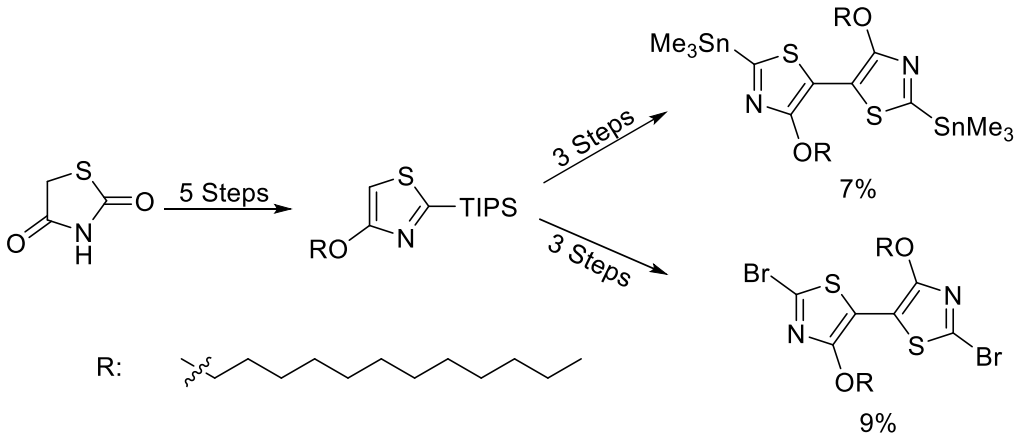

Scheme 12 Guo et al. *Starting Material Synthesis: Starting material synthesis for the polymerization performed by Guo et al. yielding 7% for the organo tin and 9% for the dibromo-thiazole*[69]

Following this example, Wei *et al.* investigated poly(4-hexyloxythiazole) as a low band gap polymer.[70] Their goal was to create a polymer similar in structure to one that is commonly used in organic electronics, and was discussed in the previous chapter, poly(3-hexylthiophene). It was found that the polymer could be easily synthesised from 4-bromothiazole which was converted into the hydroxythiazole through an Ullmann reaction. This was then prepared for polymerization through bromination using NBS. The monomer was then homopolymerized through a Stille coupling using hexamethylditin and palladium tetrakis.[70] This polymer allowed for a more direct comparison to an existing polymer that is in use.

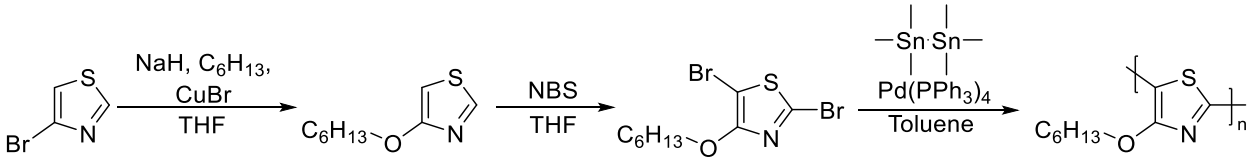

Scheme 13 Synthesis of Poly(4-hexyloxythiazole): Polymer synthesis performed by Wei et al. *through Stille cross coupling*

Once again, the band gap of these polymers was compared and it was found that the poly(4-hexylthiazole) had a smaller band gap than poly(3-hexylthiophene) allowing longer wavelengths of light to enable the transport of electrons/holes. The thiazole polymers were also

found to have lower energy when compared to the vacuum level as determined by cyclic voltammetry. This also lent credence to the idea that using hexylthiazoles as a substrate would lead to polymers that would be less readily oxidized by environmental oxidants.

3.2: Proposal

The goal of this project was to create a facile synthesis of polymer with 4,4-dialkoxybithiazole and an aryl spacer. Ideally this synthesis should be applicable to any di-bromo aryl spacer and create a conductive polymer. If successful it would allow for the creation of a wide variety of polymers with differing electrical properties while also allowing for the mass production of the monomer required to create the desired product. The other benefit of creating this synthesis was that, as previously stated, if these polymers were created on a large scale, there is no toxic or difficult waste to dispose of as the by-product of direct arylation is not a metal halide as it is with many other cross coupling reactions.

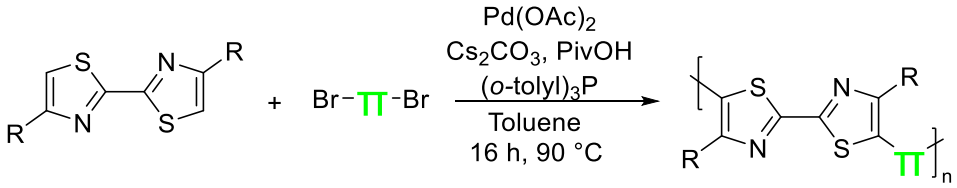

Scheme 14 Proposed General DArP: Proposed general synthesis of 4,4' substituted bithiazole polymer where a bithiazole is combined with a dibromo aryl spacer through direct arylation

3.3: Discussion

In order to determine if our targeted monomers were a viable substrate for DArP a computational study was performed to model the CMD transition state. To achieve this, a disruption-interaction analysis of 4-methoxythiazole was performed. This was done through the creation of DFT optimized structures for the ground state of both the palladium, 4-methoxythiazole, the CMD, and the final complex. Combining all of these simulations, the Gibbs

free energy was calculated for the most important aspects of the reaction. Namely the energy of the transition state as well as the two energies contributing to it discussed in Chapter 1: the energy of interaction of the 4-methoxythiazole (E_{int}) and the energy of distortion of the aryl hydrogen bond (E_{dist}(ArH)). These energies were compared to those of unsubstituted thiophenes that are known to react at the 5 position through DArP to determine the viability of the chosen substrate.

When compared to an unsubstituted thiazole, the E_{dist}(ArH) of the methoxythiazole was nearly identical. Conversely the E_{int} was calculated to be 1.7 kcal/mol larger for the methoxythiazole. This is as predicted as the E_{int} is tied to the nucleophilicity of the substrate. Therefore, when comparing the nucleophilicity of the 5 positions, a compound with an electron donating atom attached to the 4 position should be more nucleophilic. The result of this calculation indicates that the energy required to access the CMD transition state for the methoxythiazole is lower thereby increasing the reactivity.

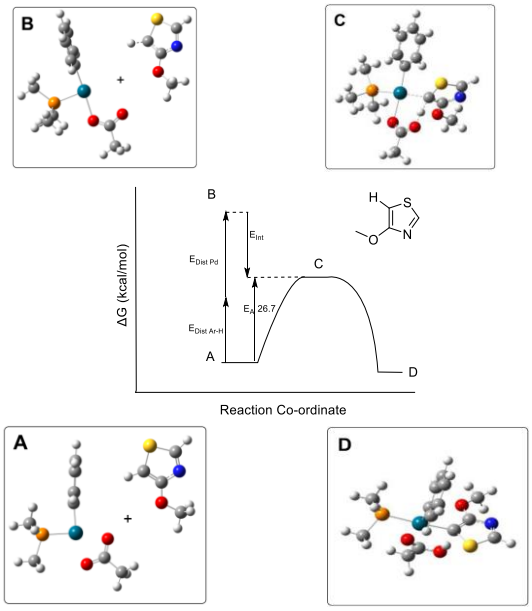

Figure 35 CMD DFT Calculations: DFT calculations performed by Dr. Sinclair concerning the CMD step between 4-methoxythiazole

3.4 Synthesis

The first goal of this project was to develop a concise synthesis of the 4,4'-dialkoxybithiazole monomer. The importance of this step is to guarantee access to the monomer for large scale production. This is due to the fact that the monomer is not commercially available and existing synthesis requires many steps with low final yield.

Beginning with a retrosynthesis our targeted bithiazole is able to be joined through the usage of an oxidative homocoupling using $Cu(OAc)_2$ with oxygen as a terminal oxidant as has been previously reported.[71] The 4-alkoxythiazole could be created through the usage of an Ullmann type coupling of a 4-halothiazole with nearly any alcohol.

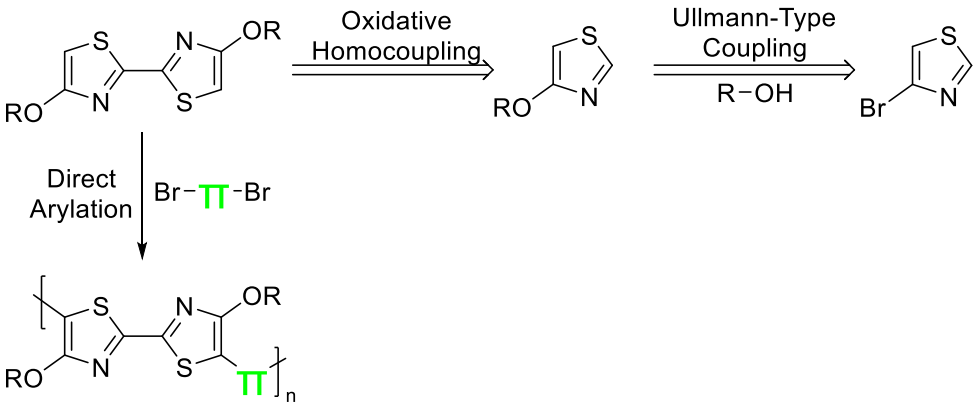

Scheme 15 Retrosynthesis of Bithiazole Monomer: Thiazoles are coupled through oxidative homocoupling that had the alkoxy side chain added through an Ullman-type coupling.

Our targeted synthesis began with a 2,4-dibromothiazole. This is due to the fact that, although commercially available, 4-bromothiazole is significantly much more expensive than 2,4-dibromothiazole *($23 USD/g via Oakwood Chemical versus $30 USD/25g via Oakwood Chemical*). The unnecessary bromine at the 2-position was removed through the use of lithium halogen exchange through the introduction of *n*-BuLi at -78 °C. This exchange will occur more favourably at the 2-position leading to the desired product after quenching with methanol. The

produced bromothiazole was retrieved in 99% yield and was then coupled with an alcohol through an Ullmann coupling. This is accomplished using NaH to first deprotonate the alcohol at room temperature over an hour forming the alkoxide. CuI and 4-bromothiazole are then introduced and the mixture is refluxed in a sealed tube forming the final product (Scheme 16**).** The product was then purified through column chromatography and retrieved in 60% yield. This is the first area of potential differentiation between the polymers as the alkoxy group alkyl chain can be varied based on the alcohol used in the Ullmann type coupling.

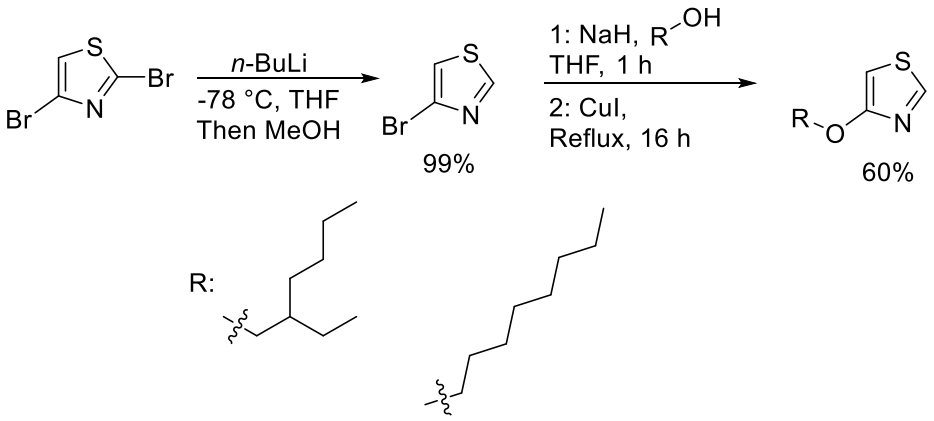

Scheme 16 Synthesis of Substituted Thiazole Monomer: Beginning with 2,4 dibromothiazole the bromine on the 2 position was removed through lithium-halogen exchange followed by an Ullmann-type coupling to add the alkoxy side chain.

Following the synthesis of the alkoxy thiazole, two units were coupled through an oxidative coupling. This coupling uses copper (II) acetate with oxygen as a terminal oxidant. All reactants are combined in xylenes and refluxed at 140 °C for 48 hours. This creates the final monomer 4,4-dialkoxybithiazole which is then purified through column chromatography and retrieved in 96% yield.

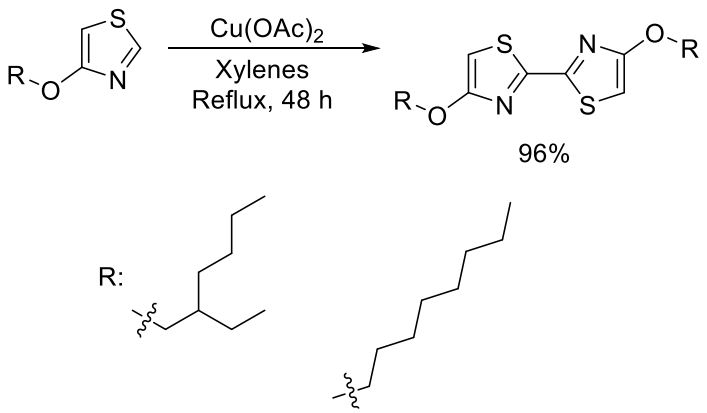

Scheme 17 Synthesis of 4,4' -Alkoxybithiazole: Synthesis of 4,4' -alkoxybithiazole through oxidative homocoupling with $Cu(OAc)_2$ in xylenes at reflux.

The synthesis of these polymers was performed through the use of direct arylation. The method was developed from that of Kambara *et al*. with a variety of modifications being tested to determine if the efficiency of the reaction could be increased with the differing substrates. Through this testing, octyl chains were determined to be ideal for not only the synthesis of the polymer but also its purification. When chains significantly shorter than octyl chains were used, the resulting polymer would either precipitate out of solution before it had reached an appropriate size or the monomer would prove too volatile, evaporating during its recovery.

A Hantzsch synthesis was also attempted to reduce the amount of steps and increase the overall yield of the monomer. The attempts at this synthesis were based on previous work by Täucher *et al*. in which the target bithiazole was similar with the primary difference being the phenols in the 5 and 5' positions. This was attempted through the mixing of dithiooxamine and ethyl bromoacetate in pyridine at 110 °C for 1 hour. To the resulting mixture, ethanol was added and it was cooled to room temperature over 30 minutes. This reaction only produced alkylated pyridines instead of the targeted dimer. The reaction was attempted with a variety of other conditions but the desired product was not obtained.

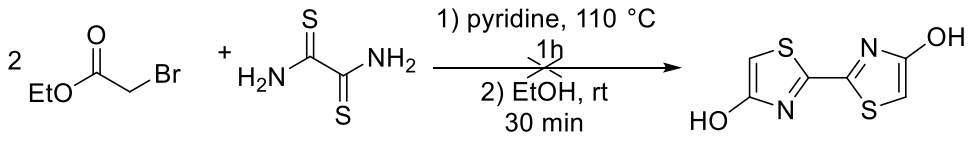

Scheme 18 Attempted 4,4'-Hydroxybithiazole Synthesis: Attempted Hantzsch synthesis of 4,4'-hydroxybithiazole

The other polymer that was synthesised for these experiments was a proof of concept. This was not only to expand the scope of polymers that could be synthesised through this method but also to practically display what was calculated through DFT by Dr. Sinclair. Namely the fact that, although an alkyl side chain in the 4 and 4' positions would allow for a greater level of solubility, they would disrupt the planar structure of the polymer thereby increasing its bandgap.

The route to the starting material is different for the alkyl monomer due to the fact that, when not requiring a halogen at the 4 position, a Hantzch synthesis can be used. Therefore, the first step was similar to that employed by Täucher *et al*. In this case, a thiazole dimer with nonyl chains at the 4 and 4' positions was produced in 87% yield through the combination of bromoundecanone and dithiooxamide in ethanol at reflux.

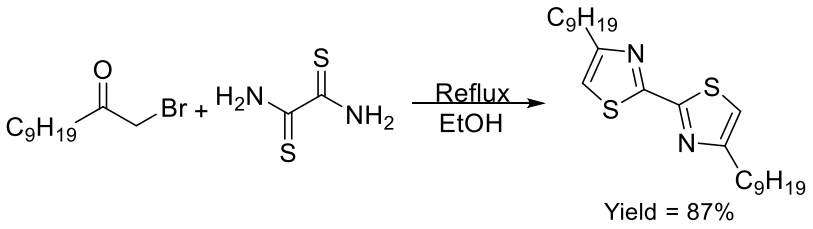

Scheme 19 Hantzsch synthesis of 4,4'-Alkylbithiazole: Hantzsch synthesis of 4,4'-nonylbithiazole

The two types of monomers were then combined through DArP with an aryl spacer. This is accomplished through the introduction of the dry reagents to a flame dried vial. The bithiazole monomer is produced as a viscous oil and was therefore diluted in toluene before its addition. The reaction was then allowed to proceed for 12 hours at 90 °C before being removed from the heat. The mixture was then sonicated to attempt to solubilize as much polymer as possible. The

polymer was then precipitated through introduction to cold methanol and purified through vacuum filtration.

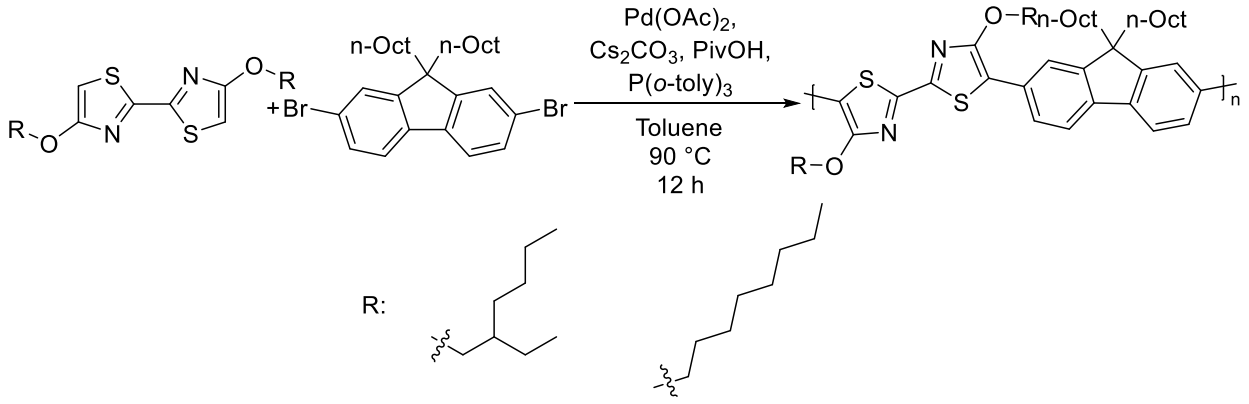

Scheme 20 Polymerization of Bithiazoles: DArP was used to polymerize the syntehsized bithiazoles and an aryl spacer (in this case 2,7-dibromo-9,9-dinonylfluorene).

3.5: Polymer Analysis

The synthesis of these polymers was the first step in the exploration of replacing thiophenes with thiazoles in conducting polymers and determining their properties. The properties of the polymer were determined using some of the same methods explained in Chapter 1. Following our success synthesising these polymers, the scope of the reaction was explored to determine if the synthesis was applicable to a wide variety of aryl spacers.

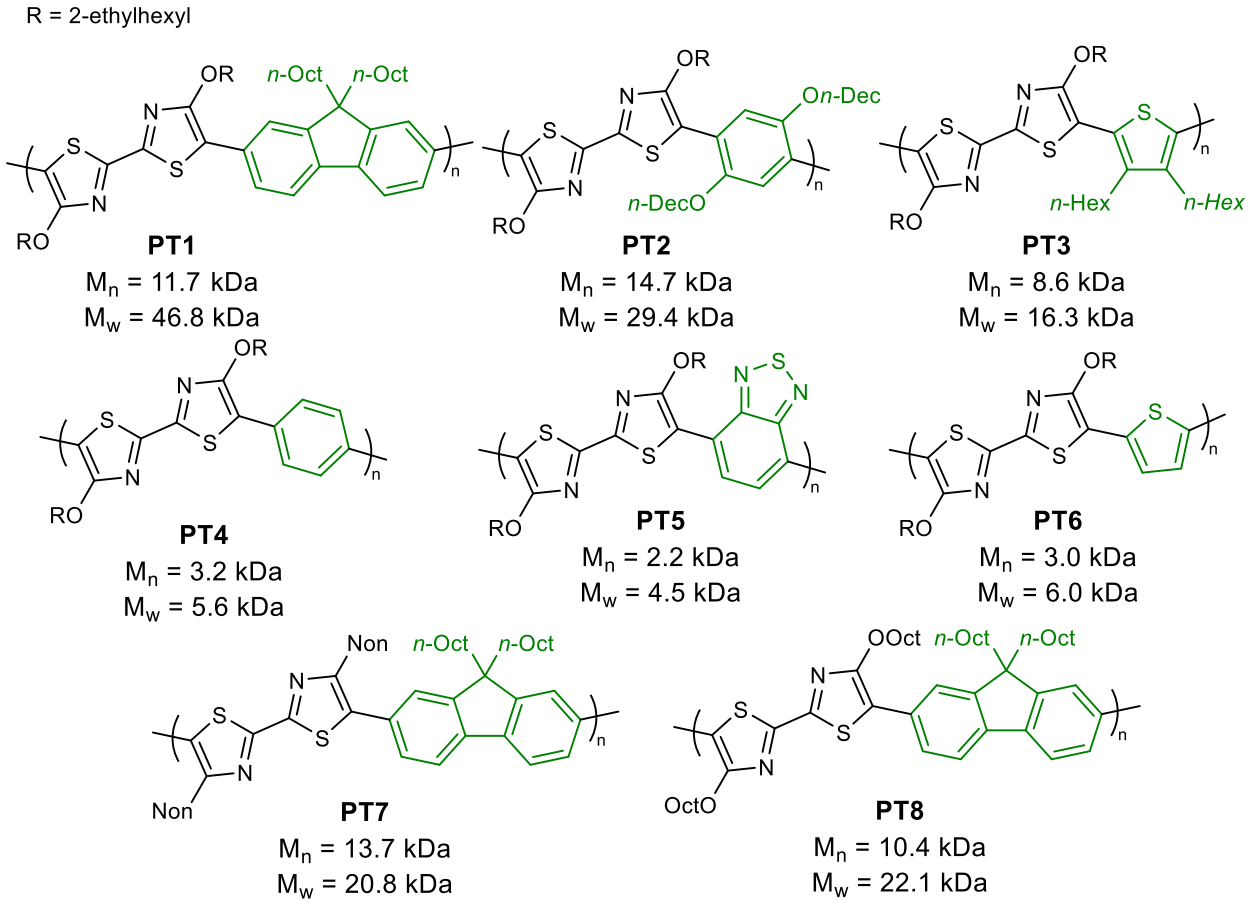

Figure 36 Polymerization Scope: Summary of the polymers investigated using the method shown in Scheme 20

After the synthesis of a variety of polymers using the method shown in Fig. 36, UV-visible spectra were taken of the different polymers to determine if there were significant differences caused by the varying length of the alkoxy side chains as well as the effect of the aryl spacers used to separate the 4,4-dialkoxybithiazole monomers. As is made evident through this figure, there is a significant amount of variation, not only in the onset of the shift but also in the wavelength of maximum absorbance. This indicates that the method used is not only effective in the synthesis of a variety of polymers but that these polymers have a large variety of optical and electronic properties.

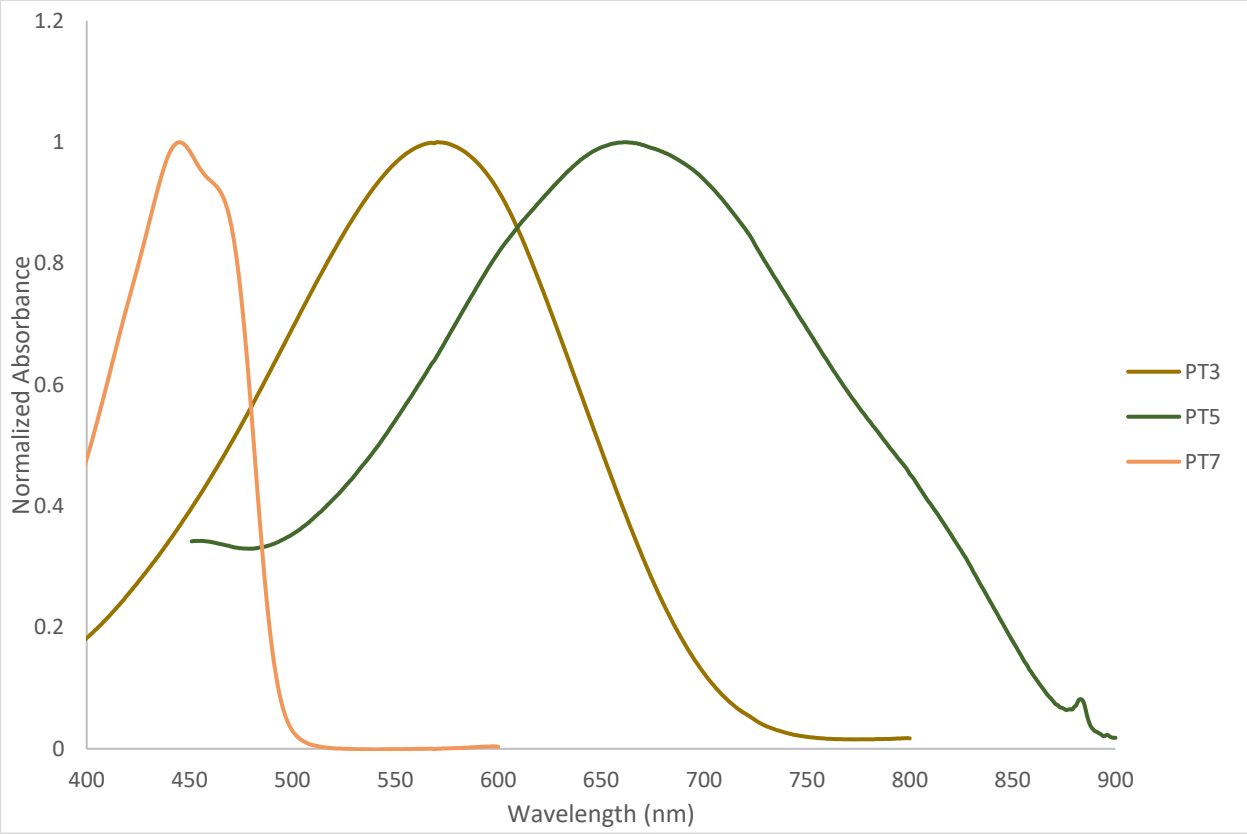

Figure 37 UV-Vis Polymer Comparison: Comparison of the polymers shown in Fig 38. Polymers were measured while solubilized in THF.

The UV-vis spectra are a clear visual indication for the amount of variation seen. The onset of the shift varying over 300 nm while the wavelength of maximum absorbance varied up to 200 nm. This indicates that through the variation of one substrate within the synthesis of the polymer, there is a massive potential for variation of electronic properties.

Following the UV-visible spectra, cyclic voltammetry was then used to further explore the electronic properties of the polymers. These tests were performed to both confirm the results of the UV-visible experiments and determine the position of the polymers in relation to the vacuum level.

As was shown in (Fig. 37), the amount of variation in the energy levels of reduction vary greatly based on the aryl spacer used. While in complement to the UV-vis spectra, cyclic voltammetry allows the HOMO-LUMO to be confirmed, while giving a clearer picture of where the HOMO and LUMO are located.

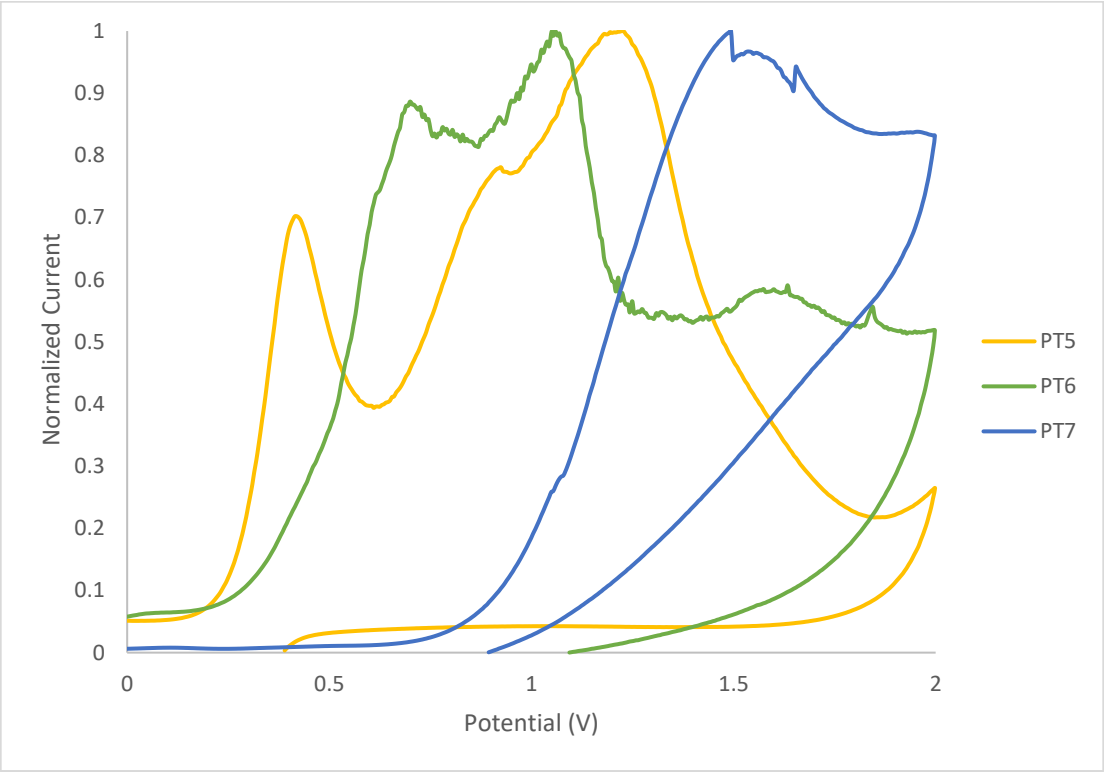

Figure 38 CV Comparison: Polymers shown in Fig 36 compared through CV. Only the forward sweep is shown for clarity

Polymer	Eg (Opt)	Eg (CV)	Abs Max (nm)	HOMO (eV)	LUMO (eV)
PT1	2.11	2.17	553	-6.33	-4.16
PT2	1.90	2.2	592	-6.75	-4.55
PT3	1.77		571		
PT4	1.85	2.11	551	-6.52	-4.41
PT5	1.43	1.58	675	-6.28	-4.70
PT6	1.62	1.7	606	-6.15	-4.45
PT7	2.7	2.61	506	-6.56	-4.05
PT8	2.1	2.13	549	-6.40	-4.27

Table 3 Polymer Properties: Compiled data of the polymers shown in Fig 36 including the band gap (Eg) measured both through UV-vis and CV as well as the wavelength of max absorbance and the LUMO and HOMO locations determined through comparison to an internal ferrocene standard.

While analyzing both of these data sets, there were a few points of interest. Firstly, the band gap of PT7, the polymer with the alkyl side chain has the largest band gap of any polymers synthesised (Table 3). This is once again due to the fact that, although necessary for solubility reasons, the alkyl chain breaks the planarity of the molecule thereby affecting its conductivity. It was also observed that the aryl spacer heavily impacted where the HOMO was located. For instance, PT5, having benzothiadiazole as its spacer, had a significantly higher max absorbance than any other polymer. This is positive as it further emphasises the ability to create a variety of electronic properties in materials through the changing of one reactant.

3.6: Conclusions

In conclusion, alkoxythiazoles are a relatively underexplored area in the realm of conjugated polymers. They address some of the issues seen in polythiophenes such as large band gap, low solubility, and air stability. Based on these factors a general synthesis was investigated.

We have outlined a method by which 4,4'-alkoxybithiazoles can be synthesised and polymerized using a wide variety of aryl spacers. The synthesis that was developed is high yielding and consists of a low number of steps when compared to other currently existing syntheses. It also allows for the use of DArP thereby reducing the amount of toxic waste produced when compared to both Stille and Suzuki couplings.

Through changing the aryl spacer used in the polymerization, the band gap can be heavily influenced allowing for a wide variety of electronic properties to be achieved. Due to the fact that the only required change to the synthesis is the aryl spacer, this indicates that the synthesis is potentially widely applicable.

Chapter 4: Polymer Wrapping

4.1: Carbon Nanotubes

Carbon nanotubes are an emerging material gaining traction in the field of materials science. This is largely due to the wide range of functions that they can serve. Ranging from healthcare applications, such as drug delivery, to those in the field of electronics such as transistors, CNTs have proven to be a useful material.[72,73] This variety of applications has much to do with the range of properties that the CNTs can take on based on their: chirality, number of walls, length, and diameter. [72]

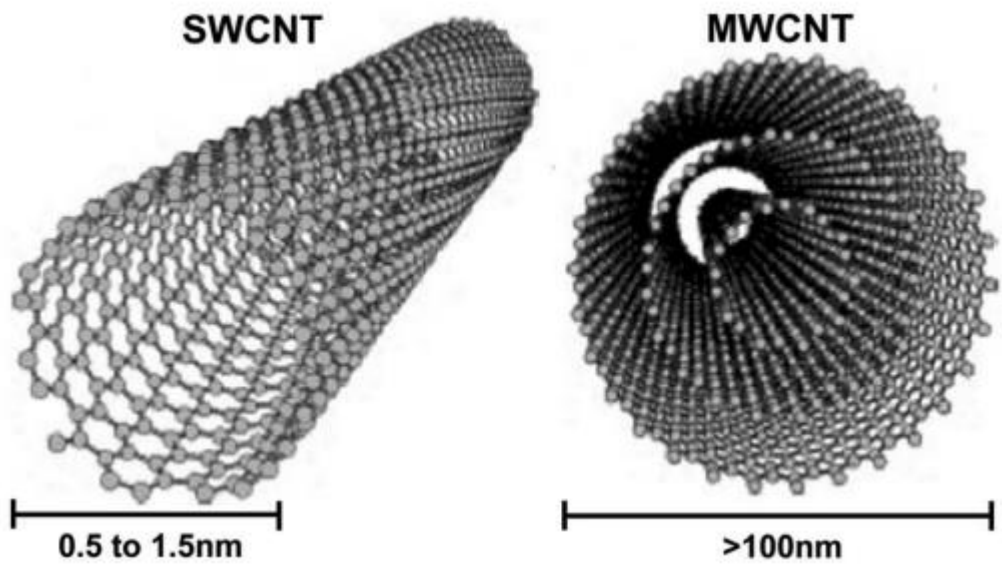

Figure 39 Carbon Nanotube Visualization: Depiction of Carbon nanotubes showing a single walled carbon nanotube on the left and a multi walled carbon nanotube on the right[74]

Many applications for carbon nanotubes use primarily SWNTs. Within the category of SWNTs, there is further division between metallic and semiconducting SWNTs. What differentiates metallic carbon nanotubes from those that are semiconducting is their band gap or, in the case of metallic nanotubes, the lack thereof. The electronic properties of these tubes follow

the rules outlined in Chapter 1 regarding organic materials. The distinction between the two is based on the diameter and chirality of the tubes (Fig 40). When there is no band gap, electrons can freely move through a substance as the amount of energy required to excite an electron from the valence band, or LUMO, to the conduction band, or HOMO is very small.[75] While this can be useful for some applications, for most electronic applications the semiconducting materials are desired as the flow of electrons through a material can be controlled by the amount of energy entering the material.

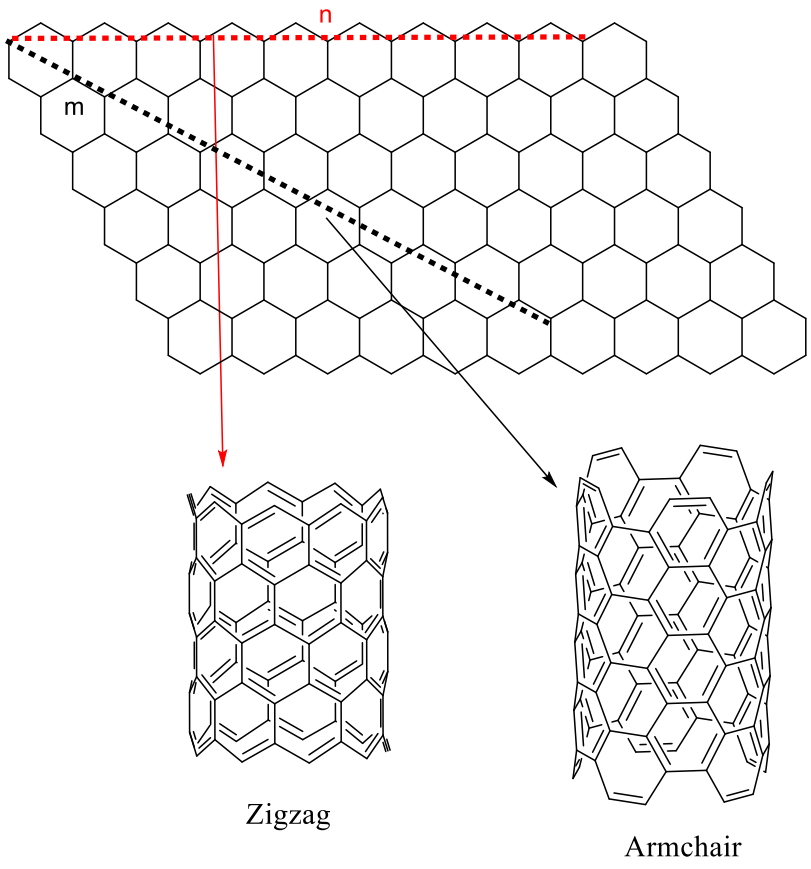

Figure 40 SWNT Chirality Visualization: Depiction of differing chiralities with zigzag tubes having one of the directional vectors equal to 0. Armchair nanotubes have the directional vectors that are equal to each other.

Chiralities of CNTs play a large role in how they react to electric currents. Based on the chirality, the band gap of the CNT changes. CNTs can have a range of chiralities affecting not only their diameters but also their properties. Different chiralities are generally separated into three categories based on the appearance of the carbon-carbon bonds as well as the attributes they imbue. They are termed: armchair, zig-zag, and chiral. Armchair nanotubes are the CNTs whose vector (n,m) and n=m.[76,77] When n is equal to m, the band gap of the materials is zero.[76,77] When n - m = 3i where i does not equal zero, the nanotubes have a low band gap.[76,77] Both of these cases mean that the CNTs are considered metallic. When the vectors n - m = 3i ±1 the tube is considered semi-conducting.[76,77] Zig-zag nanotubes are defined by either the m or the n vector being equal to zero. Zig-zag nanotubes produce a mix of semiconducting and metallic nanotubes where starting at (0,0) every 3n tubes will be semiconducting while the others are metallic.[76] This means that 2/3 of zigzag nanotubes are semiconducting while 1/3 are metallic.

The usage of semiconducting single walled carbon nanotubes (SWNTs) in electronic applications has to do with how electrons are transported through the systems. Due to the extensive π network, CNTs can make use of a phenomenon termed ballistic electron transport. This type of electron transport allows the movement of electrons through the materials without significant scattering.[78] This is particularly relevant in transistors where, as the demand for smaller electronics grows, the amount of transistors that must be packed into a material increases. Carbon nanotubes are particularly important for this due to the increased efficiency of the electron movement and reducing the scattering has the potential to increase the density of transistors in a circuit. The other effect of this is increased demand on the amount of transistors being produced which in turn increases the demand for silicon. Therefore, due to the limited availability of silicon, there is an increased demand for more easily accessible alternatives.

The nanotubes themselves can be synthesised in a variety of ways. The most common way is chemical vapour deposition (CVD).[79] This method uses heat to create hydrocarbon vapours which are passed through a reactor using a carrier gas. This reactor contains a metal catalyst which is adhered onto a substrate or support system.[79] The chamber containing the catalyst is kept at a high enough temperature to decompose the hydrocarbons, generally ranging from 100-600°C. The CNTs will then deposit on the catalyst allowing for collection. CVD is currently the most popular method for manufacturing CNTs as the materials required are relatively cheap and the number of walls contained within the tubes can be controlled based on the catalyst.[79]

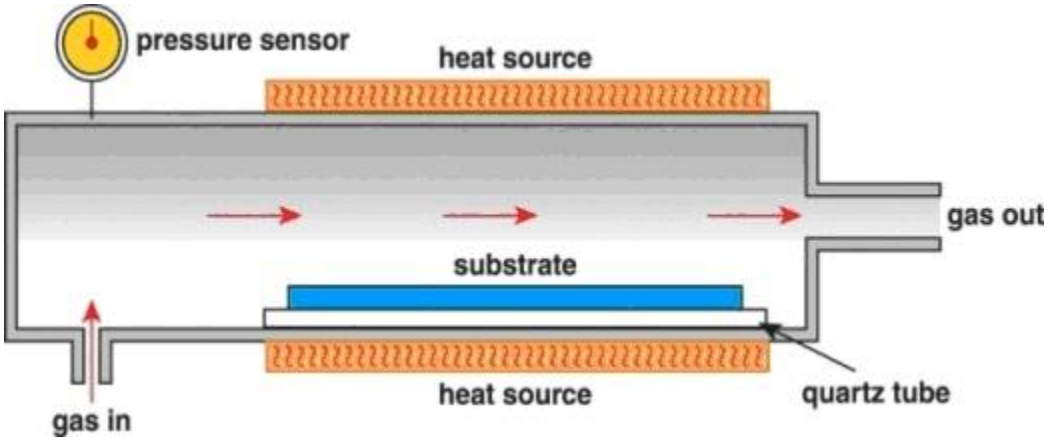

Figure 41 Carbon Nanotube Synthesis: Chemical vapor deposition instrument sublimated carbon is mixed with a carrier gas and passed through the pressurized device. The carbon is then deposed on the substrate

The primary problem found with this method of synthesis, as it is with many others including arc-discharge, laser ablation, and induction by thermal plasma, is that the different chiralites and types of CNTs are produced with little control over exactly what is produced. This is largely due to the fact that the synthesis occurs at a high enough energy that a large mixture of chiralities are generated.[77] The end result of this drawback is that another process must be created to separate the target variety of CNTs.

4.2 Existing methods of Purification

Due to the fact that current methods of CNT synthesis cannot exclusively create a given type of nanotube, there is a demand for a facile method of separation. There are many ways in which nanotubes can be separated. Some of the more prevalent ways to separate carbon nanotubes include: dielectrophoresis, polymer wrapping, and DNA wrapping.

Dielectrophoresis functions through the use of the polarizability difference between metallic and semi-conducting nanotubes. The dielectric constant for semiconducting SWNTs being 5 ϵ whereas metallic SWNTs have a dielectric constant closer to 1000 ϵ leading them to separate under a non-uniform electric field. The primary problem with this method is that it lacks the ability to separate tubes based on their chirality, only separating them based on whether they are metallic or semi-conducting. The scale of this method is also very low which could potentially lead to problems with the scale up required for an industrial separation.

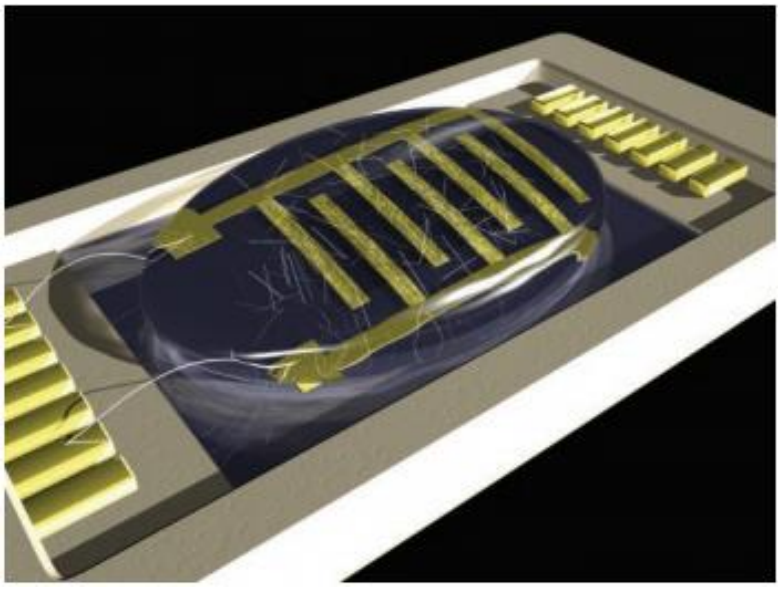

Figure 42 Dielectrophoresis Separation: CNTs are separated based on their dielectric constant.[80]

DNA wrapping is another method that has been explored for the separation of CNTs. This method works by taking advantage of the overall negative charge of the polyphosphate backbone. The negative charge allows for tubes that are wrapped by the DNA to be separated through the use of ion chromatography or GPC. The challenges for this method lie with the selectivity. Based on the sequence of the DNA that is used, the diameter or the type of nanotube can be selected but not both. This means that if this method where to be applied industrially, a minimum of two large scale columns would have to be used to select the desired diameter and type of tube. Another recurring issue is how the DNA can be removed from the CNTs after the separation requiring further processing.

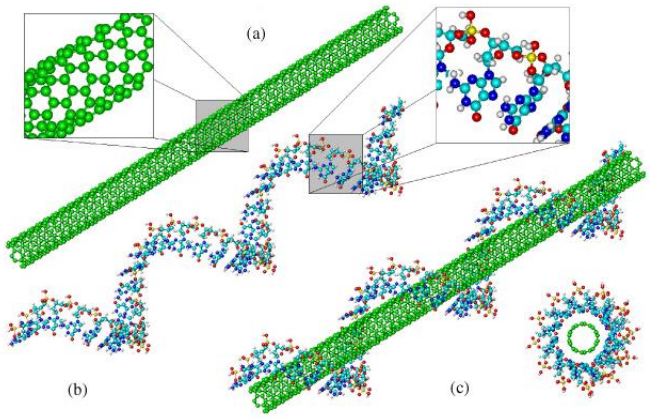

Figure 43 DNA wrapping: CNTs (a) and DNA (b) are mixed, and the DNA becomes associated with the CNT (c) which can then be separated via column chromatography[81]

Polymer wrapping is a technique that has been gaining popularity for selective separation of SWNTs as, based on the composition of the polymer, SWNTs can be separated based on both type and chirality. Aromatic polymers are the most common type used to separate SWNTs. This is due to the π-π stacking interactions between the tubes and the polymer that cause them to interact favourably. This allows the SWNTs, that are insoluble in most common solvents, to be solubilized through their interaction with the polymers. The SWNTs in this process are separated

by the favourability of their interactions with the polymer as only specific types and chiralities of SWNTs will be suspended. Polymer wrapping is particularly appealing as, with the exception of sonication and centrifugation, no specialized equipment is required to separate the nanotubes. When compared to other methods that require equipment such as specialized columns, HPLCs or electrodes, this technique is not only easy and cheap to utilize but could also be easily scaled up based on the demand. The primary drawback of this technique has been the difficulty of completely removing the polymer from the nanotubes after they are separated. As the materials do not interact through covalent or ionic bonding, their interaction is difficult to disrupt. This leads to the suspended nanotubes often being coated with the polymer used to separate them. Once the nanotubes are isolated through the evaporation of the solvent they are suspended and they remain coated with the polymer significantly affecting their properties. This severely limits the potential applications for the SWNTs that are separated by these techniques. Not only can the polymer used affect the properties of the SWNTs potentially lowering their efficiency, but they also cannot be aligned which can damage the potential effectiveness for electrical applications.

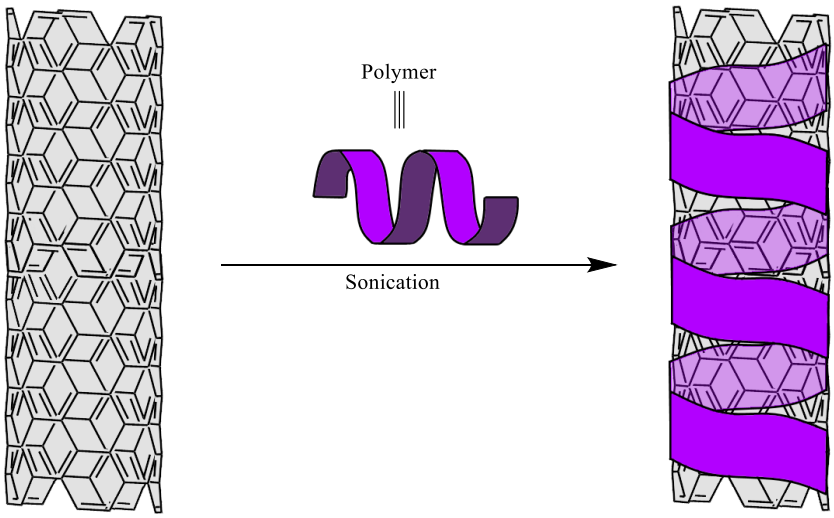

Figure 44 Polymer wrapping: Polymer and CNTs are suspended in solution through sonication. The polymer will associate with the CNTs generally through π-π stacking.

Some polymers have been created that can be removed from the SWNTs. These polymers are divided into two categories: degradable polymers and those who undergo conformation change. Degradable polymers range drastically in their structure as different monomers interact favourably with varying types of SWNTs and the backbone of each polymer is modified to be labile to a given stimulus. Fluorene is one of the most commonly used monomers for the backbone due to its versatility and stability. The range of degradation techniques for the polymers is somewhat narrower being limited to primarily acidic conditions with some success being seen with photocleavable groups.[72]

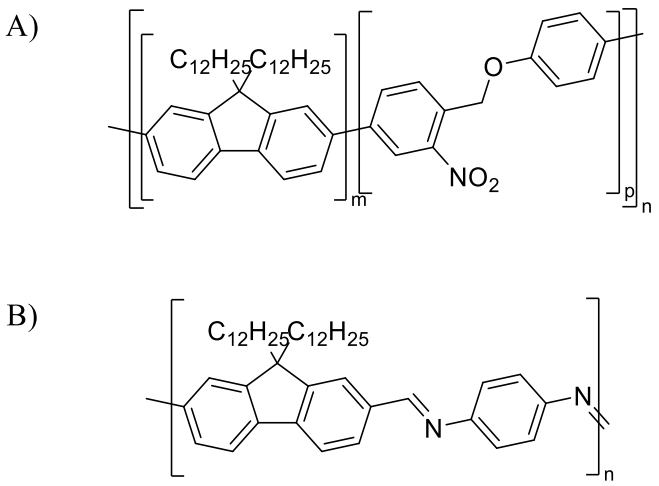

Figure 45 Polymer Wrapping Candidates: Polymers with aromatic backbone required for CNT separation. A) can be degraded through UV light while B) is degraded through the introduction of acid.[72,82]

Acid degradable polymers are further divided based on the reversibility of their degradation. Some polymers are created using traditional polymerization methods, namely condensation or radical polymerisation. This introduces acid labile groups that can easily be removed through the use of catalytic amounts of TFA.[72] The other category of acid catalysed depolymerization is polymers that are created with re-polymerisation in mind. For these polymers the primary goal is to make the monomers retrievable through non-covalent polymerization methods. This is achieved through the use of hydrogen bonding to or metal

chelation to coordinate the monomers creating high molecular weight complexes of up to 2.6 kDa.[83,84] After the addition of catalytic acid, the monomers will then dissociate and remain in solution while the SWNTs will precipitate. Each can then be collected, and the monomers can then be re-polymerized after purification through column chromatography lowering the overall cost of the procedure.[72] The main drawback of this method is the introduction of an additional purification step in column chromatography to retrieve the monomer. [83]

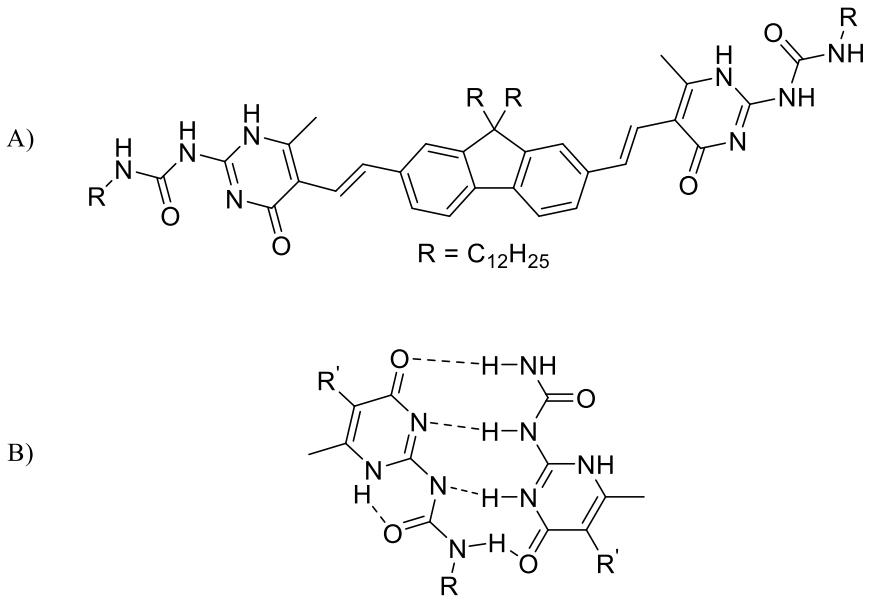

Figure 46 Small Molecule Separation: Small molecule developed to separate CNTs A) that associate through hydrogen bonding B). Can be dissociated and retrieved through the introduction of acid.

The other category of polymers used to reversibly separate carbon nanotubes are those that change conformation upon being introduced to one of a few potential compounds**.** For a polymer to solubilize a SWNT it must be able to wrap around its surface therefore, once the backbone of the polymer is rigidified or its conformation is changed preventing this, the separated nanotubes can be retrieved.[85] This method has been primarily used by varying a multitude of different conditions: solvent, pH, or metal and oxidant levels.[85] Upon introduction

of different factors the polymer cannot wrap the SWNTs and they precipitate from the solution. Using solvent plays on the polarity of the polymer backbone. A hydrophobic solvent, such as chloroform is used to allow free movement of the backbone of the polymer followed by the introduction of a more polar solvent such as acetonitrile. This causes the polymer to fold in upon itself exposing its more polar side chains and rendering it unable to wrap the SWNTs. The other conditions play primarily on changing the rigidity of the backbone.[86] Upon oxidation or protonation, the polymer becomes charged and linear thereby preventing wrapping. When using metals, the goal is to have motifs that will readily associate with ions. Upon introduction of the metals, the polymer will then be chelated changing the polymer conformation and releasing the wrapped SWNTs.[72] The primary drawback of these techniques is the difficulty in completely removing the polymer. Often times some polymer will remain associated to the SWNT even after precipitation changing its characteristics and rendering it significantly less useful due to the low conductivity of the polymers when compared to the SWNTs.[72]

4.3: Objective

Our objective in this project is to synthesise a degradable polymer that will allow for the wrapping of SWNTs, allowing the dispersal and separation of target chiralities. The synthesis involves using direct arylation to polymerise the monomers allowing for higher average molecular weights as well as minimal toxic by-products. Breakdown of the polymer will be performed via oxidation allowing for robust solvent and separation conditions. Various oxidants and solvents will be tested to attempt to achieve high concentrations of nanotubes in solution while remaining selective for targeted chiralities.

These polymers include those with both fluorene and dithiazole monomers to facilitate breakdown as well as selective wrapping. The testing of these polymers will involve wrapping

and breakdown. The goal is to identify polymers that will not only wrap SWNTs the most effectively and selectively but also degrade quickly leaving naked SWNTs to precipitate out of solution.

4.4: Desired Polymer

Targeted polymers have included those with fluorene and dithiazole monomers. These are coupled through direct arylation to give conjugated aromatic polymers that will interact with SWNTs selectively. These polymers must be long and flexible enough to wrap the SWNTs solubilizing them while also degrading to a small enough size that the SWNTs can be retrieved without any polymer remaining attached.

The primary area of interest for the development of this polymer is modifying the side chains on the degradable backbone. Changing the sidechains could potentially vary the selectivity of the polymer for SWNTs as well as the solubility. As there are two modifiable positions on the polymer, there are a variety of sidechains that could be introduced. The benefits of introducing various side chains are two-fold. Firstly side chains are important on large polymers to increase their solubility. The solubility of the polymer can also be influenced through the usage of either a polar or non-polar side chain based on the target solvent. It has also been shown that varying the side chains on the fluorene monomer in polyfluorenes can change the chirality of the nanotube it favours interacting with.[84] It stands to reason that this could hold true for not only fluorene but its co-monomer as well.

4.5: Polymer Synthesis

Two polymer backbones have been synthesised for the isolation of carbon nanotubes. Although these polymers appear similar, the routes taken to synthesize them vary based on the

ease of obtaining the thiazole dimer required. These polymers were chosen due to the presence of the fluorene group which has shown a tendency to be selective for certain nanotube chiralities as well as their potential to degrade in the presence of oxidants.[84]

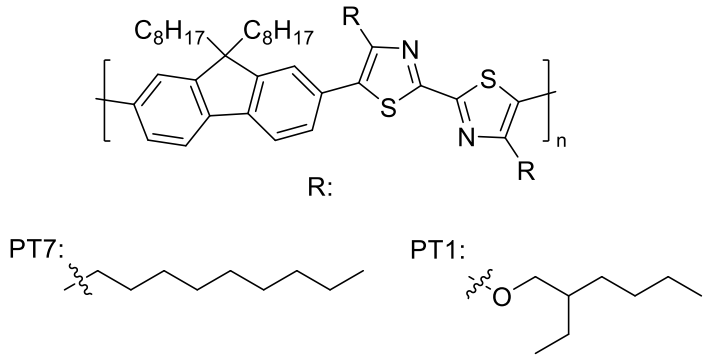

Figure 47 Target Polymer: Target polymers with potential variability at the R position

The polymer containing the alkyl chain attached to the thiazolyl dimer is obtainable in one step by combining dithiooxamide with bromo-2-undecanone at reflux. This yields one of the monomers at 87%. This monomer can be used for polymerization directly without having to produce the thiazoles individually followed by dimerization through oxidative coupling.

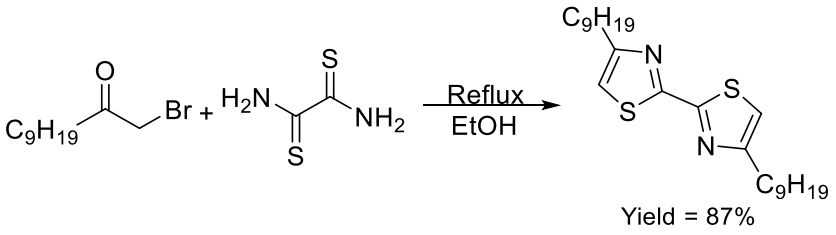

Scheme 21 Alkyl Monomer Synthesis: Production of an bithiazole with an alkyl chain at the 4 and 4' positions

The polymer containing an alkoxy group requires additional steps to retrieve the monomer for polymerization. The thiazole dimer is produced through first reacting 2,4-dibromothiazole with n-BuLi producing 4-bromothiazole though lithium halogen exchange followed by protonation with methanol. 4-Bromothiazole is then coupled with an alcohol, in this case 2-ethylhexanol, through an Ullmann coupling. The product is then homocoupled with an

oxidative coupling to retrieve the dimer. Due to both the Ullmann coupling and the oxidative polymerization having lower yields, the overall yield for the alkoxy thiazole dimer is significantly lower than that of the alkyl thiazole dimer.

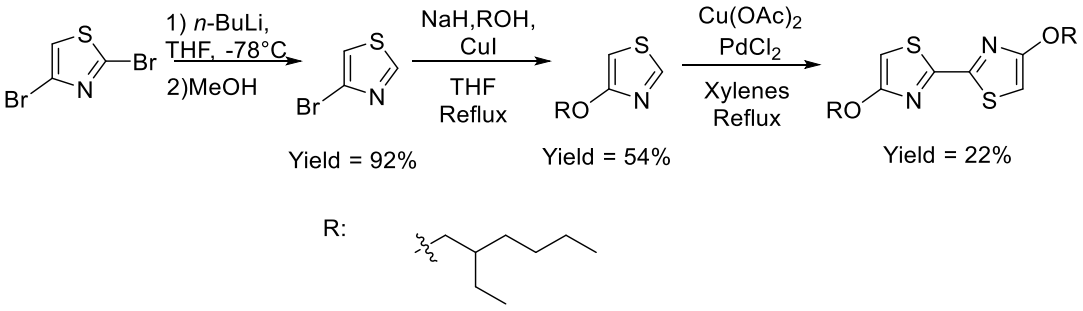

Scheme 22 Alkoxy Monomer Synthesis: production of bithiazole with an alkoxide in the 4 and 4' positions

The polymerization then proceeds through DArP with dibromo-fluorene to produce the final product. The flexibility of DArP allows for both types of monomers to be used without any further modification allowing for a higher overall yield of product. This also allows for an increased level of flexibility in the synthesis as the fluorene can react regardless of the side chain attached to the bithiazole.

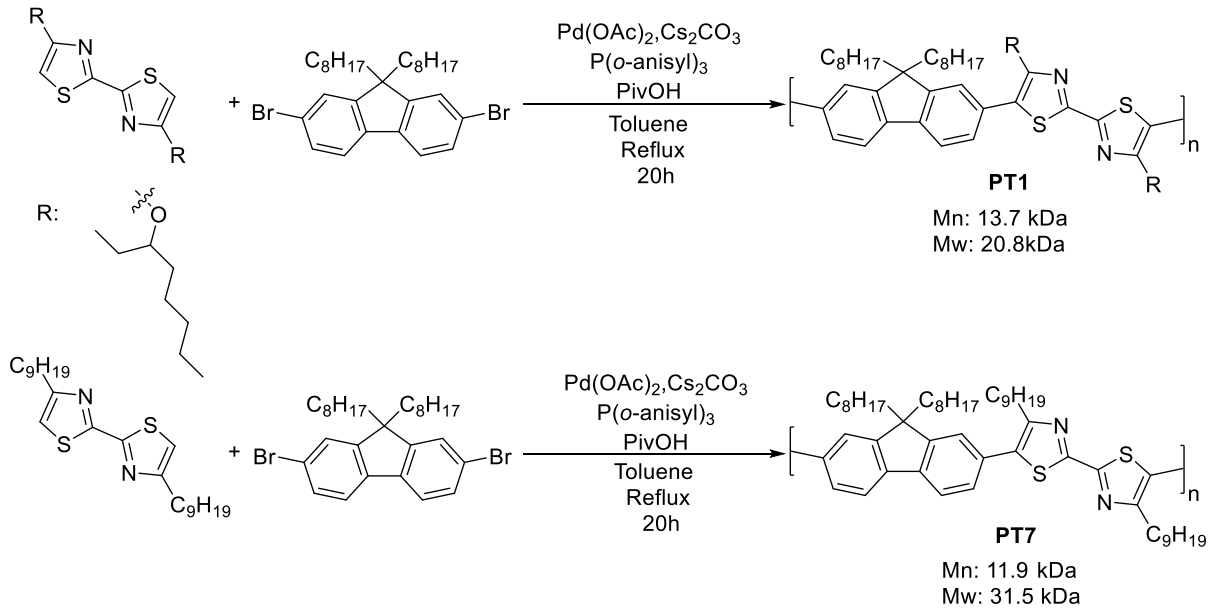

Scheme 23 CNT Polymer Wrapping Synthesis: Polymerization of both dithiazole monomers with dibromo-dioctyl fluorene using DArP

The polymerization resulted in PT1**,** produced from the bithiazole monomer with the alkoxy chains, having a M_n of 13.7 Da, a M_w of 20.8 kDa, and a PDI of 1.52. PT7 has a M_n of 11.9 kDa, M_w of 31.5 kDa and PDI of 2.65. Both polymers were large enough, when compared to past results, to be used to solubilize SWNTs.

4.6: Degradation

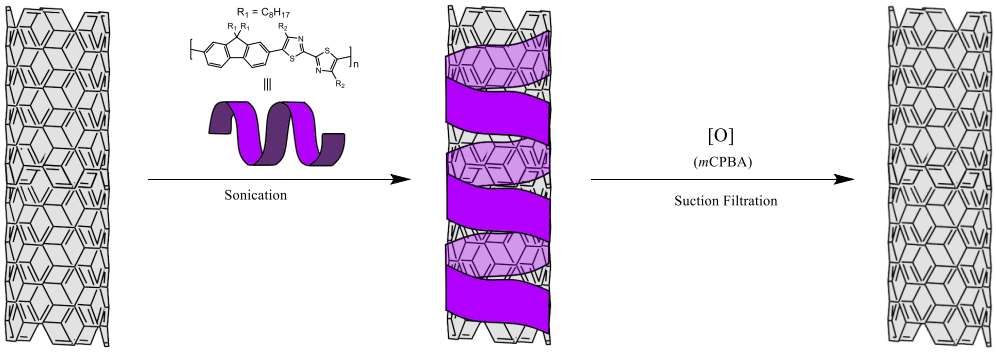

Figure 48 Proposed CNT Retrieval: Process for the retrieval of semi-conducting CNTs. The CNT mixture is first suspended with the polymer through sonication followed by the separation of the unsolubilized nanotubes through suction filtration and centrifugation. The polymer is then degraded through oxidation and the resulting nanotubes are once again suction filtered to retrieve the final product.

Breakdown of the polymer is induced through the introductions of an oxidant. Within a matter of hours the size of the polymer shrinks to below half. Although not fully characterised we are able to estimate how it degrades based on past work performed by Sinclair *et al.* (Scheme 24).[87] In this work the oxidation of thiazole-based heterocycles is seen to cause ring opening. This offers one potential route to degradation. Pictured is the predicted mechanism in which either a proton source or a Lewis-acid would allow for the opening of the thiazole ring followed by the oxidation of the sulfur. This reaction draws comparisons to our polymer as we observed degradation based on the equivalents of oxidant added, which in our case was *m*CPBA. This along with the similar heterocycle being used led us to believe that this mechanism was a potential route for polymer degradation.

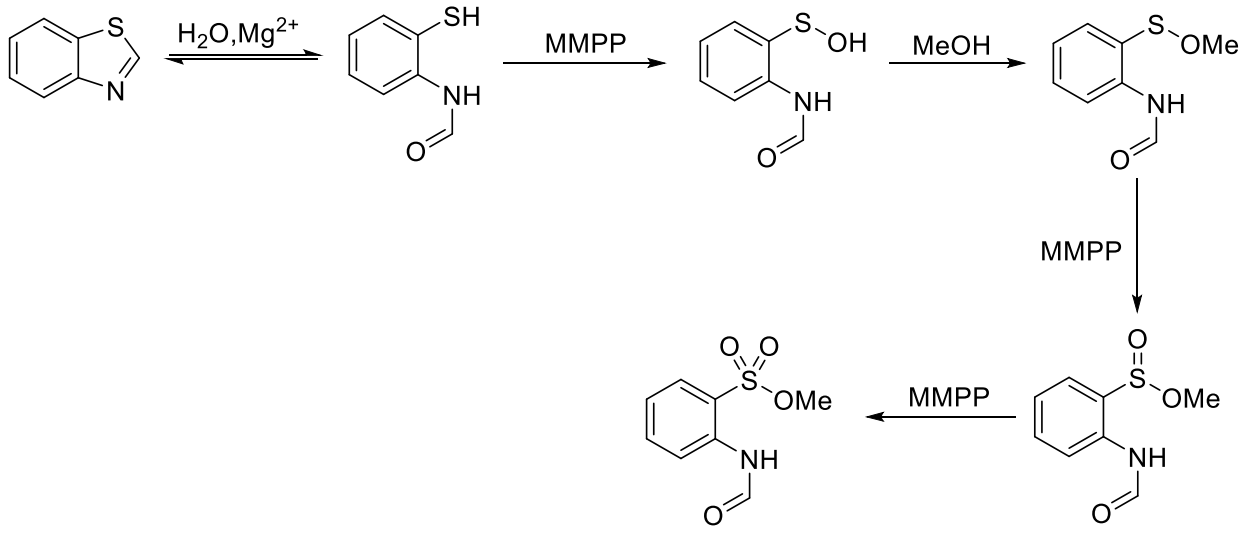

Scheme 24 Potential Route for Polymer Degradation: Potential route for polymer degradation in which the thiazole is opened and repeatedly oxidized through the use of either mCPBA or MMPP.[87]

The degradation itself saw significant variability based not only on the concentration of oxidant added but also in the solvent used. While a variety of oxidants were tested, *m*CPBA was found to yield the best results largely due to its solubility overlap with the targeted polymers while maintaining an appropriate strength. With both polymers being tested in a variety of

solvents, the three that saw the highest degree of success were DCE, THF, and toluene. In the appropriate solvent, the polymers saw as much as a 2/3 reduction in size (Tables 4 and 5).

Taking the GPC traces of this polymer before and after the breakdown, there is little trace of the higher molecular weight polymers with PDIs significantly closer to 1 than in the original synthesis. This is not unique to one of the polymers. Both polymers were tested and saw significant degradation when exposed to *m*CPBA in DCE or THF.

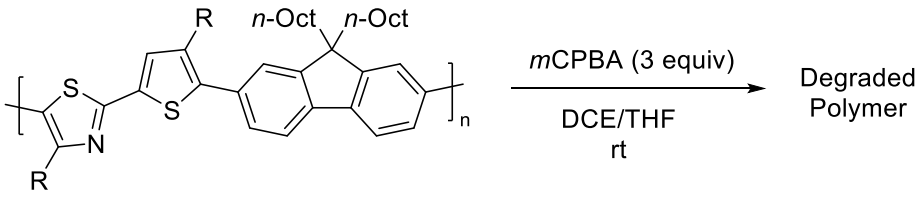

Scheme 25 Polymer Degradation Scheme: General scheme for the degradation of PT1 and PT7

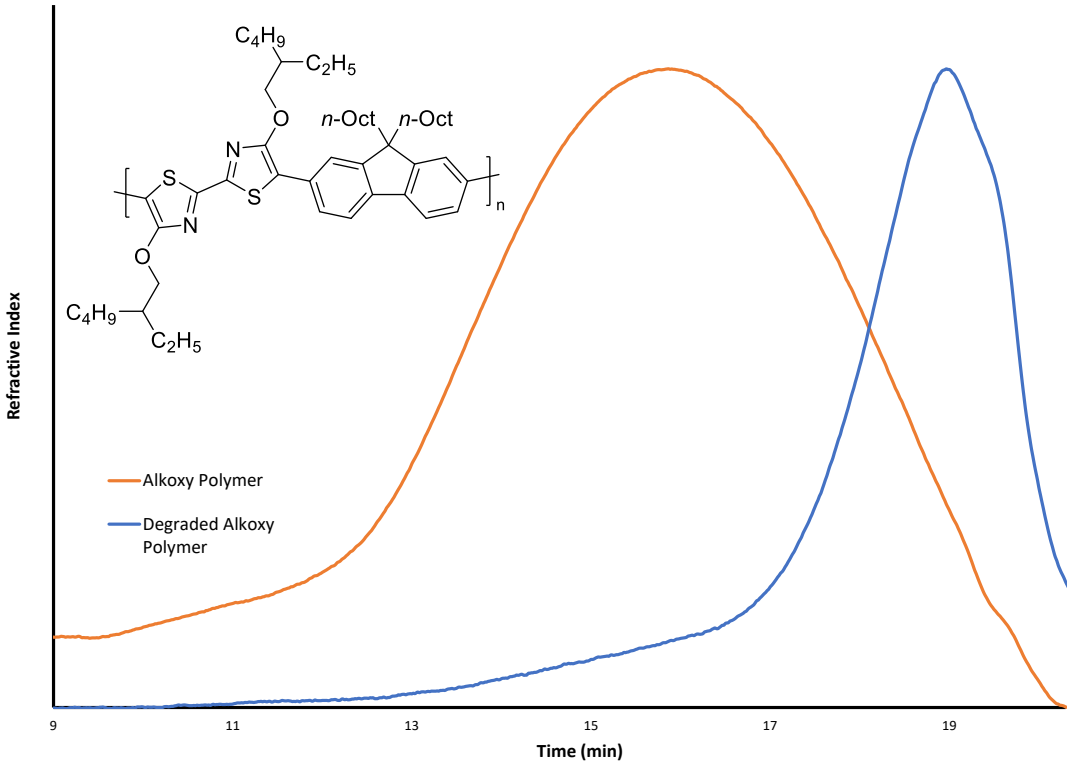

Figure 49 PT1 Degradation: GPCs of PT1 (alkoxy) sample overlayed from before the introduction of m*CPBA (blue) and after (orange)*

Sample	Polymer	Initial M_n (kDa)	Solvent	Oxidant Equivalents	Degraded M_n (kDa)
1	PT1	11.2	DCE	3	4.6
2	PT1	13.7	DCE	1.5	7.8
3	PT1	13.7	THF	3	9.4

Table 4 PT1 Degradation: Samples taken to determine levels of degradation of polymer in differing solvents and with differing equivalents of oxidant.

The polymer with an alkoxy side chain was first tested to determine the ideal conditions for the polymer degradation. Multiple solvents and equivalents of oxidant, in this case *m*CPBA, were tested. Through these tests it was determined that adding 3 equivalents of oxidant in DCE were the ideal conditions. Using these conditions the M_n of PT1 (alkoxy) was able to be reduced to 41% of its original size.

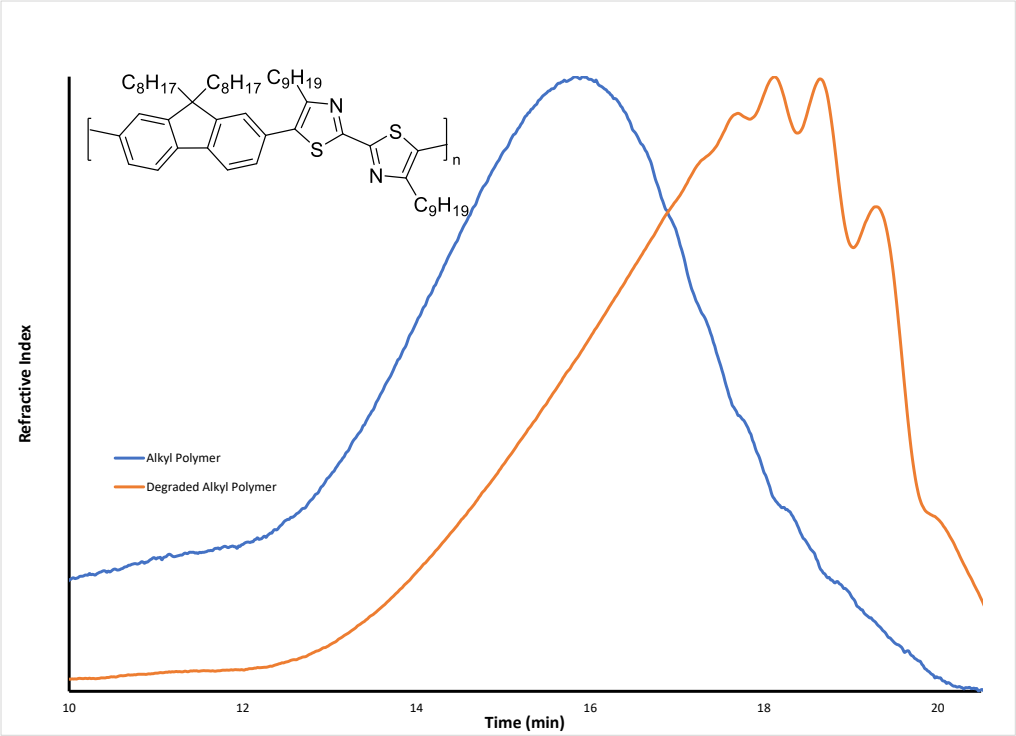

Figure 50 PT7 Degradation: GPCs of PT7 (alkyl) sample overlayed from before the introduction of m*CPBA (blue) and after (orange).*

Sample	Polymer	Initial M_n (kDa)	Solvent	Oxidant Equivalents	Degraded M_n (kDa)
5	PT7	11.6	DCE	3	3.3
6	PT7	11.9	THF	3	1.2

Table 5 PT7 Degradation: Samples of PT7 taken to determine levels of degradation in differing solvents.

The other synthesized polymer, that with alkyl chains in the 4 and 4' positions of the bithiazole, was also tested in a variety of solvents. It was found to have the largest amount of degradation in THF decreasing from 11.9 kDa to 1.2 kDA. Success was also found when using DCE, although to a lesser extent merely decreasing from 11.3 kDa to 3.3 kDa.

There is a significant difference in degradation when the polymers are tested in different solvents (full GPC traces in supporting information). PT1 will breakdown in one of the more common suspension solvent, toluene, although the degree is limited compared to what is seen in DCE. When tested in THF, one of the other most commonly used solvents for suspension of similar polymers, there is no breakdown observed. The degredation of PT7 in THF is promising as it proceeds even better than that in DCE.

4.7: Solvents

For polymer wrapping experiments, toluene is generally used as its low polarity helps to separate the CNTs that are in solution before the polymer is introduced. Metallic nanotubes, which are more hydrophilic, will aggregate making it more difficult for the polymer to interact with them. Since their interaction is required to solubilize the CNTs, the lack thereof between the polymer and the metallic CNTs has been shown to severely hinder the amount of metallic nanotubes able to be suspended. This can allow for additional selectivity achieved simply by changing the solvent. Semiconducting SWNTs that are more able to be dispersed in these

solvents as they are more hydrophobic further increasing the effects that solvents can have on the dispersion. THF can also be considered as a solvent for the polymer being used. As it is a polar solvent, the selectivity it imparts is lessened but the potential concentration of nanotubes suspended increases due to the increase in the solubility of the polymer being used.

For the final separations, the solvent chosen was therefore a mixture of both toluene and THF. This was chosen in an attempt to achieve the higher selectivity afforded by the toluene while retaining the higher solubility seen when using THF.

4.8: Testing of Suspended CNTs

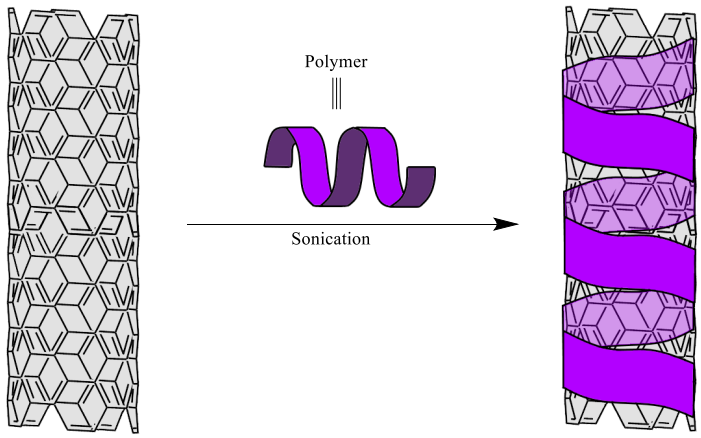

Figure 51 CNT Suspension: Process of suspension of nanotubes being tested through Raman spectroscopy. Nanotube mixture is first suspended with either PT1 or PT7 through sonication. CNTs not in solution are then separated through centrifugation.

The selective suspension of nanotubes, with the goal of degradation to retrieve them, is the primary driving force for this project. As such, the number of nanotubes, as well as the selectivity of the polymers, must be carefully investigated.

In order to separate the nanotubes, they were first suspended through sonication and left in solution with our polymers for 4 hours allowing for the polymers to bind to the nanotubes. Following this suspension, the mixture is centrifuged forcing all insolubilized nanotubes into a

pellet which is then filtered out. The final solution was then treated with *m*CPBA in order to degrade the polymers forcing the remaining nanotubes to precipitate out of solution.

In order to determine the types of nanotubes present in the solution before the precipitation, the solution was examined using Raman spectroscopy. The use of Raman spectroscopy allows for the characterization of the types of nanotubes present in solution as well as their purity.[88] Another significant aspect of using Raman spectroscopy is that the SWNTs could be tested in solution without the need to remove the polymers thereby allowing for the suspension to be tested before degradation.

The following Raman spectra display three different wavelengths at which the nanotube dispersions were tested. They include both variations of the target polymer, namely PT1 (alkoxy) and PT7 (alkyl), suspended in both THF and toluene. The grey regions display areas in which a signal will be recovered from a semiconducting nanotube and the red regions display signals received from the metallic nanotubes that remained in the solution. The final reading in black is a control, meaning a mixture of nanotubes that is yet unseparated.

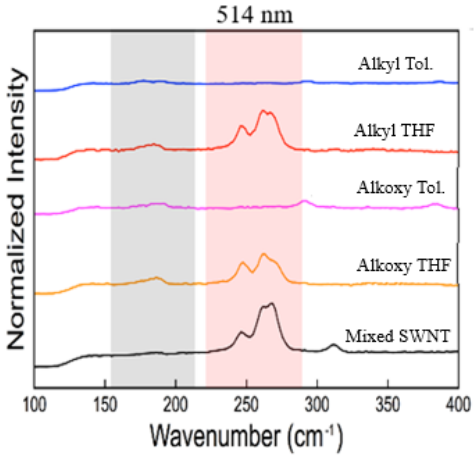

Figure 52 514 nm Raman Analysis: Raman spectra of the CNTs at 514 nm. Grey area displays the signals seen from semi-conducting CNTs while the red area displays signals from metallic CNTs.

The nanotubes in solution were first measured at 514 nm. The purpose of this measurement is primarily to observe if there are any metallic nanotubes suspended. Although there is some response from the semiconducting nanotubes at this wavelength, it is not enough for analysis. When observing PT1 and PT7 suspended in THF shown as the red and yellow traces respectively, the nanotubes in solution displayed signals characteristic of metallic CNTs between 250 cm^{-1} and 300 cm^{-1}. Suspending the polymers in toluene, as seen in the blue and pink traces, appears to address this issue seeing a significant decrease in the signal when either polymer was solubilized in it.

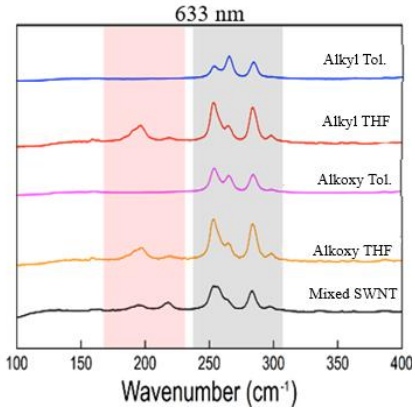

Figure 53 633 nm Raman Analysis: Raman spectra of the CNTs at 633 nm. Grey area displays the signals seen from semi-conducting CNTs while the red area displays signals from metallic CNTs.

The following test was to observe the solution at 633 nm. This wavelength allows simultaneous observation of semiconducting as well as metallic nanotubes which allows comparison of the amounts of the types of nanotubes in a suspension. Once again it was observed that the suspensions of PT1 and PT7 in THF showed metallic signals at approximately 200 cm^{-1} while there was no signal seen from the suspensions in toluene. All traces showed signals from semiconducting nanotubes in the 250 cm^{-1} to 300 cm^{-1} region indicating that all suspensions were able to separate the targeted nanotubes. Overall this measurement indicated that, although the THF suspensions did contain metallic nanotubes they were primarily

composed of semiconducting CNTs while emphasizing that the toluene based suspensions separated only semiconducting nanotubes.

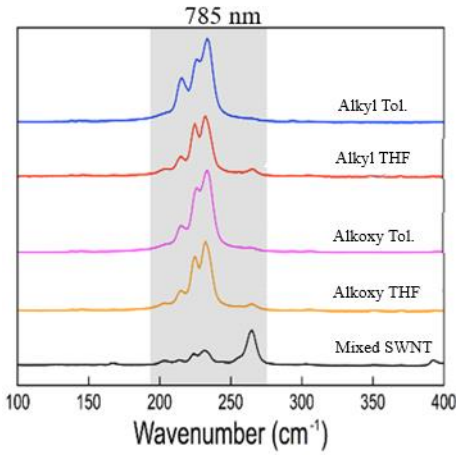

Figure 54 785 nm Raman Analysis: Raman spectra of the CNTs at 789 nm. Grey area displays the signals seen from semi-conducting CNTs.

Finally, the suspensions were tested at 785 nm. This test allows a clearer view of the number of semiconducting tubes suspended. All four suspensions of PT1 and PT7 allowed for the separation of semiconducting nanotubes between 200 cm^{-1} and 300 cm^{-1}. The other conclusion that can be reached from this measurement has to do with the selectivity of the polymers. When compared to the control sample in black, all four of the polymer suspensions showed significant signal from 200 cm^{-1} to 250 cm^{-1} while showing almost no signal from 250 cm^{-1} to 300 cm^{-1}. This result led to the hypothesis that out polymer suspensions were selectively solubilizing CNTs based on their chiralities.

As was predicted, it is not only the polymer that affects solubility and selectivity but the solvent as well. When solubilized in THF, the polymer shows lower selectivity, as is indicated by the peaks in the metallic regions of the Raman spectra but did display higher overall solubility for the nanotubes. The mixtures were also tested in toluene which did show higher selectivity for

semiconducting nanotubes but seemed to solubilize significantly less polymer and thereby less CNTs were left in solution after the isolation procedure. This could cause problems with the pure volume of solvent required to retrieve any relevant number of nanotubes. The potential solution at the time was to use mixtures of solvents. Mixing both THF and toluene to increase the solubility of the polymer while retaining the selectivity. When suspended in a 75:25 mixture of THF:toluene, there was an increase in solubility seen from both polymers compared to pure toluene and an increase in selectivity, particularly from the alkyl polymer, seen towards the nanotubes suspended.

4.9 Thermogravimetric analysis

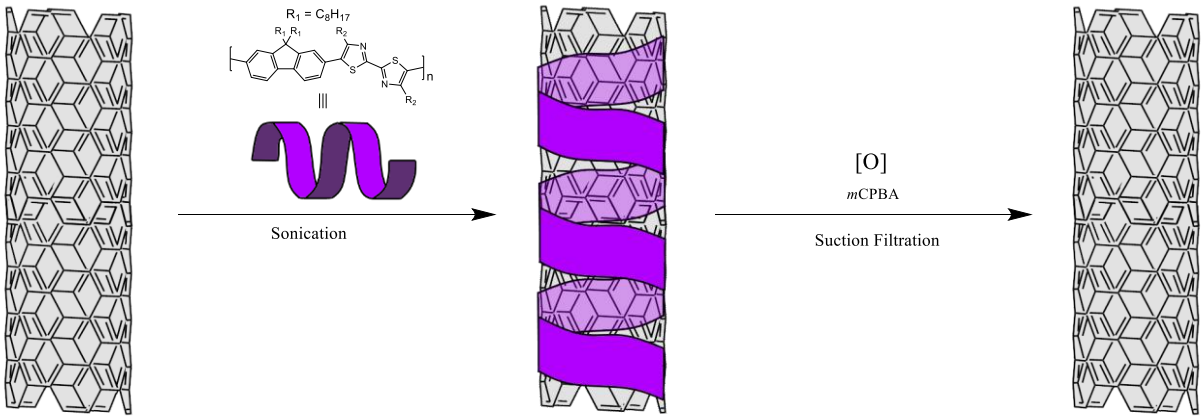

Figure 55 CNT Separasion: Nanotubes tested through TGA were fully separated through suspension followed by centrifugation degradation and suction filtration.

The next most important aspect of the polymer CNT solution to test is how complete the removal of the polymer is from the precipitated CNTs. To do this, thermogravimetric analysis was employed. This process involved heating the precipitated CNTs to extremely high temperatures, reaching above 600°C while measuring the mass of the sample, to determine if there was any polymer remaining attached to the nanotubes after their precipitation as any

remaining polymer will be incinerated while the carbon nanotubes will remain intact. The nanotube suspension was separated at different times to determine if the amount of time spent in the wrapping process before being degraded and washed off caused a difference in the percentage of the final mass that was CNTs. These trials were performed along with a control of pure polymer to determine how much polymer remained attached to the nanotubes after degradation. Ideally Fig. 58 would show a straight line indicating that no mass percentage was polymer.

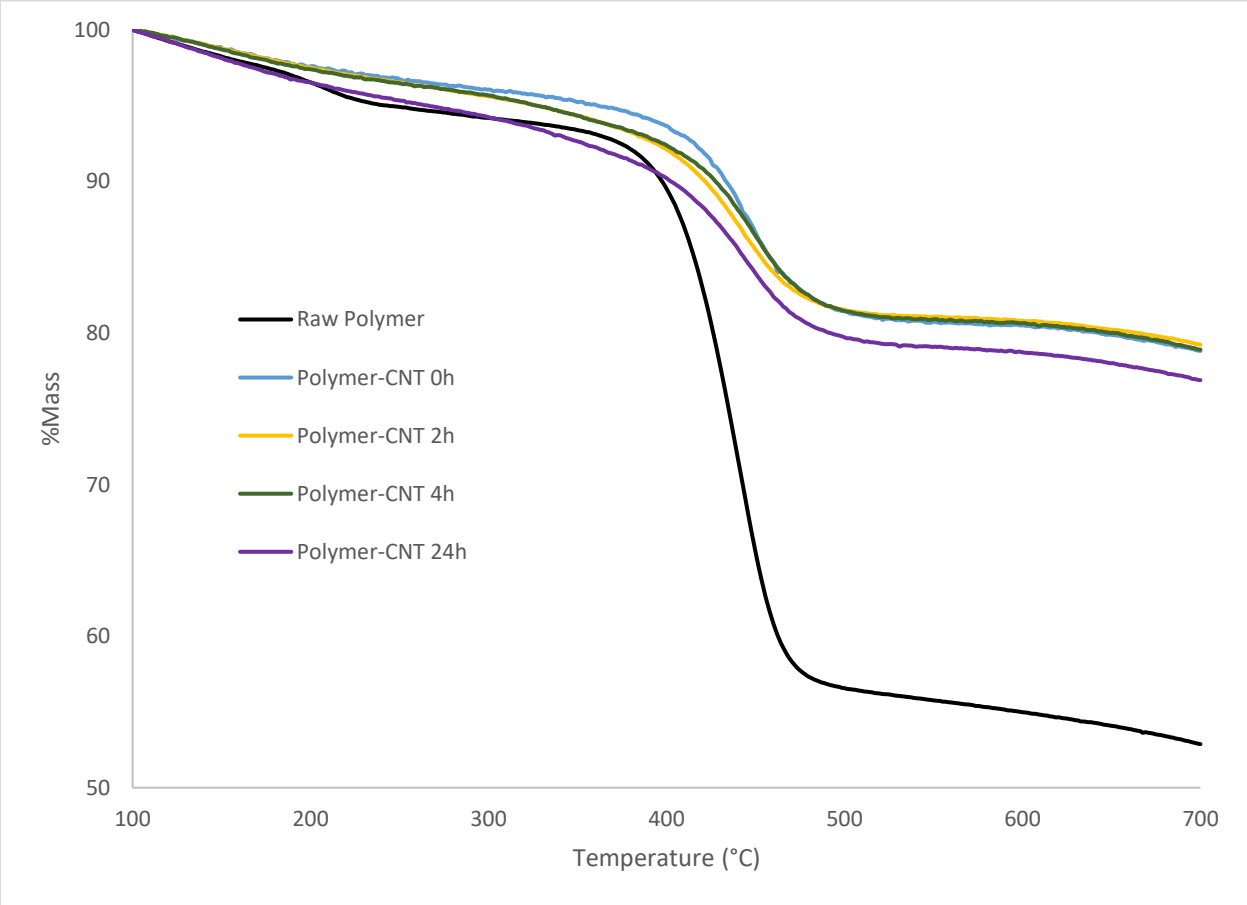

Figure 56 TGA Analysis: TGA results from nanotubes separated with PT1 measured up to 700 °C

As is visible, while a significant amount of polymer is removed from the nanotubes, some remains attached. This is visible through the observation of the steep mass percentage decrease

between 400 °C and 500 °C. The temperature of this percentage mass decrease aligns with that seen in the control indicating that upwards of 20% of the final mass was PT1. As previously discussed, polymers remaining associated with the CNTs can effect their electrical properties. This would mean that, while the final result may have less interference than some other methods, the CNTs would not be completely pure, and some amount of polymer would remain attached. Although further degradation was attempted after this result, lower masses could not be attained. This means that the synthesised polymer would not be a suitable candidate for the separation of pure CNTs.

4.10 Conclusions

In conclusion, a facile synthesis of a polymer that was easily degraded was achieved. This polymer, when combined with a mixture of carbon nanotubes was able to achieve a rapid separation. The polymer was then able to be degraded while adhered to the nanotubes but was not able to be completely removed regardless of the amount of oxidant introduced. This means that, although the separation was successful, the isolation of the CNTs was incomplete. While the separated nanotubes could find some uses, the failure to completely remove the polymer would either introduce an additional step in the isolation process or the uses of the CNTs would be significantly impacted. While polymer wrapping does provide a facile method of selectively separating SWNTs, finding a motif that can be fully degraded and removed from the resulting SWNTs has yet to be discovered.

5.0 Projects Summary

As was illustrated in the previous chapters, significant research can be done with conjugated polymers and a lot of work remains to be done until they achieve their full potential. In Chapter 1 a precatalyst for the synthesis of conjugated polymers was presented. This precatalyst allowed for higher efficiency in the synthesis of polymers while reducing the number of defects seen. This was primarily shown through NMR analysis of the polymers that displayed significantly fewer defects in the aromatic region for polymers synthesized using the precatalyst. This could represent a step forwards for DArP as a method with regards to the regioregularity able to be achieved.

In Chapter 2 a synthesis was outlined that allowed for the production of a variety of polymers using a bithiazole monomer. This synthesis was easily reproducible and resulted in polymers that had greatly differing electronic and optical properties. Further development and testing of the polymers could potentially allow for advancement of the commercial production of conjugated polymers.

Finally in Chapter 3 a potential method for separating carbon nanotubes was outlined. This method utilized the π-π interactions seen between conjugated polymers and CNTs. This interaction allows for the polymers to solubilize CNTs based on the properties of the polymer and the CNT. Although the polymers did allow for the selective separation of semi-conducting CNTs, their degradation did not allow for full purification. For this reason, this method is limited in its application. Overall conjugated polymers are a promising area of research with developments being seen in the usage of DArP to facilitate their synthesis.

References

(1) Martin Pope; Swenberg, C. E. Electronic Processes in Organic Crystals and Polymers - 2nd Edition, ISBN: 9780195129632. **1999**, 1360.

(2) Liu, M.; Makuta, S.; Tsuda, S.; Russo, S.; Seki, S.; Terao, J.; Tachibana, Y. Fluorene−Thiophene Copolymer Wire on TiO 2 : Mechanism Achieving Long Charge Separated State Lifetimes. *J. Phys. Chem. C* **2017**, *121* (46), 25672–25681. https://doi.org/10.1021/acs.jpcc.7b07295.

(3) Chen, R.; Zheng, C.; Li, C.; Li, H.; Wang, Z.; Tang, Y.; Jiang, H.; Tan, Z.; Huang, W. Efficient Synthesis and Photovoltaic Properties of Highly Rigid Perylene-Embedded Benzothiazolyls. *Polym. Chem.* **2016**, *7*, 11–16. https://doi.org/10.1039/c5py01791b.

(4) Dimitrakopoulos, C. D.; Malenfant, P. R. L. Organic Thin Film Transistors for Large Area Electronics. *Adv. Mater.* **2002**, *14*, 99–117. https://doi.org/10.1002/1521-4095.

(5) Yamashita, Y. Organic Semiconductors for Organic Field-Effect Transistors. *Sci. Technol. Adv. Mater.* **2009**, *10* (2), 24313–24322. https://doi.org/10.1088/1468-6996/10/2/024313.

(6) Clayden, J.; Greeves, N.; Warren, S. *Organic Chemistry*, 2nd ed.; Oxford University Press, 2012.

(7) Skoog, D. a; Holler, F. J.; Nieman, T. a. *Principles of Instrumental Analysis*, *Brooks/Cole*; 1998.

(8) Harris, D. C.; Lucy, C. A. *Quantitative Chemical Analysis*, 8th ed.; W. H. Freeman and Company: New York, 2010.

(9) Bredas, J. L. Mind the Gap! *Mater. Horizons* **2013**, *1* (1), 17–19.

https://doi.org/10.1039/C3MH00098B.

(10) Coropceanu, V.; Cornil, J.; da Silva Filho, D. A.; Olivier, Y.; Silbey, R.; Brédas, J. L. Charge Transport in Organic Semiconductors. *Chem. Rev.* **2007**, *107* (4), 926–952. https://doi.org/10.1021/CR050140X.

(11) Kahn, A. Fermi Level, Work Function and Vacuum Level Materials Horizons FOCUS. *Cite this Mater. Horiz* **2016**, *3*, 7–10. https://doi.org/10.1039/c5mh00160a.

(12) Sun, H.; Guo, X.; Facchetti, A. High-Performance n-Type Polymer Semiconductors: Applications, Recent Development, and Challenges. *Chem* **2020**, *6* (6), 1310–1326. https://doi.org/10.1016/J.CHEMPR.2020.05.012.

(13) McCulloch, I.; Heeney, M.; Bailey, C.; Genevicius, K.; MacDonald, I.; Shkunov, M.; Sparrowe, D.; Tierney, S.; Wagner, R.; Zhang, W.; Chabinyc, M. L.; Kline, R. J.; McGehee, M. D.; Toney, M. F. Liquid-Crystalline Semiconducting Polymers with High Charge-Carrier Mobility. *Nat. Mater.* **2006**, *5* (4), 328–333. https://doi.org/10.1038/NMAT1612.

(14) Burroughes, J. H.; Bradley, D. D. C.; Brown, A. R.; Marks, R. N.; Mackay, K.; Friend, R. H.; Burns, P. L.; Holmes, A. B. Light-Emitting Diodes Based on Conjugated Polymers. *Nature* **1990**, *347* (6293), 539–541. https://doi.org/10.1038/347539A0.

(15) Friend, R. H.; Gymer, R. W.; Holmes, A. B.; Burroughes, J. H.; Marks, R. N.; Taliani, C.; Bradley, D. D. C.; Dos Santos, D. A.; Brédas, J. L.; Lögdlund, M.; Salaneck, W. R. Electroluminescence in Conjugated Polymers. *Nat. 1999 3976715* **1999**, *397* (6715), 121–128. https://doi.org/10.1038/16393.

(16) Bernius, M. T.; Inbasekaran, M.; O'brien, J.; Wu, W. Progress with Light-Emitting Polymers. *Adv. Mater.* **2000**, *12*, 1737–1750. https://doi.org/10.1002/1521-4095.

(17) Elgrishi, N.; Rountree, K. J.; McCarthy, B. D.; Rountree, E. S.; Eisenhart, T. T.; Dempsey, J. L. A Practical Beginner's Guide to Cyclic Voltammetry. *J. Chem. Educ.* **2018**, *95* (2), 197–206. https://doi.org/10.1021/ACS.JCHEMED.7B00361/SUPPL_FILE/ED7B00361_SI_002.DOCX.

(18) Wade, L. *Organic Chemistry*, 8th ed.; Pearson: Illinois, 2013.

(19) Chemler, C.; Trauner, D.; Danishefsky, S. The B-Alkyl Suzuki-Miyaura Cross-Coupling Reaction: Development, Mechanistic Study, and Applications in Natural Product Synthesis. *Angew. Chemie* **2001**, *40* (24), 4544–4568.

(20) Wang, J.; Ma, X.; Ding, Y.; Wang, Y.; Yang, Z. Measurement and Correlation of the Solubility of Tin Compounds and β-Diketimine in Selected Solvents. *J. Mol. Liq.* **2019**, *296*, 111784. https://doi.org/10.1016/J.MOLLIQ.2019.111784.

(21) Farina, V.; Krishnamurthy, V.; Scott, W. J. The Stille Reaction. *Org. React.* **1997**, 1–652. https://doi.org/10.1002/0471264180.OR050.01.

(22) Sonogashira, K. Development of Pd–Cu Catalyzed Cross-Coupling of Terminal Acetylenes with Sp2-Carbon Halides. *J. Organomet. Chem.* **2002**, *653* (1–2), 46–49. https://doi.org/10.1016/S0022-328X(02)01158-0.

(23) de Meijere, A.; Diederich, F. *Metal-Catalyzed Cross-Coupling Reactions*, 2nd ed.; Wiley, 2004. https://doi.org/10.1002/9783527619535.

(24) Wang, Q.; Takita, R.; Kikuzaki, Y.; Ozawa, F. Palladium-Catalyzed Dehydrohalogenative Polycondensation of 2-Bromo-3-Hexylthiophene: An Efficient Approach to Head-to-Tail Poly(3-Hexylthiophene). *J. Am. Chem. Soc.* **2010**, *132* (33), 11420–11421. https://doi.org/10.1021/JA105767Z.

(25) Lapointe, D.; Fagnou, K. Overview of the Mechanistic Work on the Concerted Metallation-Deprotonation Pathway. **2010**. https://doi.org/10.1246/cl.2010.1118.

(26) Lavenot, L.; Gozzi, C.; Ilg, K.; Orlova, I.; Penalva, V.; Lemaire, M. Extension of the Heck Reaction to the Arylation of Activated Thiophenes. *J. Organomet. Chem.* **1998**, *567*, 49–55.

(27) Iwasawa, T.; Tokunaga, M.; Obora, Y.; Tsuji, Y. Homogeneous Palladium Catalyst Suppressing Pd Black Formation in Air Oxidation of Alcohols. *J. Am. Chem. Soc.* **2004**, *126* (21), 6554–6555. https://doi.org/10.1021/JA031936L/SUPPL_FILE/JA031936LSI20040414_064457.PDF.

(28) Herrmann, W. A.; Brossmer, C.; Reisinger, C. P.; Riermeier, T. H.; Öfele, K.; Beller, M. Palladacycles: Efficient New Catalysts for the Heck Vinylation of Aryl Halides. *Chem. - A Eur. J.* **1997**, *3* (8), 1357–1364. https://doi.org/10.1002/chem.19970030823.

(29) Mueller, J. A.; Goller, C. P.; Sigman, M. S. Elucidating the Significance Of-Hydride Elimination and the Dynamic Role of Acid/Base Chemistry in a Palladium-Catalyzed Aerobic Oxidation of Alcohols. **2004**. https://doi.org/10.1021/ja047794s.

(30) Wakioka, M.; Ichihara, N.; Kitano, Y.; Ozawa, F. A Highly Efficient Catalyst for the Synthesis of Alternating Copolymers with Thieno[3,4-c]Pyrrole-4,6-Dione Units via Direct Arylation Polymerization. *Macromolecules* **2014**, *47* (2), 626–631.

https://doi.org/10.1021/ma4023668.

(31) González, J. J.; Garćia, N.; Gómez-Lor, B.; Echavarren, A. M. Synthesis of Spiro Polycyclic Aromatic Hydrocarbons by Intramolecular Palladium-Catalyzed Arylation. *J. Org. Chem.* **1997**, *62* (5), 1286–1291. https://doi.org/10.1021/JO962059N/SUPPL_FILE/JO1286.PDF.

(32) García-Cuadrado, D.; Braga, A. A. C.; Maseras, F.; Echavarren, A. M. Proton Abstraction Mechanism for the Palladium-Catalyzed Intramolecular Arylation. *J. Am. Chem. Soc.* **2006**, *128* (4), 1066–1067. https://doi.org/10.1021/JA056165V/SUPPL_FILE/JA056165VSI20051125_120148.PDF.

(33) Campeau, L. C.; Parisien, M.; Leblanc, M.; Fagnou, K. Biaryl Synthesis via Direct Arylation: Establishment of an Efficient Catalyst for Intramolecular Processes. *J. Am. Chem. Soc.* **2004**, *126* (30), 9186–9187. https://doi.org/10.1021/JA049017Y/SUPPL_FILE/JA049017YSI20040622_105614.PDF.

(34) Lafrance, M.; Blaquière, N.; Fagnou, K. Direct Intramolecular Arylation of Unactivated Arenes: Application to the Synthesis of Aporphine Alkaloids. *Chem. Commun.* **2004**, No. 24, 2874–2875. https://doi.org/10.1039/B410394G.

(35) Parisien, M.; Valette, D.; Fagnou, K. Direct Arylation Reactions Catalyzed by Pd(OH)2/C: Evidence for a Soluble Palladium Catalyst. *J. Org. Chem.* **2005**, *70* (19), 7578–7584. https://doi.org/10.1021/JO051039V/SUPPL_FILE/JO051039VSI20050712_104002.PDF.

(36) Campeau, L. C.; Parisien, M.; Jean, A.; Fagnou, K. Catalytic Direct Arylation with Aryl Chlorides, Bromides, and Iodides: Intramolecular Studies Leading to New Intermolecular

Reactions. *J. Am. Chem. Soc.* **2006**, *128* (2), 581–590. https://doi.org/10.1021/JA055819X/SUPPL_FILE/JA055819XSI20051109_104035.PDF.

(37) Gorelsky, S. I.; Lapointe, D.; Fagnou, K. Analysis of the Concerted Metalation-Deprotonation Mechanism in Palladium-Catalyzed Direct Arylation across a Broad Range of Aromatic Substrates. *J. Am. Chem. Soc.* **2008**, *130* (33), 10848–10849. https://doi.org/10.1021/JA802533U/SUPPL_FILE/JA802533U.PDF.

(38) Liégault, B.; Petrov, I.; Gorelsky, S. I.; Fagnou, K. Modulating Reactivity and Diverting Selectivity in Palladium-Catalyzed Heteroaromatic Direct Arylation through the Use of a Chloride Activating/Blocking Group. *J. Org. Chem.* **2010**, *75* (4), 1047–1060. https://doi.org/10.1021/JO902515Z/SUPPL_FILE/JO902515Z_SI_001.PDF.

(39) Gorelsky, S. I.; Lapointe, D.; Fagnou, K. Analysis of the Palladium-Catalyzed (Aromatic)C–H Bond Metalation–Deprotonation Mechanism Spanning the Entire Spectrum of Arenes. *J. Org. Chem.* **2012**, *77* (1), 658–668. https://doi.org/10.1021/jo202342q.

(40) Hazari, N.; Melvin, P. R.; Beromi, M. M. Well-Defined Nickel and Palladium Precatalysts for Cross-Coupling. *Nat. Rev. Chem. 2017 13* **2017**, *1* (3), 1–16. https://doi.org/10.1038/S41570-017-0025.

(41) Bruno, N. C.; Tudge, M. T.; Buchwald, S. L. Design and Preparation of New Palladium Precatalysts for C–C and C–N Cross-Coupling Reactions. *Chem. Sci.* **2013**, *4* (3), 916–920. https://doi.org/10.1039/C2SC20903A.

(42) Shaughnessy, K. H. Development of Palladium Precatalysts That Efficiently Generate LPd(0) Active Species. *Isr. J. Chem.* **2020**, *60* (3–4), 180–194.

https://doi.org/10.1002/IJCH.201900067.

(43) Hills, I. D.; Fu, G. C. Elucidating Reactivity Differences in Palladium-Catalyzed Coupling Processes: The Chemistry of Palladium Hydrides. *J. Am. Chem. Soc.* **2004**, *126* (41), 13178–13179. https://doi.org/10.1021/JA0471424/SUPPL_FILE/JA0471424SI20040808_110157.PDF.

(44) Nakashima, Y.; Hirata, G.; Sheppard, T. D.; Nishikata, T. The Mizoroki-Heck Reaction with Internal Olefins: Reactivities and Stereoselectivities. *Asian J. Org. Chem.* **2020**, *9* (4), 480–491. https://doi.org/10.1002/AJOC.201900741.

(45) Amatore, C.; Broeker, G.; Jutand, A.; Khalil, F. Identification of the Effective Palladium(0) Catalytic Species Generated in Situ from Mixtures of Pd(Dba) 2 and Bidentate Phosphine Ligands. Determination of Their Rates and Mechanism in Oxidative Addition. **1997**.

(46) De Meijere, A. *Metal-Catalyzed Cross-Coupling Reactions*, 2nd ed.; De Meijere, A., Diederich, F., Eds.; Wiley-VCH: Weinheim, 2004.

(47) Cope, A. C.; Siekman, R. W. Formation of Covalent Bonds from Platinum or Palladium to Carbon by Direct Substitution. *J. Am. Chem. Soc.* **1965**, *87* (14), 3272–3273. https://doi.org/10.1021/ja01092a063.

(48) Cope, A. C.; Friedrich, E. C. Electrophilic Aromatic Substitution Reactions by Platinum (II) and Palladium (II) Chlorides on N,N-Dimethylbenzylamines. *J. Am. Chem. Soc.* **1968**, *90* (4), 909–913. https://doi.org/10.1021/JA01006A012/ASSET/JA01006A012.FP.PNG_V03.

(49) Beller, M.; Fischer, H.; Kühlein, K.; Reisinger, C. P.; Herrmann, W. A. First Palladium-Catalyzed Heck Reactions with Efficient Colloidal Catalyst Systems. *J. Organomet. Chem.* **1996**, *520* (1–2), 257–259. https://doi.org/10.1016/0022-328X(96)06398-X.

(50) Zim, D.; Nobre, S. M.; Monteiro, A. L. Suzuki Cross-Coupling Reaction Catalyzed by Sulfur-Containing Palladacycles: Formation of Palladium Active Species. *J. Mol. Catal. A Chem.* **2008**, *287* (1–2), 16–23. https://doi.org/10.1016/J.MOLCATA.2008.02.015.

(51) Gorunova, O. N.; Novitskiy, I. M.; Grishin, Y. K.; Gloriozov, I. P.; Roznyatovsky, V. A.; Khrustalev, V. N.; Kochetkov, K. A.; Dunina, V. V. When Applying the Mercury Poisoning Test to Palladacycle-Catalyzed Reactions, One Should Not Consider the Common Misconception of Mercury(0) Selectivity. *Organometallics* **2018**, *37* (17), 2842–2858. https://doi.org/10.1021/ACS.ORGANOMET.8B00363/SUPPL_FILE/OM8B00363_SI_002.PDF.

(52) Biscoe, M. R.; Fors, B. P.; Buchwald, S. L. A New Class of Easily Activated Palladium Precatalysts for Facile C-N Cross-Coupling Reactions and the Low Temperature Oxidative Addition of Aryl Chlorides. *J. Am. Chem. Soc.* **2008**, *130* (21), 6686–6687. https://doi.org/10.1021/JA801137K/SUPPL_FILE/JA801137K-FILE003.PDF.

(53) Kinzel, T.; Zhang, Y.; Buchwald, S. L. A New Palladium Precatalyst Allows for the Fast Suzuki-Miyaura Coupling Reactions of Unstable Polyfluorophenyl and 2-Heteroaryl Boronic Acids. *J. Am. Chem. Soc.* **2010**, *132* (40), 14073–14075. https://doi.org/10.1021/JA1073799/SUPPL_FILE/JA1073799_SI_001.PDF.

(54) Bruno, N. C.; Tudge, M. T.; Buchwald, S. L. Design and Preparation of New Palladium

Precatalysts for C-C and C-N Cross-Coupling Reactions. *Chem. Sci.* **2013**, *4* (3), 916. https://doi.org/10.1039/C2SC20903A.

(55) Pappenfus, T. M.; Almyahi, F.; Cooling, N. A.; Culver, E. W.; Rasmussen, S. C.; Dastoor T M Pappenfus, P. C.; Almyahi, F.; Cooling, N. A.; Dastoor, P. C.; Culver, E. W.; Rasmussen, S. C. Exploration of the Direct Arylation Polymerization Method for the Practical Application of Conjugated Materials: Synthetic Scale-Up, Solar Cell Performance, and Cost Analyses. *Macromol. Chem. Phys.* **2018**, *219* (21), 1800272. https://doi.org/10.1002/MACP.201800272.

(56) Osedach, T. P.; Andrew, T. L.; Bulović, V. Effect of Synthetic Accessibility on the Commercial Viability of Organic Photovoltaics. *Energy Environ. Sci.* **2013**, *6* (3), 711–718. https://doi.org/10.1039/C3EE24138F.

(57) Sperling, L. H. *Introduction to Physical Polymer Science*, 4th ed.; Wiley & Sons: Hoboken, 2006.

(58) Mirabel, R.; Buratynski, J.; Schipper, D. J. Design of Palladium Precatalysts for Direct(Hetero)Arylation Polymerization. *Manuscr. Prep.* **2022**.

(59) Morin, P. O.; Bura, T.; Sun, B.; Gorelsky, S. I.; Li, Y.; Leclerc, M. Conjugated Polymers à La Carte from Time-Controlled Direct (Hetero)Arylation Polymerization. *ACS Macro Lett.* **2015**, *4* (1), 21–24. https://doi.org/10.1021/MZ500656G/SUPPL_FILE/MZ500656G_SI_001.PDF.

(60) Lafrance, M.; Fagnou, K. Palladium-Catalyzed Benzene Arylation: Incorporation of Catalytic Pivalic Acid as a Proton Shuttle and a Key Element in Catalyst Design. *J. Am. Chem. Soc.* **2006**, *128* (51), 16496–16497.

https://doi.org/10.1021/JA067144J/SUPPL_FILE/JA067144JSI20061121_125154.PDF.

(61) Sun, H. Y.; Gorelsky, S. I.; Stuart, D. R.; Campeau, L. C.; Fagnou, K. Mechanistic Analysis of Azine N-Oxide Direct Arylation: Evidence for a Critical Role of Acetate in the Pd(OAc)2 Precatalyst. *J. Org. Chem.* **2010**, *75* (23), 8180–8189. https://doi.org/10.1021/JO101821R/SUPPL_FILE/JO101821R_SI_001.PDF.

(62) Ye, L.; Thompson, B. C. P-Cymene: A Sustainable Solvent That Is Highly Compatible with Direct Arylation Polymerization (DArP). *ACS Macro Lett.* **2021**, *10*, 714–719. https://doi.org/10.1021/ACSMACROLETT.1C00274/ASSET/IMAGES/LARGE/MZ1C00274_0002.JPEG.

(63) Wakioka, M.; Kitano, Y.; Ozawa, F. A Highly Efficient Catalytic System for Polycondensation of 2,7-Dibromo-9,9-Dioctylfluorene and 1,2,4,5-Tetrafluorobenzene via Direct Arylation. *Macromolecules* **2013**, *46* (2), 370–374. https://doi.org/10.1021/ma302558z.

(64) Frommer, J. E. Conducting Polymer Solutions. *Acc. Chem. Res.* **1986**, *19* (1), 2–9. https://doi.org/10.1021/AR00121A001/ASSET/AR00121A001.FP.PNG_V03.

(65) Huang, H.; Yang, L.; Facchetti, A.; Marks, T. J. Organic and Polymeric Semiconductors Enhanced by Noncovalent Conformational Locks. *Chem. Rev.* **2017**, *117* (15), 10291–10318. https://doi.org/10.1021/ACS.CHEMREV.7B00084/ASSET/IMAGES/MEDIUM/CR-2017-000842_0041.GIF.

(66) Pascoe, D. J.; Ling, K. B.; Cockroft, S. L. The Origin of Chalcogen-Bonding Interactions. *J. Am. Chem. Soc.* **2017**, *139* (42), 15160–15167.

https://doi.org/10.1021/JACS.7B08511/SUPPL_FILE/JA7B08511_SI_002.CIF.

(67) Wang, Q.; Wakioka, M.; Ozawa, F. Synthesis of End-Capped Regioregular Poly(3-Hexylthiophene)s via Direct Arylation. *Macromol. Rapid Commun.* **2012**, *33* (14), 1203–1207. https://doi.org/10.1002/marc.201200076.

(68) Täuscher, E.; Calderón-Ortiz, L.; Weiß, D.; Beckert, R.; Görls, H. Bis(4-Hydroxythiazoles): Novel Functional and Switchable Fluorophores. *Synthesis (Stuttg).* **2011**, *2011* (14), 2334–2339. https://doi.org/10.1055/s-0030-1260670.

(69) Guo, X.; Quinn, J.; Chen, Z.; Usta, H.; Zheng, Y.; Xia, Y.; Hennek, J. W.; Ortiz, R. P.; Marks, T. J.; Facchetti, A. Dialkoxybithiazole: A New Building Block for Head-to-Head Polymer Semiconductors. *J. Am. Chem. Soc.* **2013**, *135* (5), 1986–1996. https://doi.org/10.1021/JA3120532/SUPPL_FILE/JA3120532_SI_001.PDF.

(70) Wei, Q.; Miyanishi, S.; Zhou, E.; Hashimoto, K.; Tajima, K. Poly(4-Hexyloxythiazole): A New Low Band Gap Semiconductor for Polymer Electronics. *Synth. Met.* **2014**, *196*, 139–144. https://doi.org/10.1016/J.SYNTHMET.2014.07.028.

(71) Truong, T.; Alvarado, J.; Tran, L. D.; Daugulis, O. Nickel, Manganese, Cobalt, and Iron-Catalyzed Deprotonative Arene Dimerization. *Org. Lett.* **2010**, *12* (6), 1200. https://doi.org/10.1021/OL902970Z.

(72) Lei, T.; Pochorovski, I.; Bao, Z. Separation of Semiconducting Carbon Nanotubes for Flexible and Stretchable Electronics Using Polymer Removable Method. *Acc. Chem. Res.* **2017**, *50* (4), 1096–1104. https://doi.org/10.1021/acs.accounts.7b00062.

(73) Yomogida, Y.; Tanaka, T.; Zhang, M.; Yudasaka, M.; Wei, X.; Kataura, H. Industrial-

Scale Separation of High-Purity Single-Chirality Single-Wall Carbon Nanotubes for Biological Imaging. *Nat. Commun.* **2016**, *7* (1), 1–8. https://doi.org/10.1038/ncomms12056.

(74) PA, M.-J.; CE, A.; RR, R.; AJ, F. Carbon Nanotubes: Directions and Perspectives in Oral Regenerative Medicine. *J. Dent. Res.* **2013**, *92* (7), 18-1-18–26. https://doi.org/10.1177/0022034513490957.

(75) Suresh, B. *Solid State Devices and Technology*, 3rd ed.; Sanguine Technical Publishers: Bangalore, 2010.

(76) Saito, R.; Fujita, M.; Dresselhaus, G.; Dresselhaus, M. S. Electronic Structure of Chiral Graphene Tubules. *Appl. Phys. Lett.* **1992**, *60* (18), 2204–2206. https://doi.org/10.1063/1.107080.

(77) Ding, J.; Li, Z.; Lefebvre, J.; Cheng, F.; Dubey, G.; Zou, S.; Finnie, P.; Hrdina, A.; Scoles, L.; Lopinski, G. P.; Kingston, C. T.; Simard, B.; Malenfant, P. R. L. Enrichment of Large-Diameter Semiconducting SWCNTs by Polyfluorene Extraction for High Network Density Thin Film Transistors. *Nanoscale* **2014**, *6* (4), 2328–2339. https://doi.org/10.1039/c3nr05511f.

(78) Javey, A.; Guo, J.; Wang, Q.; Lundstrom, M.; Dai, H. Ballistic Carbon Nanotube Field-Effect Transistors. *Nature* **2003**, *424* (6949), 654–657. https://doi.org/10.1038/nature01797.

(79) Liu, L.; Zhou, H.; Cheng, R.; Yu, W. J.; Liu, Y.; Chen, Y.; Shaw, J.; Zhong, X.; Huang, Y.; Duan, X. High-Yield Chemical Vapor Deposition Growth of High-Quality Large-Area AB-Stacked Bilayer Graphene. *ACS Nano* **2012**, *6* (9), 8241–8249.

https://doi.org/10.1021/nn302918x.

(80) Krupke, R.; Hennrich, F.; Löhneysen, H. v.; Kappes, M. M. Separation of Metallic from Semiconducting Single-Walled Carbon Nanotubes. *Science (80-.).* **2003**, *301* (5631), 344–347. https://doi.org/10.1126/science.1086534.

(81) Enyashin, A. N.; Gemming, S.; Seifert, G. DNA-Wrapped Carbon Nanotubes Related Content. *Nanotechnology* **2007**, *18*, 1–10. https://doi.org/10.1088/0957-4484/18/24/245702.

(82) Lemasson, F.; Tittmann, J.; Hennrich, F.; Stürzl, N.; Malik, S.; Kappes, M. M.; Mayor, M. Debundling, Selection and Release of SWNTs Using Fluorene-Based Photocleavable Polymers. *Chem. Commun.* **2011**, *47* (26), 7428–7430. https://doi.org/10.1039/c1cc11400j.

(83) Pochorovski, I.; Wang, H.; Feldblyum, J. I.; Zhang, X.; Antaris, A. L.; Bao, Z. H-Bonded Supramolecular Polymer for the Selective Dispersion and Subsequent Release of Large-Diameter Semiconducting Single-Walled Carbon Nanotubes. *J. Am. Chem. Soc.* **2015**, *137* (13), 4328–4331. https://doi.org/10.1021/jacs.5b01704.

(84) Toshimitsu, F.; Nakashima, N. Semiconducting Single-Walled Carbon Nanotubes Sorting with a Removable Solubilizer Based on Dynamic Supramolecular Coordination Chemistry. *Nat. Commun.* **2014**, *5* (1), 1–9. https://doi.org/10.1038/ncomms6041.

(85) Liang, S.; Chen, G.; Peddle, J.; Zhao, Y. Reversible Dispersion and Releasing of Single-Walled Carbon Nanotubes by a Stimuli-Responsive TTFV-Phenylacetylene Polymer. *Chem. Commun.* **2012**, *48* (25), 3100–3102. https://doi.org/10.1039/c2cc17935k.

(86) Liang, S.; Chen, G.; Zhao, Y. Conformationally Switchable TTFV-Phenylacetylene Polymers: Synthesis, Properties, and Supramolecular Interactions with Single-Walled Carbon Nanotubes. *J. Mater. Chem. C* **2013**, *1* (35), 5477–5490. https://doi.org/10.1039/c3tc30317a.

(87) Moreira, R. E.; Sinclair, G. S.; Schipper, D. J. Oxidative Ring-Opening of Benzothiazole Derivatives. *Can. J. Chem.* **2019**, *97* (5), 360–365. https://doi.org/10.1139/CJC-2018-0459/SUPPL_FILE/CJC-2018-0459SUPPLB.CIF.

(88) Dresselhaus, M. S.; Dresselhaus, G.; Saito, R.; Jorio, A. Raman Spectroscopy of Carbon Nanotubes. *Phys. Rep.* **2005**, *409*, 47–99. https://doi.org/10.1016/j.physrep.2004.10.006.

Appendix

General Considerations

All reactions were performed under a protective argon atmosphere unless otherwise specified. Reaction solvents utilized were either reagent and/or HPLC grade. Tetrahydrofuran, toluene, acetonitrile, triethylamine, and dichloromethane were obtained from a JC Mayer solvent-purification system. Chemical reagents were primarily purchased from Millipore-Sigma or Oakwood Chemical. Thin layer chromatography to monitor reactions was performed using aluminum backed silica plates (Kieselgel 60 F_{254}, Merck) and were examined either under UV lighting (254 nm or 365 nm) or through staining. Flash chromatography was performed using 230-400 mesh silica gel with a Teledyne-isco Combiflash Rf+ system.

^{1}H and ^{13}C NMR spectra were recorded on a Brüker AVANCE300 (300 MHz) or Brüker AC300 (300MHz) NMR spectrometer. All chemical shifts are reported in parts per million (ppm) relative to chloroform found at 7.26 ppm for ^{1}H NMR and 77.00 ppm for ^{13}C NMR. Abbreviations used for NMR peaks are as follows: s, singlet; d, doublet; t, triplet; q, quartet; dd, doublet of doublets; dt, doublet of triplets; m, multiplet; and bs, broad singlet. Ultraviolet visible (UV-vis) absorption spectra were measured using a Carey-4000 spectrophotometer and the background was corrected using a solvent filled cuvette. Electrochemical measurements were taken using a WaveNano potentiostat in a three-electrode configuration: platinum button working electrode, a platinum wire counter electrode, and a platinum wire reference electrode. Ferrocene was used as an internal standard. Acetonitrile was used as a solvent with 0.1 mM nBu_4NPF_6 as an electrolyte. The experiments were performed under nitrogen and a scan rate of

0.1 V/s was employed. While measuring polymers, they were drop cast onto the working electrode.

Polymer molecular weights, both number-average (M_n) and weight-average (M_w), were measured relative to polystyrene standards. The polymers were measured through size exclusion chromatography using a Viscotek GPC MAX VE2001 with two PAS-104 styrene-divinylbenzene gel columns maintained at 35°C and detected through a VE 3580 RI detector. The flow rate was fixed at 1.0 mL/min with tetrahydrofuran as the eluent. Samples were prepared at 2 mg/mL in THF and filtered through 0.22 µM PTFE into 1 mL chromatography vials.

Synthetic Procedures

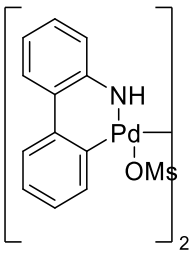

To a flame dried and purged round bottom flask was added $Pd(OAc)_2$ (243 mg, 0.942 mmol, 1 equiv) and [1,1'-biphenyl]-2-yl-l5-azaneyl methanesulfonate (253 mg, 0.949 mmol, 1 equiv) followed by toluene (4 mL, 0.25 M). The mixture was then heated and stirred for 45 min. The resulting mixture was separated through vacuum filtration and washed with toluene (10 mL) to yield as a white solid (0.344 g, 99%).

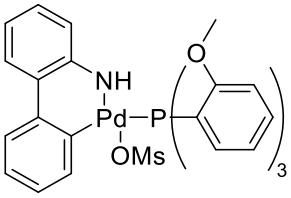

To a flame dried and purged round bottom flask was added above (50 mg, 0.068 mmol, 1 equiv) and tris(*o*-anisyl) phosphine (48 mg, 0.138 mmol, 2 equiv) followed by THF (1.1 mL, 0.1 M). The mixture was then stirred at room temperature for 45 min. 90% of the THF was removed and then the residue was triturated using hexanes. The final product was isolated using vacuum filtration to yield as a white solid (95 mg, 97%) ^{1}H NMR (300 MHz, $CDCl_3$) δ 7.50 (m, 3H), 7.47 – 7.33 (m, 6H), 7.28 (m, 8H), 6.90 (m, 4H), 6.76 (s, 2H), 6.52 (s, 2H), 4.48 (s, 1H), 3.41 (s, 9H), 2.18 (s, 3H).

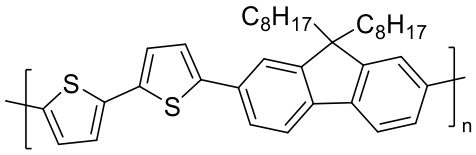

To a flame dried and argon purged vial was added: 2,2'-bithiophene (75.3 mg, 0.45 mmol, 1 equiv) and 9,9'-dioctyl-2,7-dibromofluorene (246.8, 0.45 mmol, 1 equiv), PivOH (46 mg, .45 mmol, 1 equiv), Cs_2CO_3 (429 mg, 1.35 mmol, 3 equiv), Pd_2dba_3 (16.5 mg, 0.018 mmol, 4 mol%), and tris(*o*-anisyl) phosphine (12.7 mg, 0.036 mmol, 8 mol%). The solids were then freeze dried before the addition of anhydrous toluene (3 mL, 0.15 M). The mixture was then heated to 100 °C and allowed to react for 3 h. The polymer was then precipitated through addition to cold, stirring methanol (20 mL). Solid polymer was then separated through vacuum filtration producing P1c. The resulting polymer was then purified through sonication in 50:50 methanol:water (144 mg, 55%) ^{1}H NMR (500 MHz, TCE, 90 °C) δ 7.68 (d, J = 7.8 Hz, 1H), 7.63 – 7.58 (m, 1H), 7.55 (d, J = 12.2 Hz, 1H), 7.30 (s, 1H), 7.21 (s, 1H), 2.03 (s, 2H), 1.26 – 1.01 (m, 13H), 0.80 (t, J = 6.9 Hz, 5H). M_n = 18.8 kDa, M_w = 44.5 kDa, PDI = 2.37

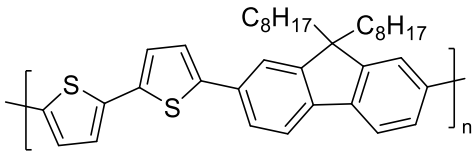

To a flame dried and argon purged vial was added: bithiophene (75.3 mg, 0.45 mmol, 1 equiv) and 9,9'-dioctyl-2,7-dibromofluorene (246.8, 0.45 mmol, 1 equiv), PivOH (46 mg, .45 mmol, 1 equiv), Cs_2CO_3 (429 mg, 1.35 mmol, 3 equiv), Pd_2dba_3 (16.5 mg, 0.018 mmol, 4 mol%), and tris(*o*-anisyl) phosphine (12.7 mg, 0.036 mmol, 8 mol%).The solids were then freeze dried before the addition of anhydrous toluene (3 mL, 0.15 M). The mixture was then heated to 100 °C and allowed to react for 3 h. The polymer was then precipitated through addition to cold, stirring methanol (20 mL). Solid polymer was then separated through vacuum filtration yielding P1b. The resulting polymer was then purified through sonication in 50:50 methanol:water (185.3 mg, 71%) ^{1}H NMR (500 MHz, TCE, 90 °C) δ 7.67 (d, J = 7.9 Hz, 2H), 7.58 (d, J = 7.7 Hz, 2H), 7.56 (s, 2H), 7.30 (s, 2H), 7.20 (s, 2H), 2.02 (m, 4H), 1.31 – 0.96 (m, 24H), 0.88 – 0.71 (m, 6H). M_n = 13.2 kDa, M_w = 47.2 kDa, PDI = 3.6

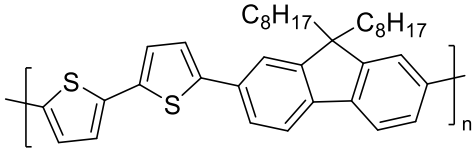

To a flame dried and argon purged vial was added: bithiophene (75.3 mg, 0.45 mmol, 1 equiv) and 9,9'-dioctyl-2,7-dibromofluorene (246.8, .45 mmol, 1 equiv), PivOH (46 mg, 0.45 mmol, 1 equiv), Cs_2CO_3 (429 mg, 1.35 mmol, 3 equiv), and precatalyst (6.5 mg, 0.009 mmol, 2 mol%). The solids were then freeze dried before the addition of anhydrous toluene (3 mL, 0.15 M). The mixture was then heated to 100 °C and allowed to react for 3 h. The polymer was then precipitated through addition to cold, stirring methanol (20 mL). Solid polymer was then

separated through vacuum filtration yielding P1a (239 mg 96%). M_n = 25.6 kDa, M_w = 75.4 kDa, PDI = 2.9

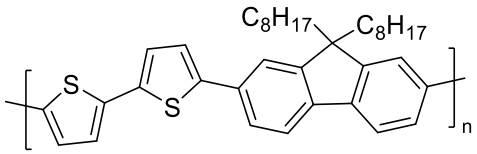

To a flame dried and argon purged vial was added: 2,2'-bithiophene (25.4 mg, 0.150 mmol, 1 equiv) and 9,9'-dioctyl-2,7-dibromofluorene (83.4 mg, 0.150 mmol, 1 equiv), PivOH (15.7 mg, 0.150 mmol, 1 equiv), Cs_2CO_3 (150 mg, 0.45 mmol, 3 equiv), precatalyst (2.3 mg, 0.003 mmol, 2 mol%), and LiO^tBu (.5 mg, 0.006 mmol, 4 mol %). The solids were then freeze dried before the addition of anhydrous toluene (1 mL, 0.15 M). The mixture was then heated to 100 °C and allowed to react for 3 h. The polymer was then precipitated through addition to cold, stirring methanol (20 mL). Solid polymer was then separated through vacuum filtration yielding P1d (72 mg, 87%). Spectral data is consistent with literature values.[59] ^{1}H NMR (300 MHz, TCE, 90 °C): δ7.68 (d, J =7.9 Hz, 2H), 7.69 (d, J =7.7 Hz, 2H), 7.57 (bs, 2H), 7.30 (d, J = 2.8 Hz, 2H), 7.21 (d, J = 2.8 Hz, 2H), 2.13 (m, 4H), 1.21 (m, 6H), 1.10 (m, 18H), 0.90 (t, J = 6.9 Hz, 6H). M_n =17.7 kDa, M_w = 65.3 kDa, PDI = 3.7

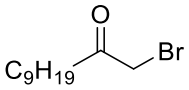

1-bromoundecan-2-one

To an argon purged flame dried round bottom flask, undecan-2-one (6.06 mL, 29.4 mmol, 1.0 equiv) was mixed with methanol (50 mL, 0.6 M) and brought to -10 °C using an ice-salt mixture. Bromine (1.5 mL, 29.7 mmol, 1.0 equiv) was then added and the mixture was stirred for 1 h and then was brought to room temperature and allowed to stir for an additional hour. To this mixture was then added water (10 mL) and concentrated sulfuric acid (17 mL, 18.0

M) and it was stirred for 24 h. The resulting mixture was then vacuum filtered and recrystalized using ethanol to retrieve the product as a white crystal (4.03g, 54%). ^{1}H-NMR ($CDCl_3$, 300 MHz) δ3.90 (s, 2H), δ2.67 (t, J = 7.3 Hz, 2H), δ1.64 (t, J = 6.8, 2H), δ1.29 (s, 14 H), δ0.90 (t, J = 6.4, 3 H).

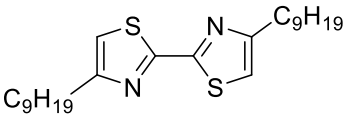

4,4'-dinonyl-2,2'-bithiazole

Above (2.74 g, 11 mmol, 2 equiv) was added to ethanol (50 mL, 0.1 M) and cooled to 0 °C in a round bottom flask in ambient conditions. Thiooxamide was then added (0.6 g, 5 mmol, 1 equiv) and the mixture was then refluxed for 12 h. The resulting solution was then poured into water and extracted with dichloromethane and washed with brine and dried with $MgSO_4$. The product was concentrated then purified by column chromatography (0-10% EtOAc in hexanes) to retrieve (1.64 g, 78%). ^{1}H NMR (300 MHz, $CDCl_3$) δ 6.94 (s, 2H), 2.83 (t, J = 7.5 Hz, 4H), 1.75 (p, J= 7.80, 4H), 1.46 – 1.17 (m, 26H), 0.90 (m, 9H).

4-bromothiazole

2,4-Dibromothiazole (5 g, 20.6 mmol, 1 equiv.) was added to THF (100 mL, 0.2 M) in a flame dried argon purged round bottom flask and brought to -78 °C with a dry ice-acetone bath. n-BuLi (14 mL, 1.6 M, 1.1 equiv.) was then added and the resulting mixture was left to stir for 30 mins. Methanol (2.1 mL, 51.5 mmol, 2.5 equiv) was then added dropwise to quench the solution which was then allowed to come to room temperature. The resulting mixture was then

filtered through a silica plug with 9:1 hexanes:EtOAc and the product was retrieved as a clear liquid (3.52 g, 92%)

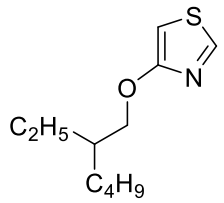

4-((2-ethylhexyl)oxy)thiazole

NaH (0.48 g, 12.2 mmol, 2 equiv) and THF (12.2 mL, 0.5M) were added to a flame dried round bottom flash. 2-Ethylhexanol (1.9 mL, 12.2 mmol, 2 equiv) was added dropwise over 5 mins and allowed to stir for 2 h. Above (1 g, 6.10 mmol, 1 equiv) and CuI (0.23 g, 1.22 mmol, 0.2 equiv) were then added and the mixture was brought to reflux in an open atmosphere for 12 h. The resulting mixture was filtered through Celite and washed with 10% NaOH (40 mL) before being dried with $MgSO_4$ and concentrated. The crude product was then purified through column chromatography (0-5% EtOAc in hexanes) to yield a yellow oil (0.71 g, 54%). ^{1}H NMR (300 MHz, $CDCl_3$) δ 8.53 (d, J = 1.8 Hz, 1H), 6.10 (d, J = 2.1 Hz, 1H), 3.99 (d, J = 5.7 Hz, 2H), 1.74 (tt, J = 12.2, 6.0 Hz, 1H), 1.39 (m, 10H), 0.90 (m, 8H).

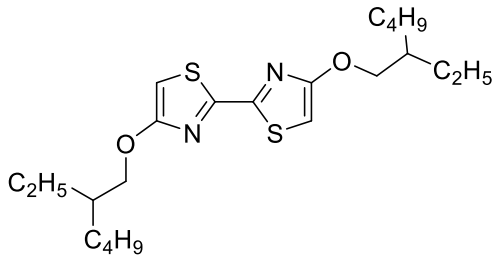

4,4'-bis((2-ethylhexyl)oxy)-2,2'-bithiazole

To a flame dried argon purged pressure vessel was added above (0.71 g, 3.3 mmol, 1 equiv) and $Cu(OAc)_2$ (0.31 g, 1.68 mmol, 0.5 equiv). These were solubilized in xylenes (11.3 mL, 0.3 M) and brought to reflux and allowed to stir for 48 h. The resulting product was then concentrated and purified via column chromatography (0-5% EtOAc in hexanes) to yield (152 mg, 23%). ^{1}H NMR (300 MHz, $CDCl_3$) δ 6.19 (s, 2H), 4.03 (d, J = 5.3 Hz, 4H), 1.79 (s, 2H), 1.45 (m, 18H), 0.96 (m, 14H).

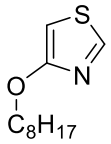

4-(octyloxy)thiazole

NaH (0.24 g, 6.10 mmol, 2 equiv) and THF (6.1 mL, 0.5 M) were added to a flame dried round bottom flash. Octanol (0.95 mL, 6.1 mmol, 2 equiv) was added dropwise over 5 mins and allowed to stir for 2 h. 4-Bromothiazole (0.5 g, 3.05 mmol, 1 equiv) and CuI (0.12 g, 0.61 mmol, 0.2 equiv) were then added and the mixture was brought to reflux in open atmosphere for 12 h. The resulting mixture was filtered through Celite and washed with 10% NaOH (40 mL) before being dried with $MgSO_4$ and concentrated. The crude product was then purified through column chromatography (0-5% EtOAc in hexanes) to yield a yellow oil (0.25 g, 52%) ^{1}H NMR (300 MHz, $CDCl_3$) δ 8.53 (d, J = 2.3 Hz, 1H), 6.11 (d, J = 2.3 Hz, 1H), 4.11 (t, J = 6.5 Hz, 2H), 1.80 (p, J = 6.66 2H), 1.47 (p, J = 6.66, 2H), 1.28 (m, 9H), 0.88 (t, J = 6.6 Hz, 3H).

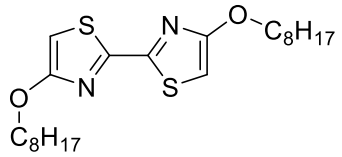

4,4'-bis(octyloxy)-2,2'-bithiazole

To a flame dried argon purged pressure vessel was added above (170 mg, 0.80 mmol, 1 equiv) and $Cu(OAc)_2$ (29 mg, 0.16 mmol, 0.2 equiv). These were solubilized in xylenes (4 mL, 0.2 M) and brought to reflux and allowed to stir for 48 h. The resulting product was then concentrated and purified via column chromatography (0-5% EtOAc in hexanes) to yield (80 mg, 46%) ^{1}H NMR (300 MHz, $CDCl_3$) δ 6.19 (s, 2H), 4.14 (t, J = 6.5 Hz, 4H), 1.83 (dt, J = 14.7, 6.6 Hz, 2H), 1.40 (M, 21H), 0.90 (m, 6H).

General Procedure

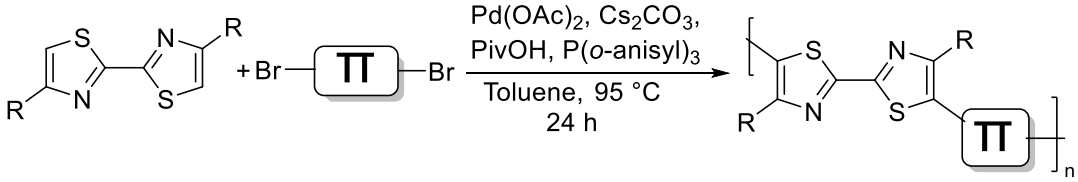

To a dried round bottom flask was added $Pd(OAc)_2$ (2.3 mg, 8 mol %), Cs_2CO_3 (133 mg, 0.36 mmol, 3 equiv), tris(*o*-methoxyphenyl)phosphine (8 mg, 16 mol %), PivOH (13 mg, 0.13 mmol, 1 equiv), the dibromoaryl spacer (0.13 mmol, 1 equiv) and the bithiazole (54 mg, 0.13 mmol, 1 equiv). This mixture was solubilized in anhydrous toluene (1.3 mL, 0.1 M) and sealed. The mixture was then stirred at 95 °C for 24 h. The resulting mixture was then cooled to room temperature and added dropwise to cooled, stirring, methanol (20 mL). The precipitate was then separated via suction filtration.

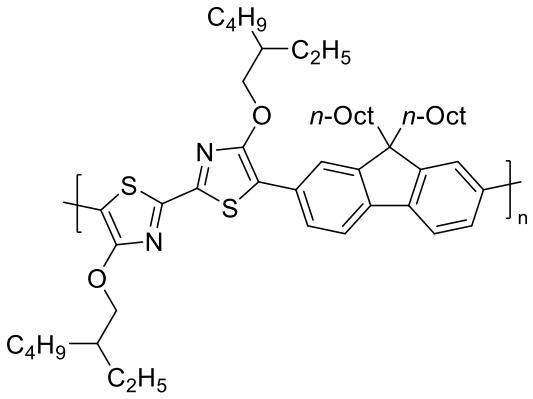

Prepared according to the General Procedure using 9,9'-dioctyl-2,7-dibromofluorene (71 mg, 0.13 mmol, 1 equiv) and 4,4'-bis((2-ethylhexyl)oxy)-2,2'-bithiazole (54mg, 0.13mmol, 1 equiv). The reaction yielded a black polymer PT1 (105 mg, quant.). ^{1}H NMR (300 MHz, $CDCl_3$) δ 7.93 (s, 2H), 7.73 (s, 4H), 4.53 (s, 4H), 2.04 (s, 13H), 1.59 (s, 7H), 1.52 – 0.88 (m, 52H), 0.83 (s, 15H). M_n = 11.7 kDa, M_w = 46.8 kDa, PDI = 4.

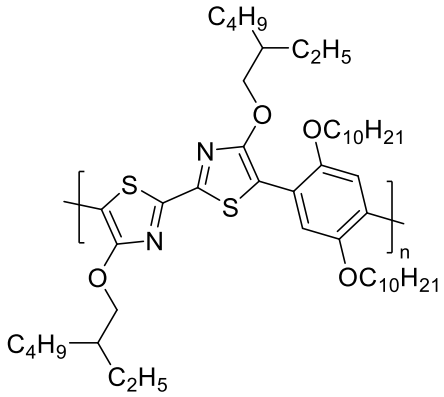

Prepared according to the General Procedure using 1,4-dibromo-2,5-bis(decyloxy)benzene (110 mg, 0.20 mmol, 1 equiv) and 4,4'-bis((2-ethylhexyl)oxy)-2,2'-bithiazole (85 mg, 0.20 mmol, 1 equiv). The reaction yielded a black polymer PT2 (162 mg, quant.). 1H NMR (300 MHz, $CDCl_3$) δ 8.07 (s, 2H), 4.53 (d, J = 4.2 Hz, 4H), 4.18 (s, 2H), 2.02 (s, 4H), 1.84 (s, 2H), 1.71 – 1.20 (m, 58H), 0.96 (m, 18H). M_n = 13.6 kDa, M_w = 27.2 kDa, PDI = 2.0.

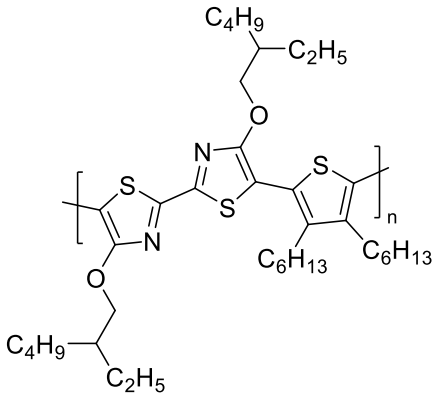

Prepared according to the General Procedure using 2,5-dibromo-3,4-dihexylthiophene (65 μL, 0.20 mmol, 1 equiv) and 4,4'-bis((2-ethylhexyl)oxy)-2,2'-bithiazole (85 mg, 0.20 mmol, 1 equiv). The reaction yielded a black polymer PT3 (116 mg, 86%.) ^{1}H NMR (300 MHz, $CDCl_3$) δ 4.41 (d, J = 5.5 Hz, 4H), 2.76 (4s, H), 1.82 (2s, 1H), 1.40 (m, 32H), 1.11 – 0.76 (m, 22H). M_n = 8.7 kDa, M_w = 16.7 kDa, PDI = 1.9.

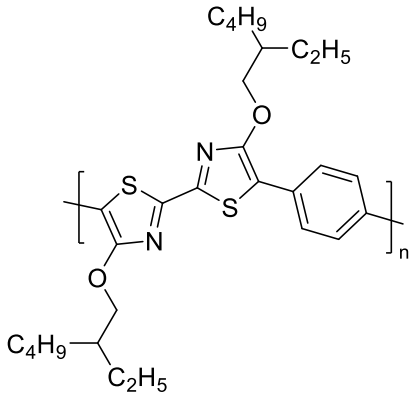

Prepared according to the General Procedure using 1,4-dibromobenzene (30.7 mg, 0.13 mmol, 1 equiv) and 4,4'-bis((2-ethylhexyl)oxy)-2,2'-bithiazole (54 mg, 0.13 mmol, 1 equiv). The reaction yielded a black polymer PT4 (59 mg, 83%). ^{1}H NMR (300 MHz, $CDCl_3$) δ 7.62 (m, 4H), 4.46 (s, 4H), 1.85 (s, 3H), 1.36 (m, 19H), 1.23 – 0.78 (m, 12H). M_n = 3.2 kDa, M_w = 5.6 kDa, PDI = 1.8.

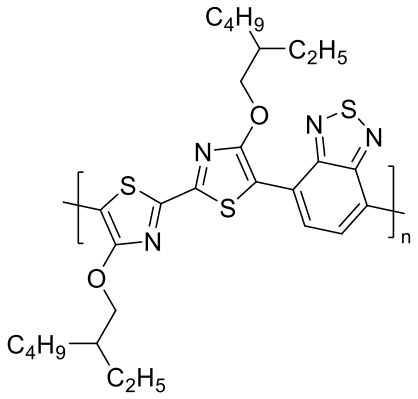

Prepared according to the General Procedure using 4,7-dibromo[c]-1,2,5-thiadiazole (38.2 mg, 0.13 mmol, 1 equiv) and 4,4'-bis((2-ethylhexyl)oxy)-2,2'-bithiazole (54 mg, 0.13mmol, 1 equiv). The reaction yielded a black polymer PT5 (59 mg, 77%). ^{1}H NMR (300 MHz, $CDCl_3$) δ 8.46 (s, 1H), 7.90 (s, 1H), 4.65 (s, 4H), 1.23 (m, 35H). M_n = 2.2 kDa, M_w = 4.5 kDa, PDI = 2.1.

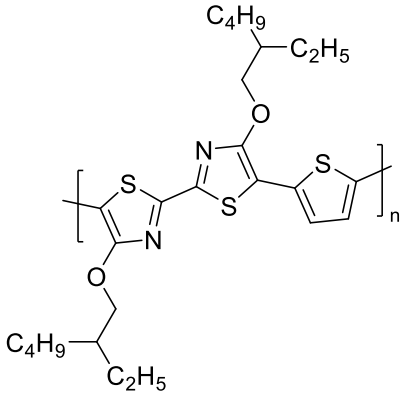

Prepared according to the General Procedure using 2,4-dibromothiophene (31.5 mg, 0.13 mmol, 1 equiv) and 4,4'-bis((2-ethylhexyl)oxy)-2,2'-bithiazole ((54 mg, 0.13 mmol, 1 equiv). The reaction yielded a black polymer PT6 (67 mg, 88%). ^{1}H NMR (300 MHz, $CDCl_3$) δ 6.99 (s, 2H), 4.46 (s, 4H), 1.85 (s, 2H), 1.50 (m, 24H), 0.99 (m, 14H). M_n = 3.4 kDa, M_w = 5.3 kDa, PDI = 1.6.

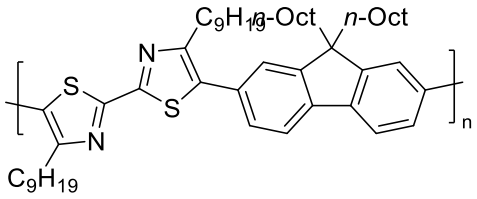

Prepared according to the General Procedure using 9,9'-dioctyl-2,7-dibromofluorene (71 mg, 0.13 mmol, 1 equiv) and 4,4'-bis((2-ethylhexyl)oxy)-2,2'-bithiazole (54 mg, 0.13 mmol, 1 equiv). The reaction yielded a black polymer PT7 (79 mg, quant.). ^{1}H NMR (300 MHz, $CDCl_3$) δ 7.82 (d, J = 7.5 Hz, 2H), 7.51 (s, 2H), 7.19 (d, J = 8.4 Hz, 2H), 3.51 (d, J = 5.2 Hz, 8H), 2.94 (s, 4H), 2.06(s, 4H), 1.85(s, 4H) 1.28 (s, 24H), 1.12 (s, 16H), 0.97 – 0.76 (m, 18H). M_n = 13.7 kDa, M_w = 24.8 kDa, PDI = 1.8.

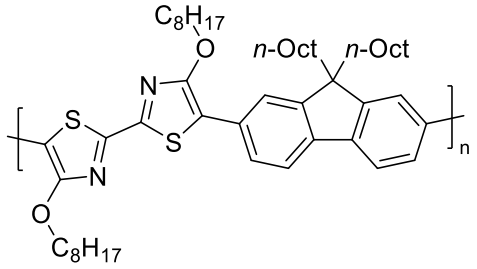

Prepared according to the General Procedure using 9,9'-dioctyl-2,7-dibromofluorene (71 mg, 0.13 mmol, 1 equiv) and 4,4'-bis((2-octyl)oxy)-2,2'-bithiazole (54 mg, 0.13 mmol, 1 equiv). The reaction yielded a black polymer PT8 (105 mg, quant.) M_n = 10.4 kDa, M_w = 22.1 kDa, PDI = 2.1.

Nuclear Magnetic Resonance

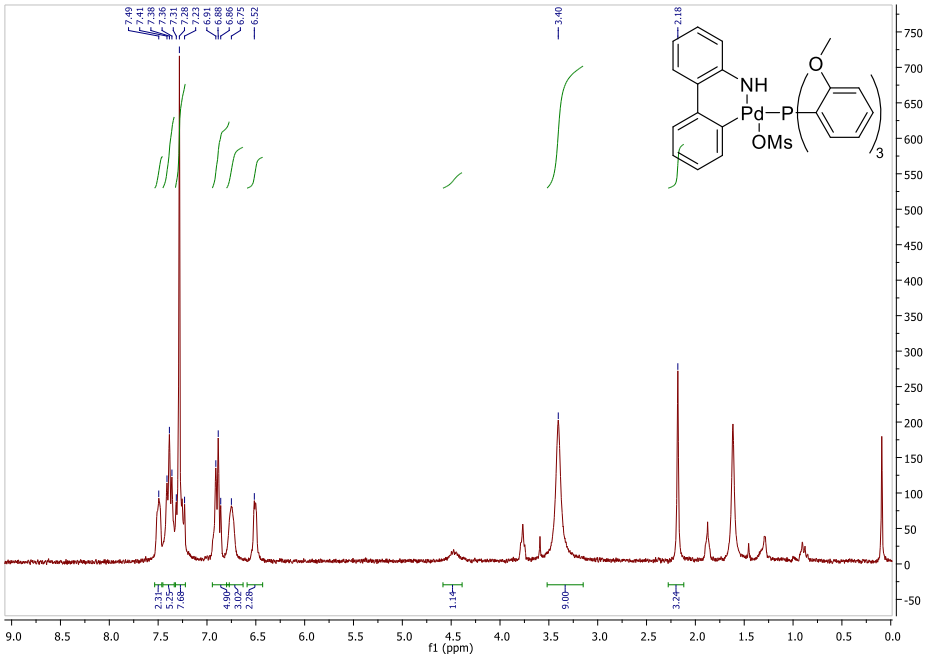

Appendix Figure 1: ^{1}H NMR of Precatalyst

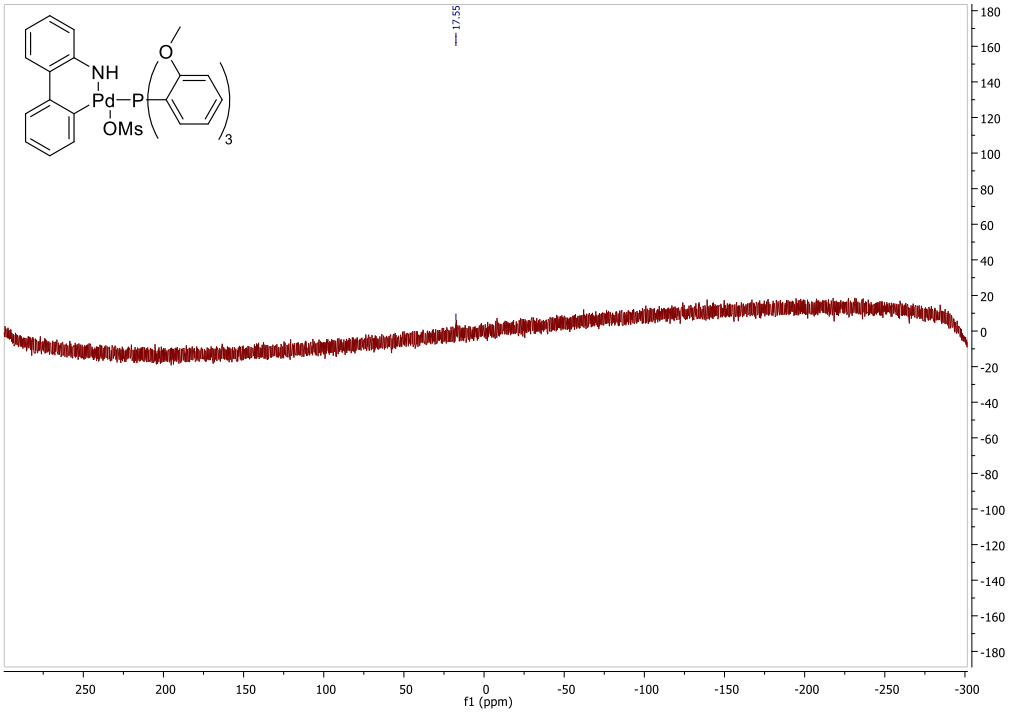

Appendix Figure 2: ^{31}P NMR of Precatalyst

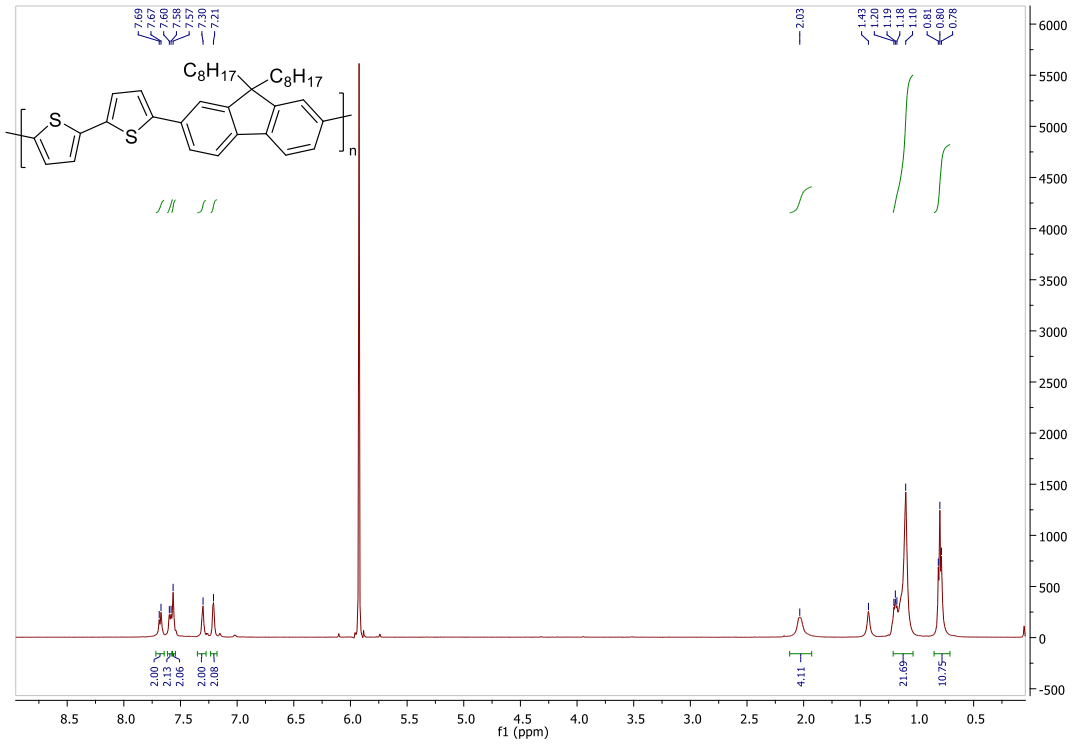

Appendix Figure 3: ^{1}H NMR of P1a

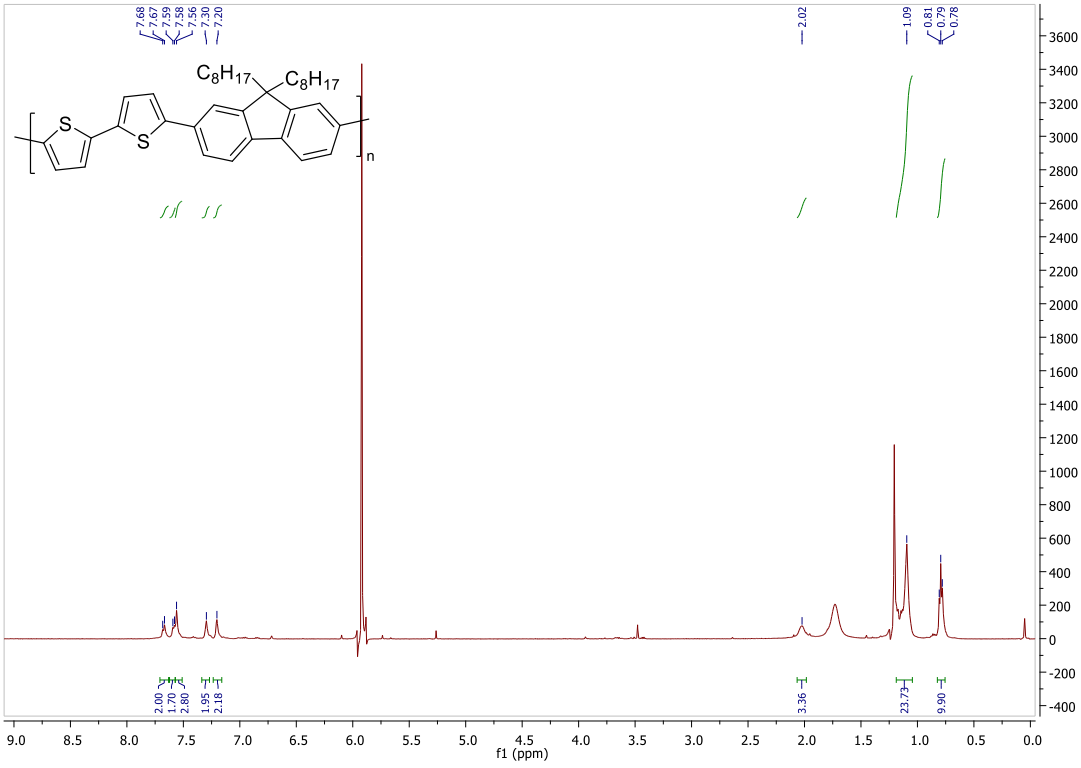

Appendix Figure 4: ^{1}H NMR of P1b

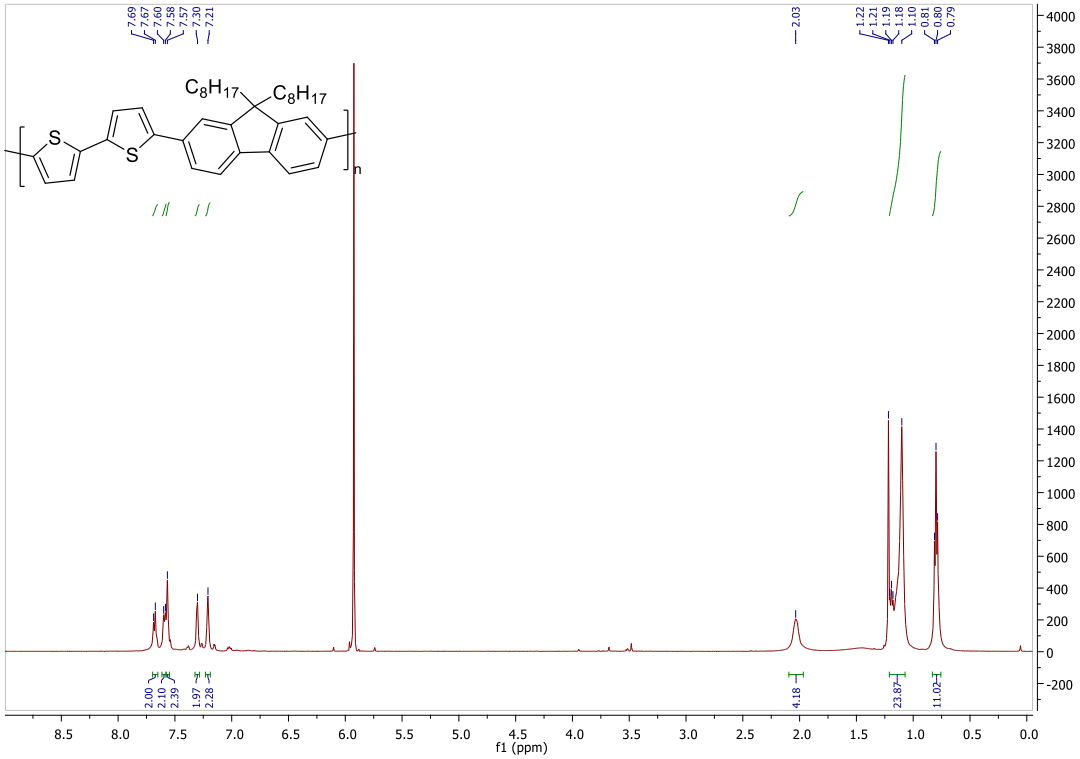

Appendix Figure 5: ^{1}H NMR of P1c

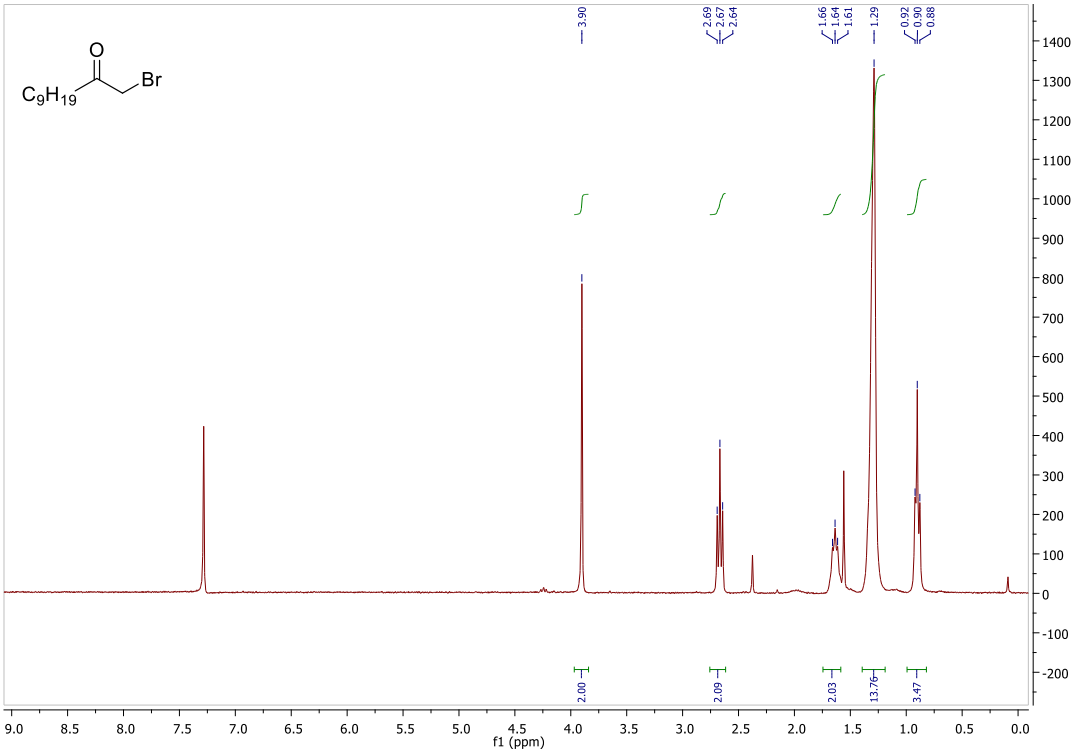

Appendix Figure 6: ^{1}H NMR of 1-bromo-2-undecanone

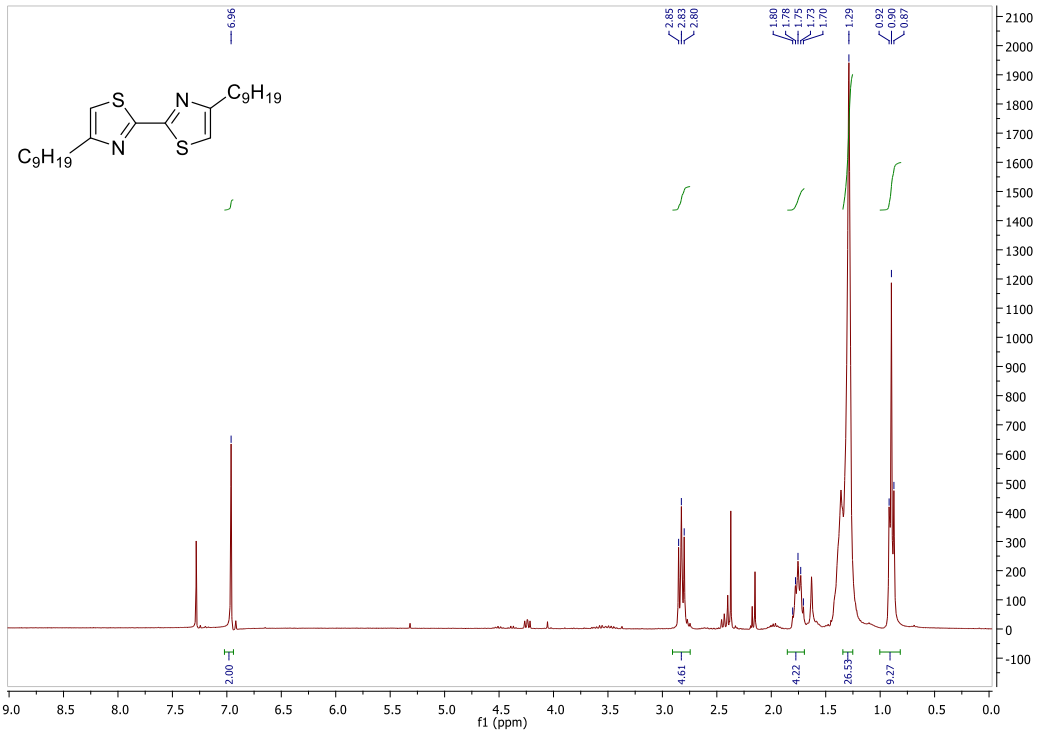

Appendix Figure 7: ^{1}H NMR of 4,4'-dinonyl-2,2'-bithiazole

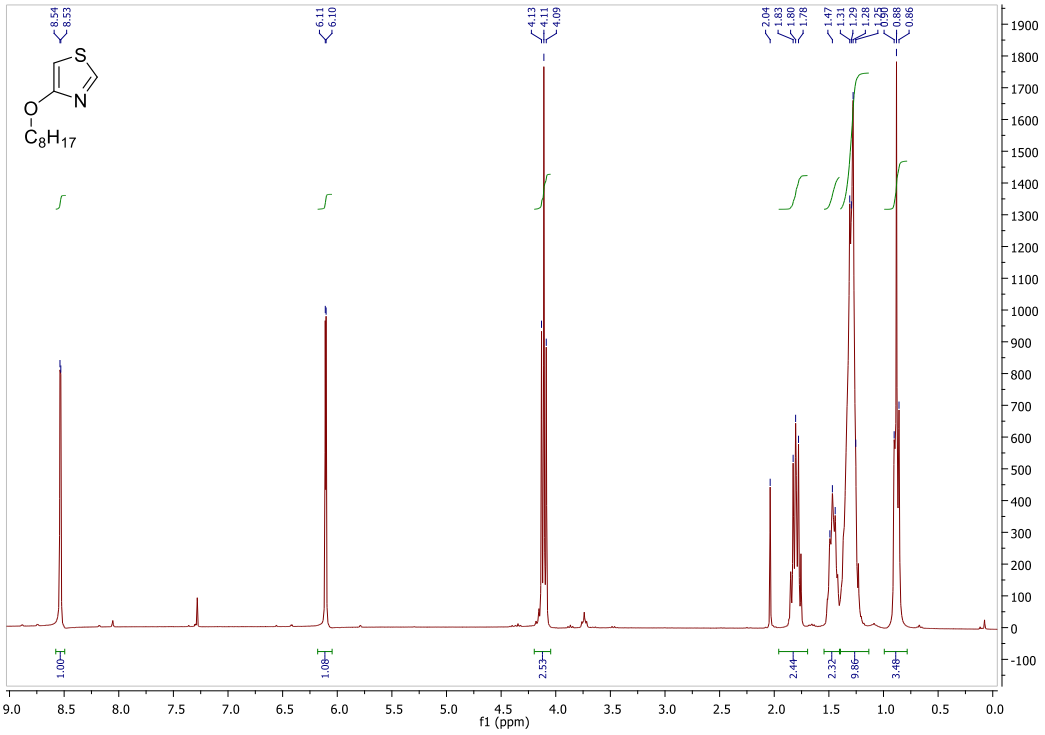

Appendix Figure 8: ^{1}H NMR of 4-(octyloxy)thiazole

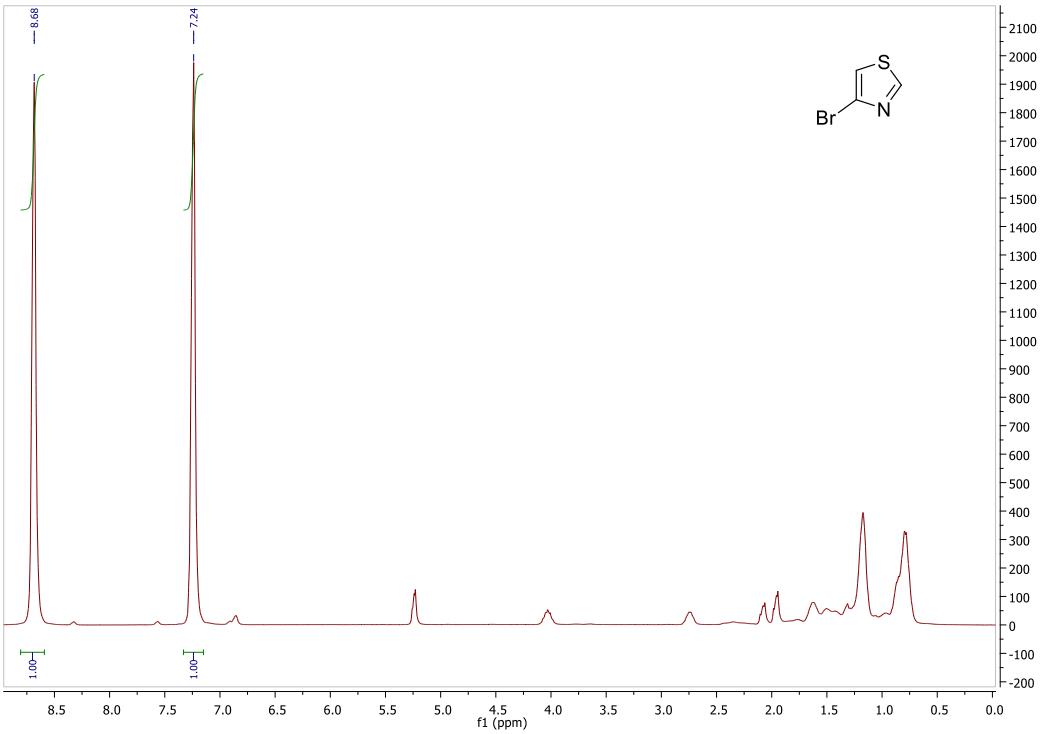

Appendix Figure 9: ^{1}H NMR of 4-bromothiazole

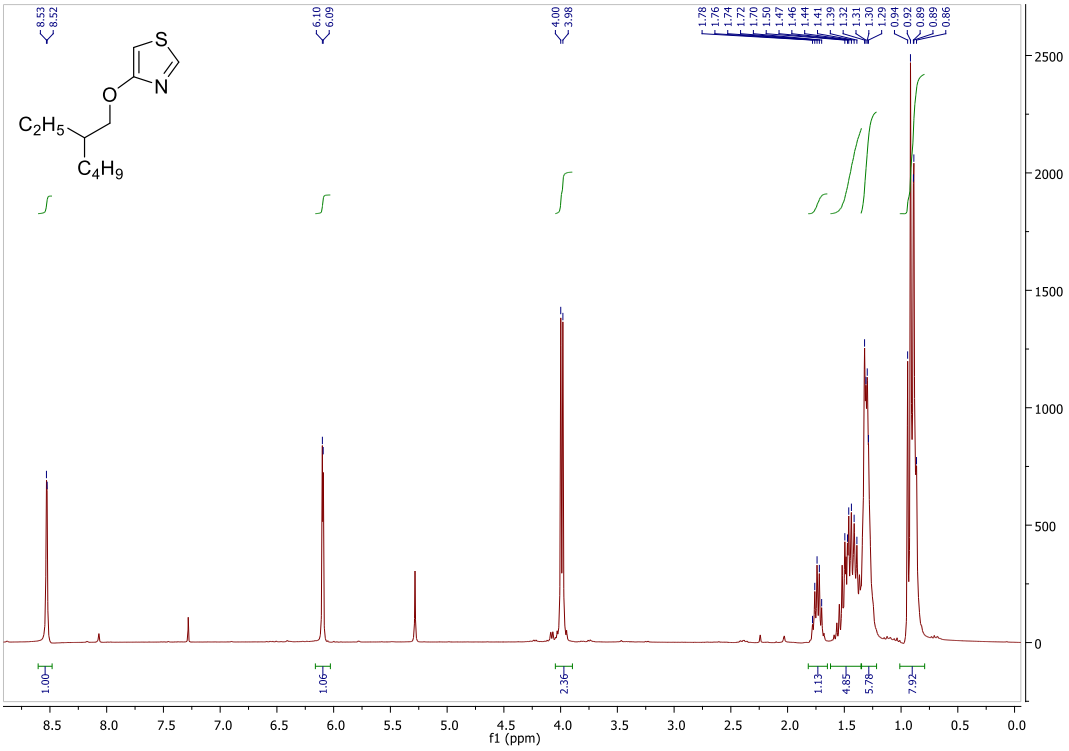

Appendix Figure 10: ^{1}H NMR of 4-((2-ethylhexyl)oxy)thiazole

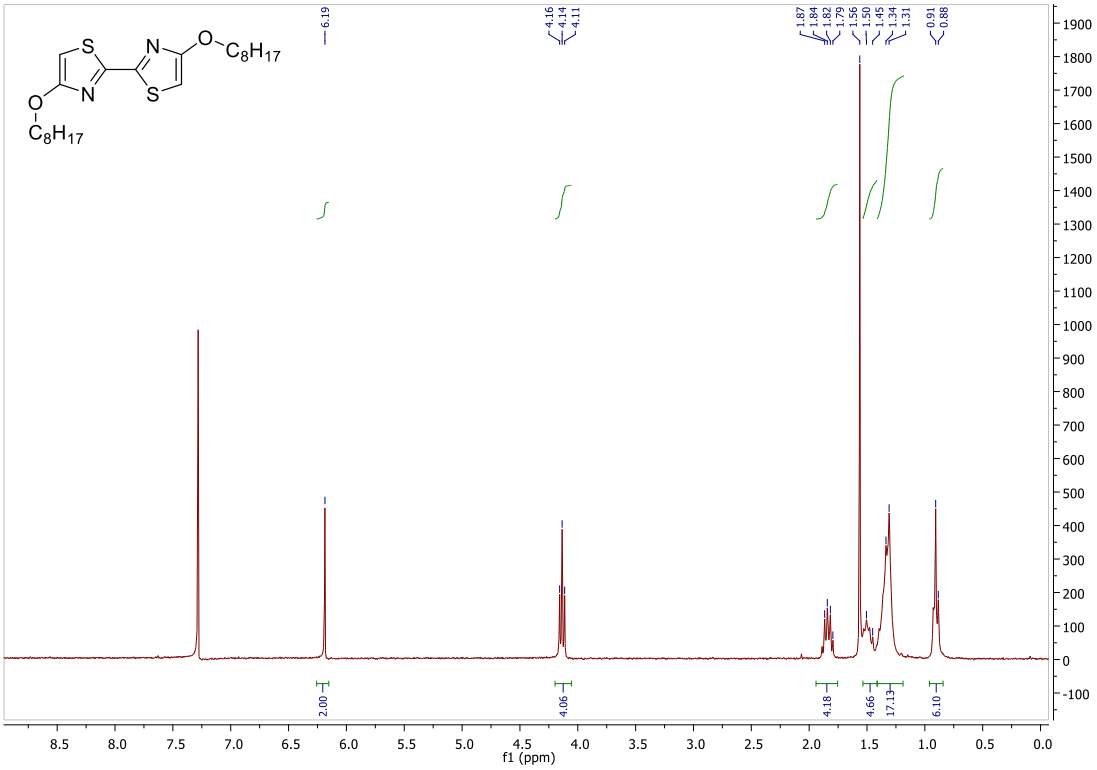

Appendix Figure 11: ^{1}H NMR of 4,4'-bis(octyloxy)-2,2'-bithiazole

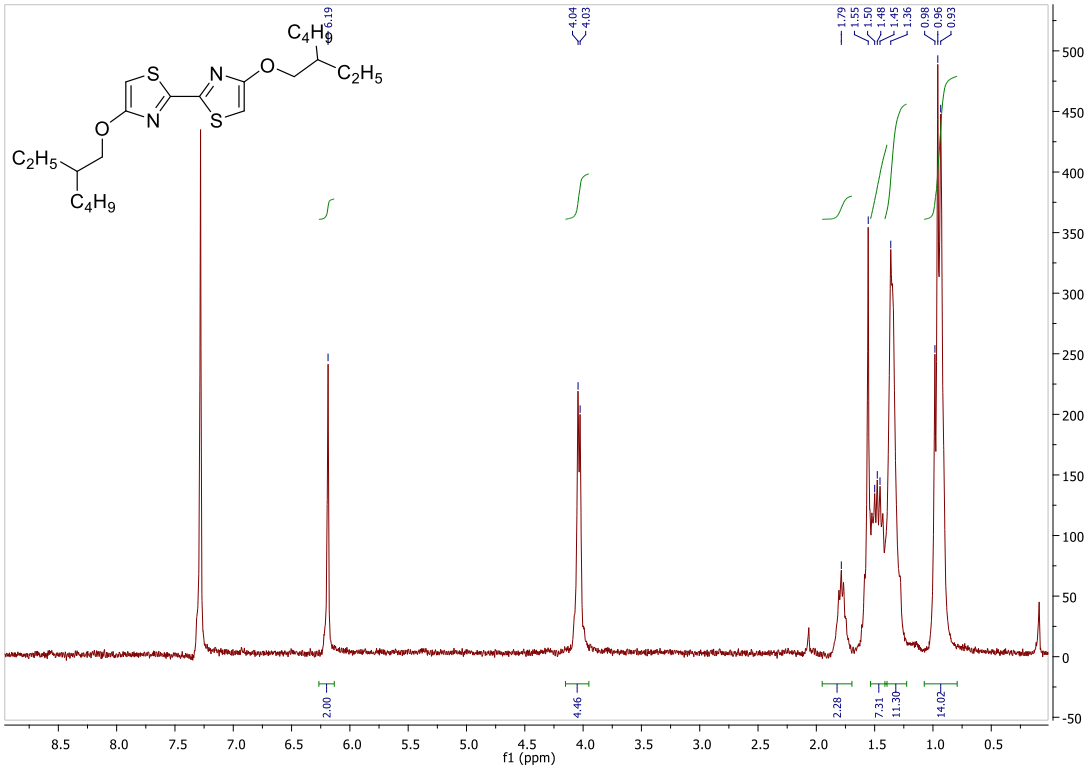

Appendix Figure 12: ^{1}H NMR of 4,4'-bis((2-ethylhexyl)oxy)-2,2'-bithiazole

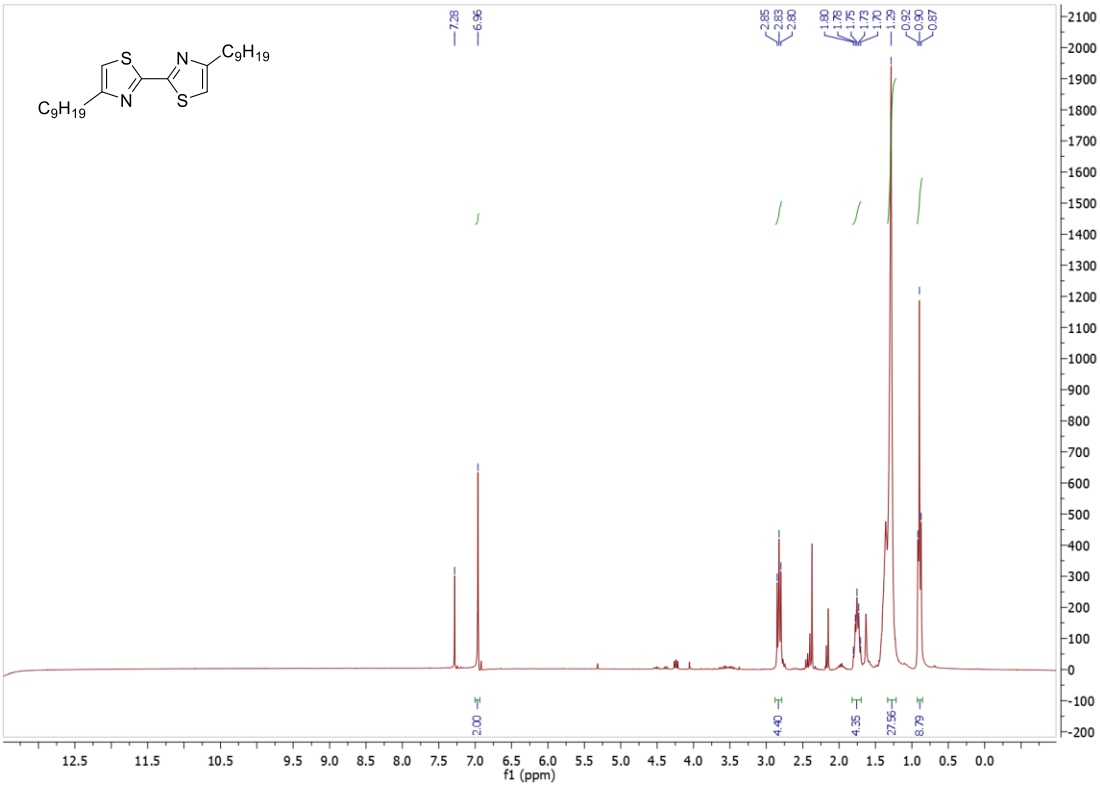

Appendix Figure 13: ^{1}H NMR 4,4'-dinonyl-2,2'-bithiazole

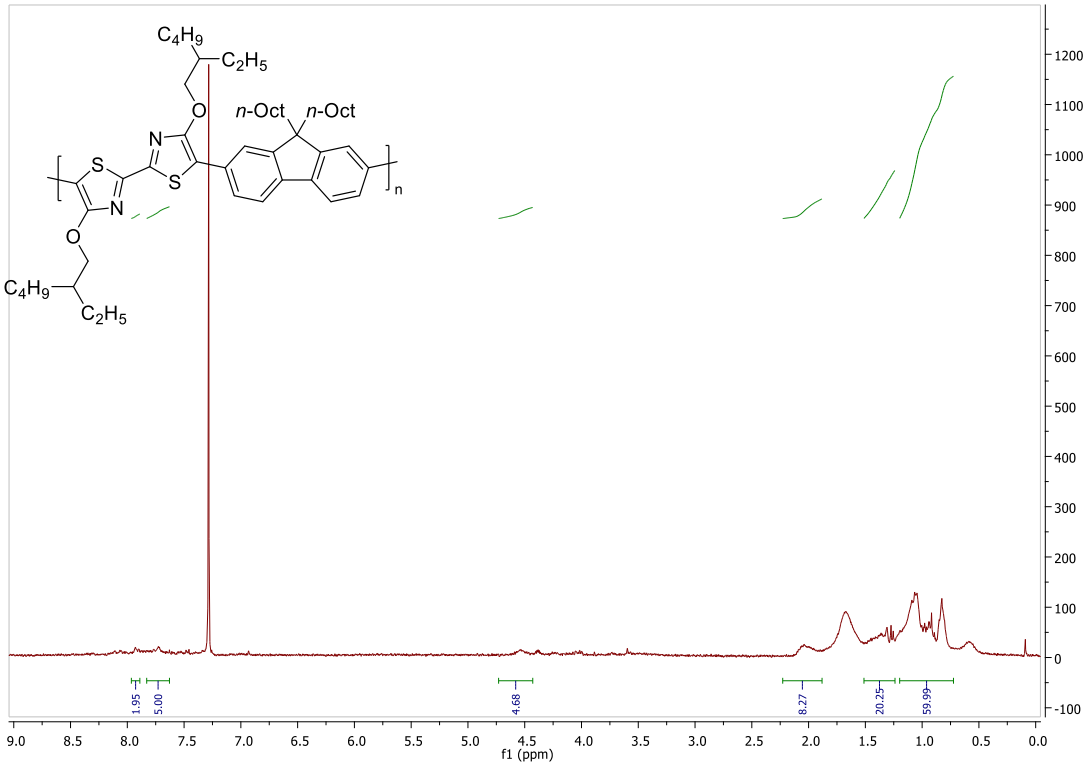

Appendix Figure 14: ^{1}H NMR of PT1

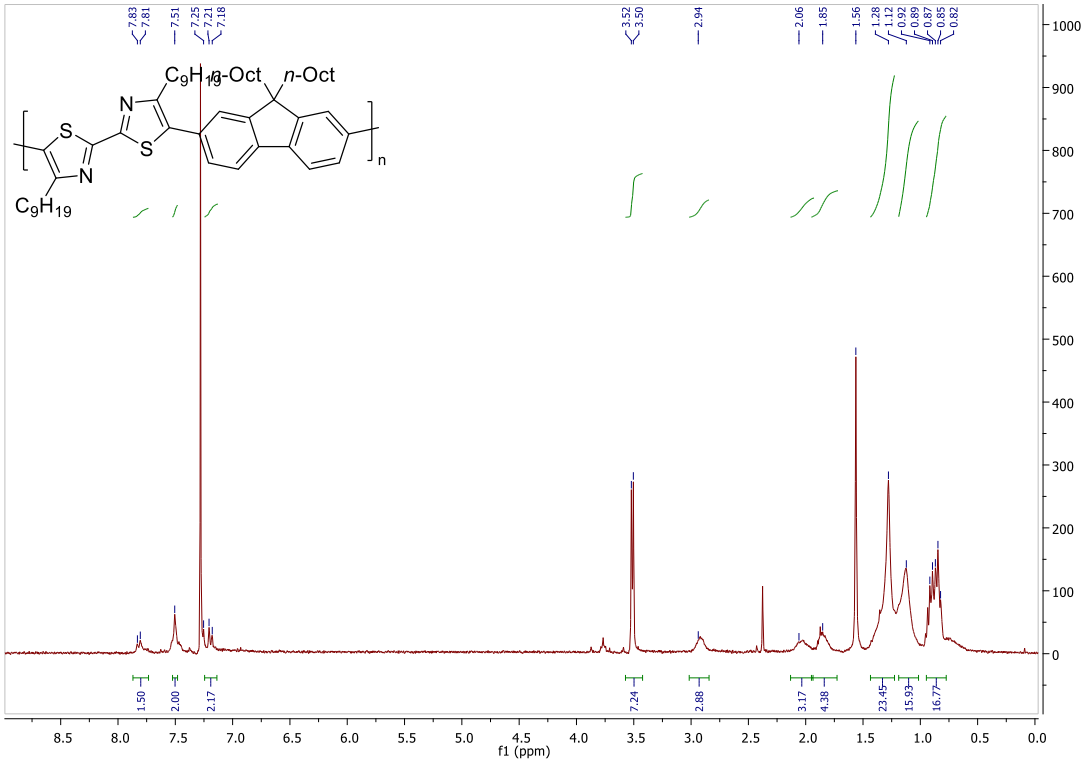

Appendix Figure 15: ^{1}H NMR of PT7

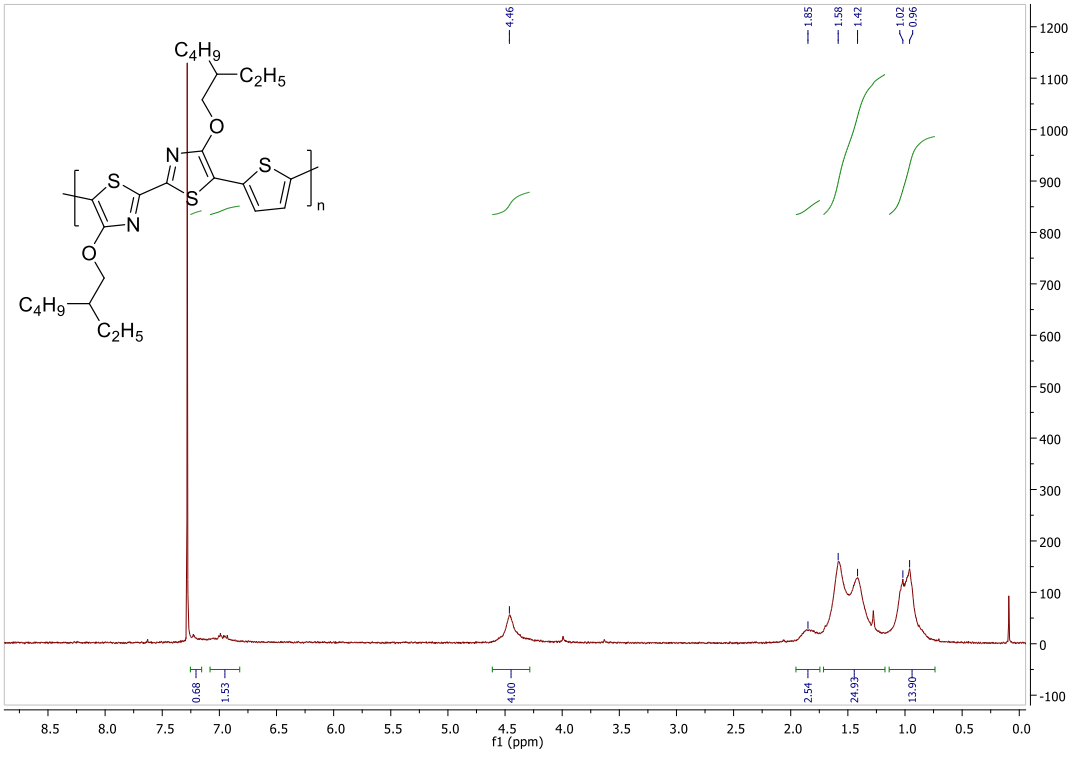

Appendix Figure 16: ^{1}H NMR of PT6

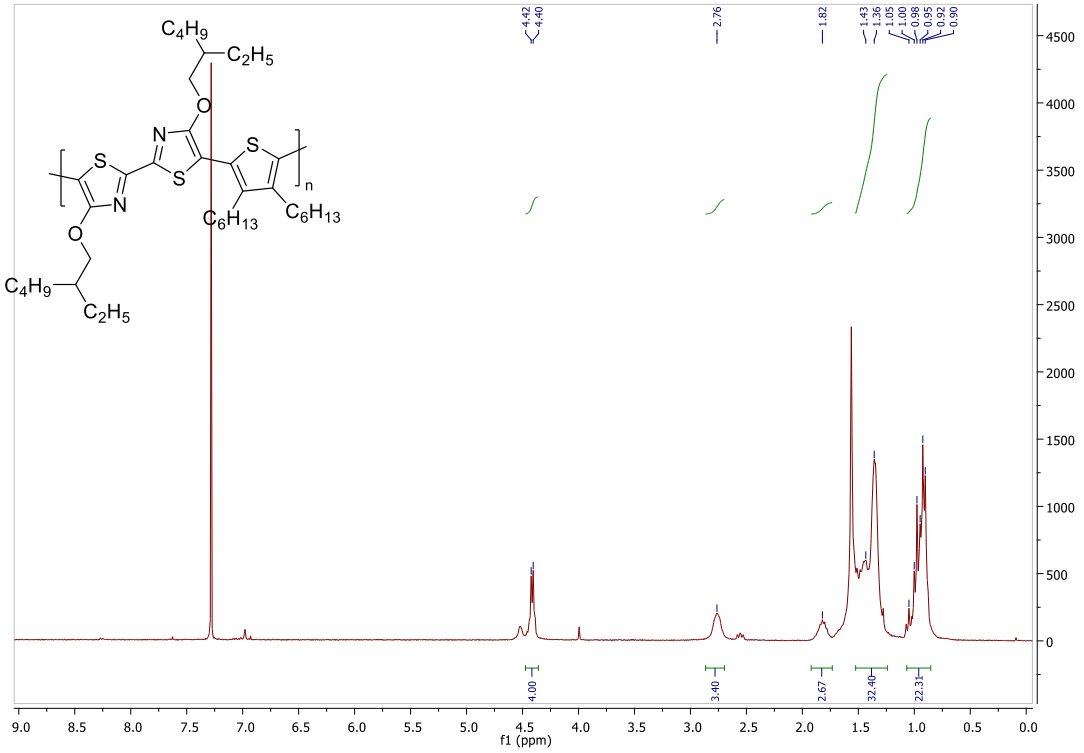

Appendix Figure 17: ^{1}H NMR of PT3

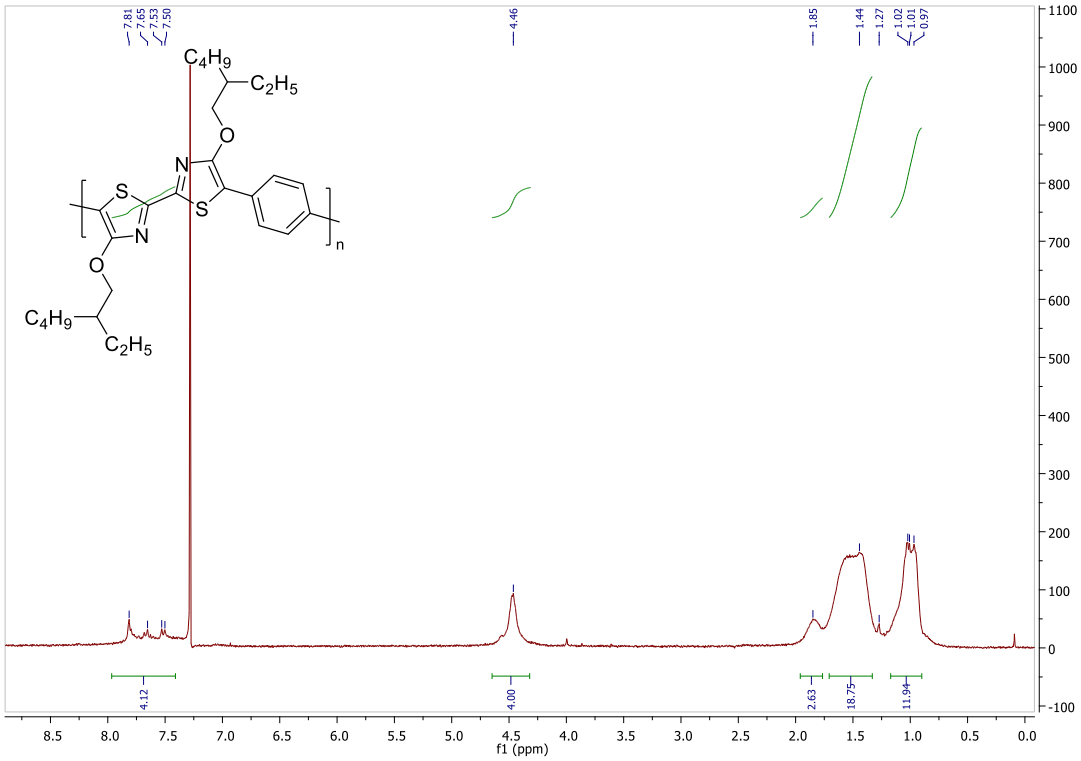

Appendix Figure 18: ^{1}H NMR of PT4

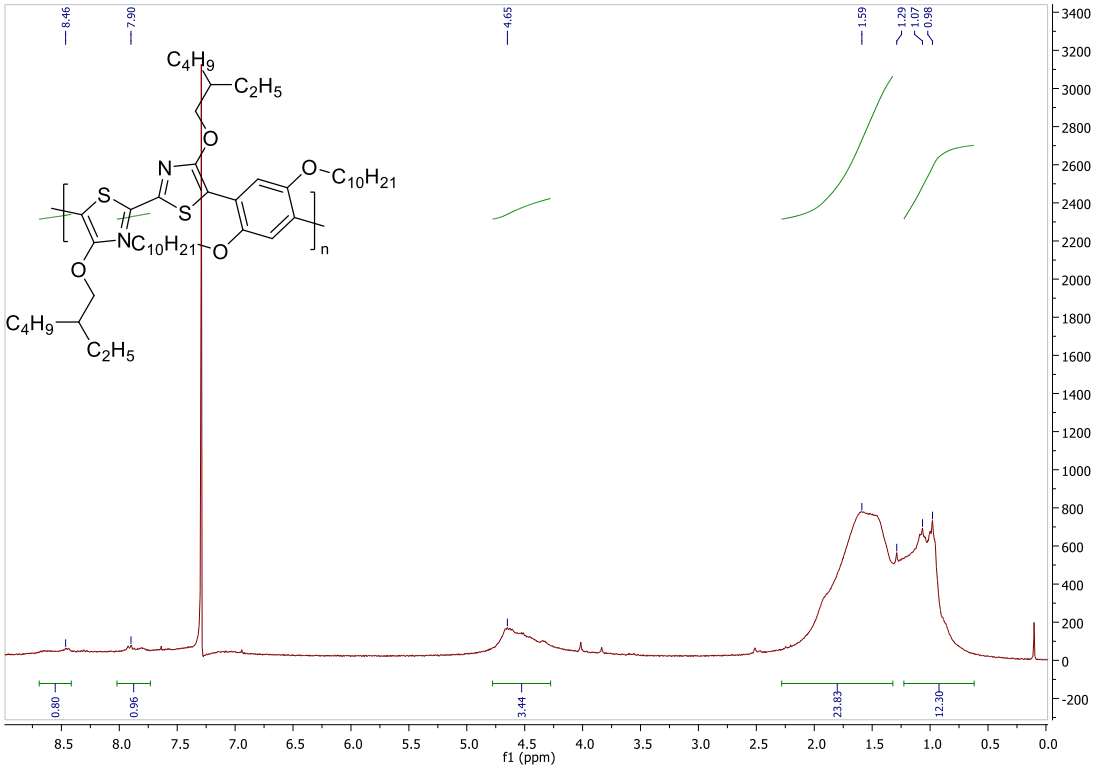

Appendix Figure 19: ^{1}H NMR of PT2

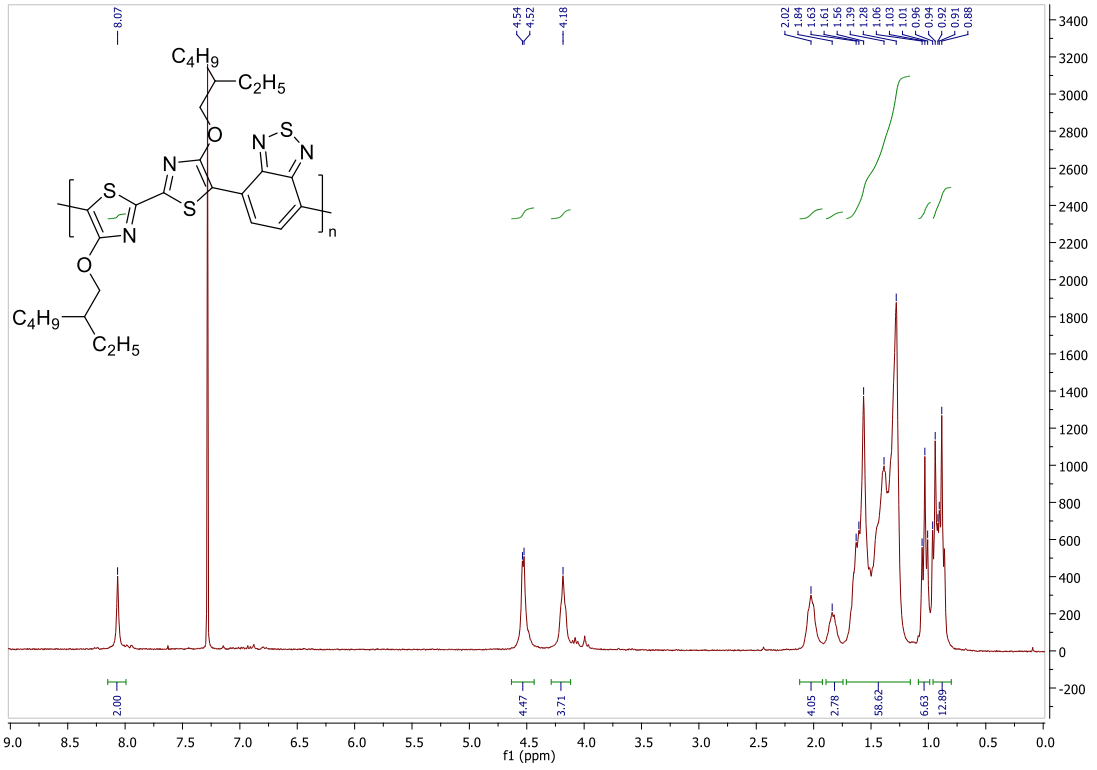

Appendix Figure 20: ^{1}H NMR of PT5

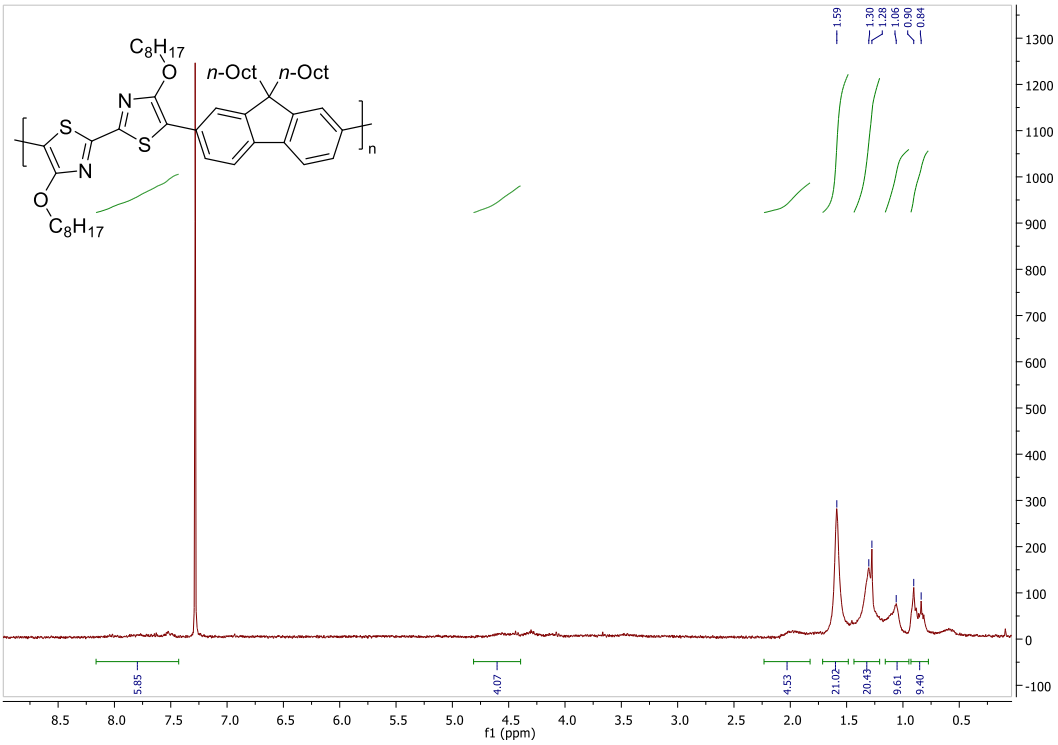

Appendix Figure 21: ^{1}H NMR of PT8

Gel Permeation Chromatography

Number-average (M_n) and weight-average (M_w) molecular weights were determined through the use of size exclusion chromatography with a Viscotek GPCmax VE2001 at 35 °C. The detector used was a VE 3580 RI detector and the columns used were two PAS-104 Styrene-Divinylbenzene gel columns. The polymers were eluted using tetrahydrofuran (THF) at a flow rate of 1 mL/min. Molecular weights were determined through comparison to an external polystyrene calibration curve. Samples were prepared in concentrations of 2 mg/mL before being filtered through 0.22 μM PTFE filters into 1 mL chromatography vials. All GPC data has been normalized.

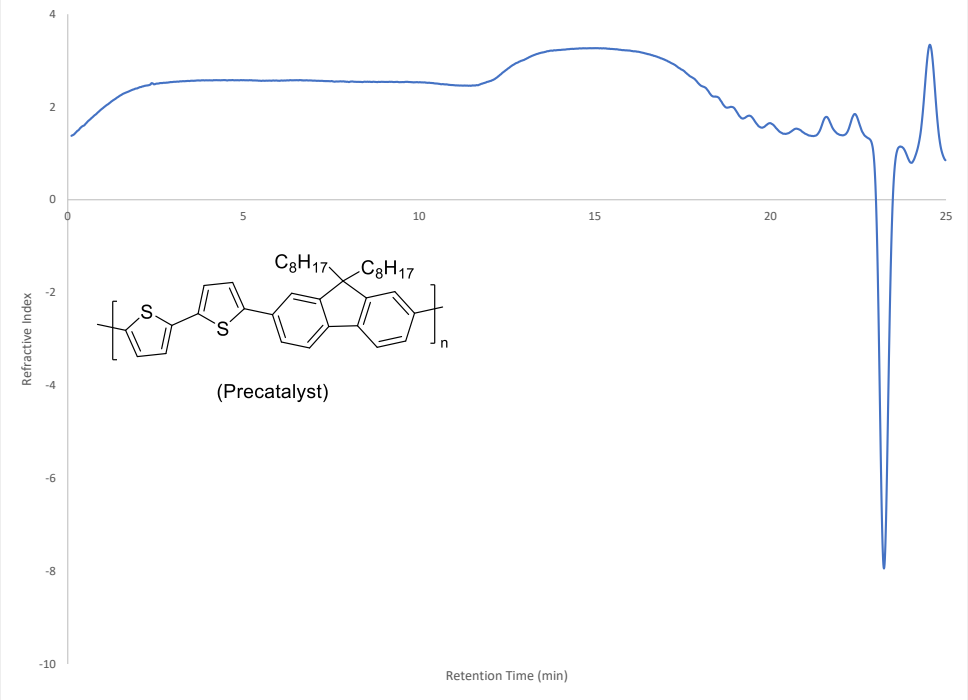

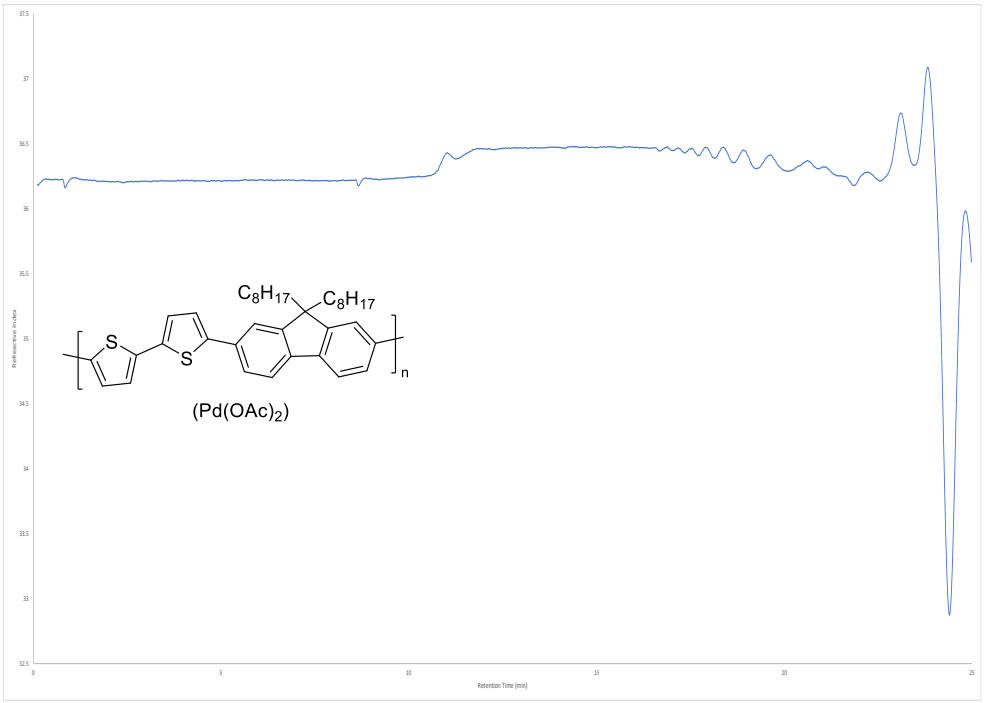
C_8H_{17}
C_8H_{17}
S
S
n
$(Pd(OAc)_2)$

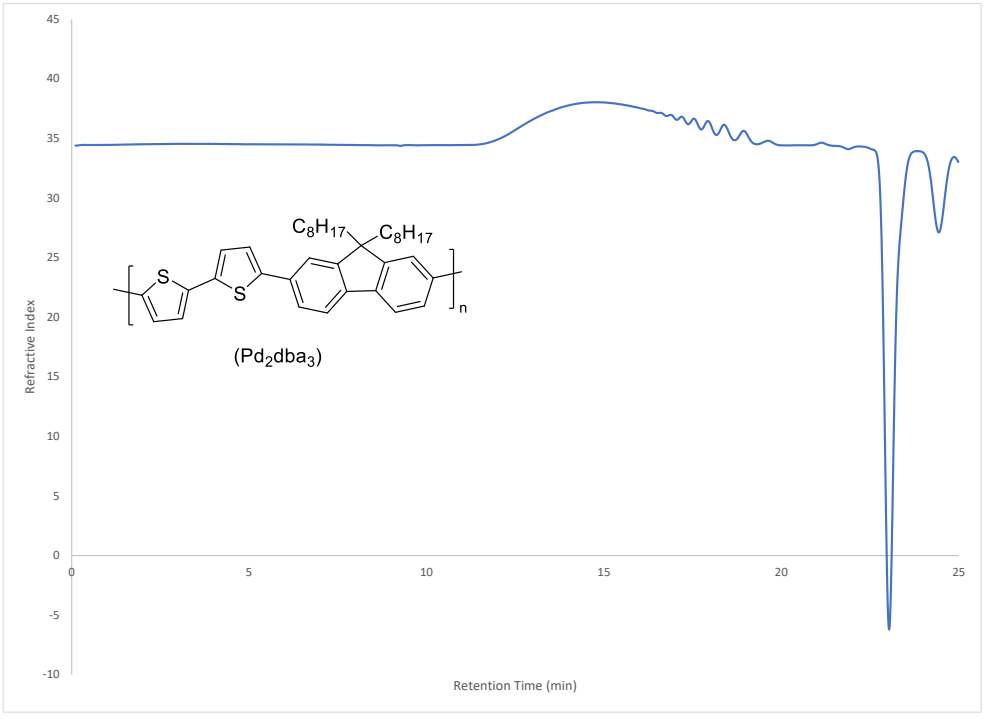
45
40
35
30
25
20
15
10
5
0
-5
-10
Refractive Index
0
5
10
15
20
25
Retention Time (min)
C_8H_{17}
C_8H_{17}
S
S
n
(Pd_2dba_3)

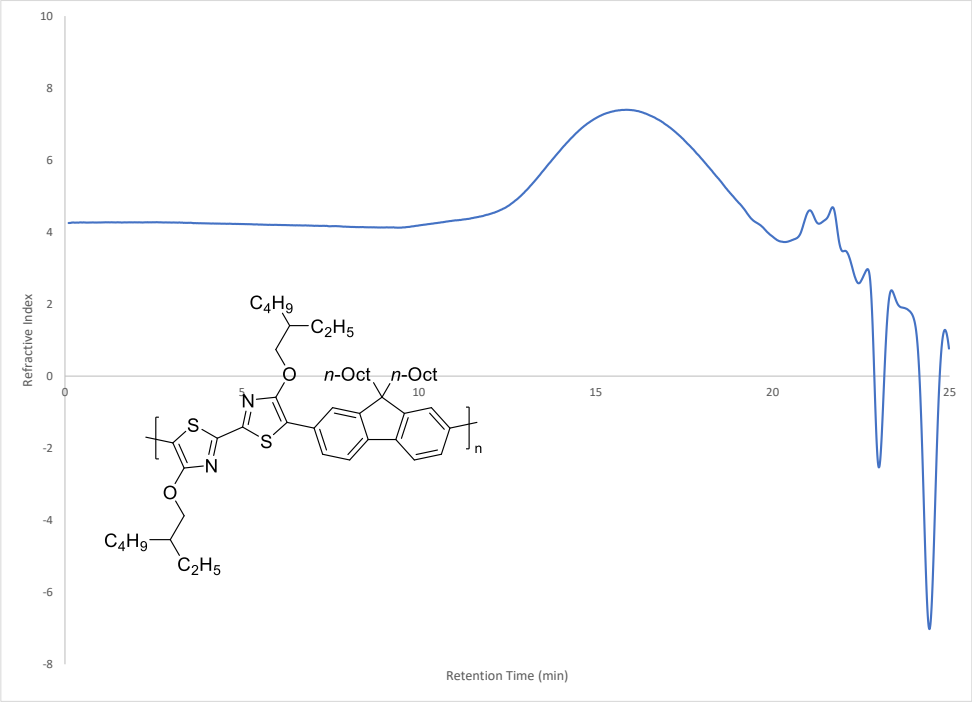
Refractive Index
Retention Time (min)
n-Oct
n-Oct

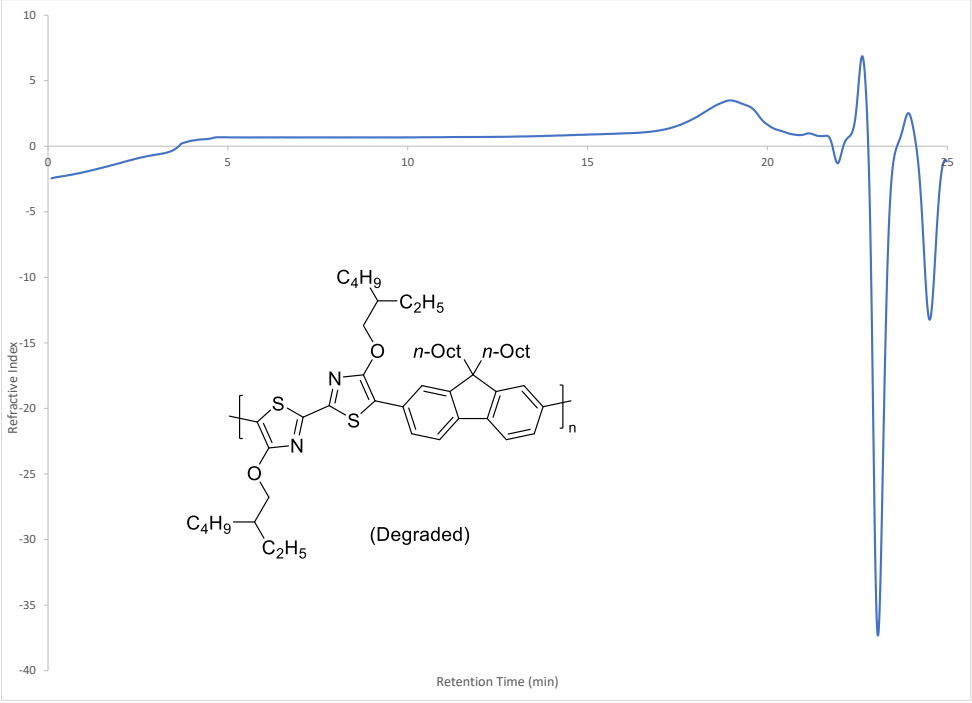
Refractive Index
Retention Time (min)
n-Oct
n-Oct
(Degraded)

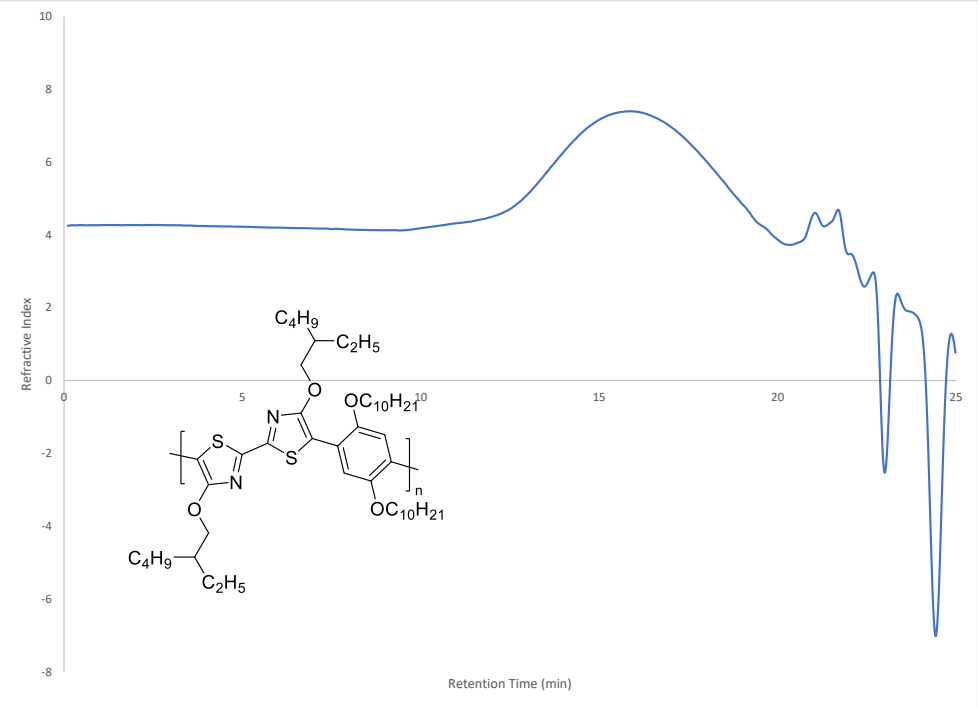
Refractive Index
Retention Time (min)
10
8
6
4
2
0
-2
-4
-6
-8
0
5
10
15
20
25
C_4H_9
C_2H_5
O
N
S
S
N
O
$OC_{10}H_{21}$
n
$OC_{10}H_{21}$
C_4H_9
C_2H_5

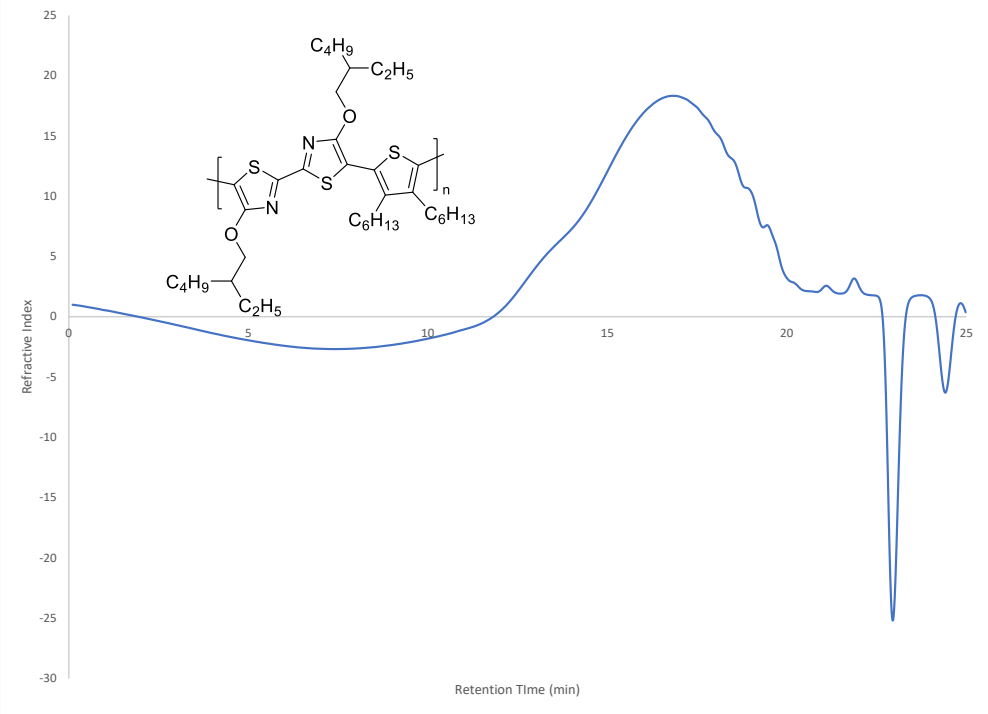
Refractive Index
Retention TIme (min)
25
20
15
10
5
0
-5
-10
-15
-20
-25
-30
0
5
10
15
20
25
C_4H_9
C_2H_5
O
N
S
S
N
O
n
C_6H_{13}
C_6H_{13}
C_4H_9
C_2H_5

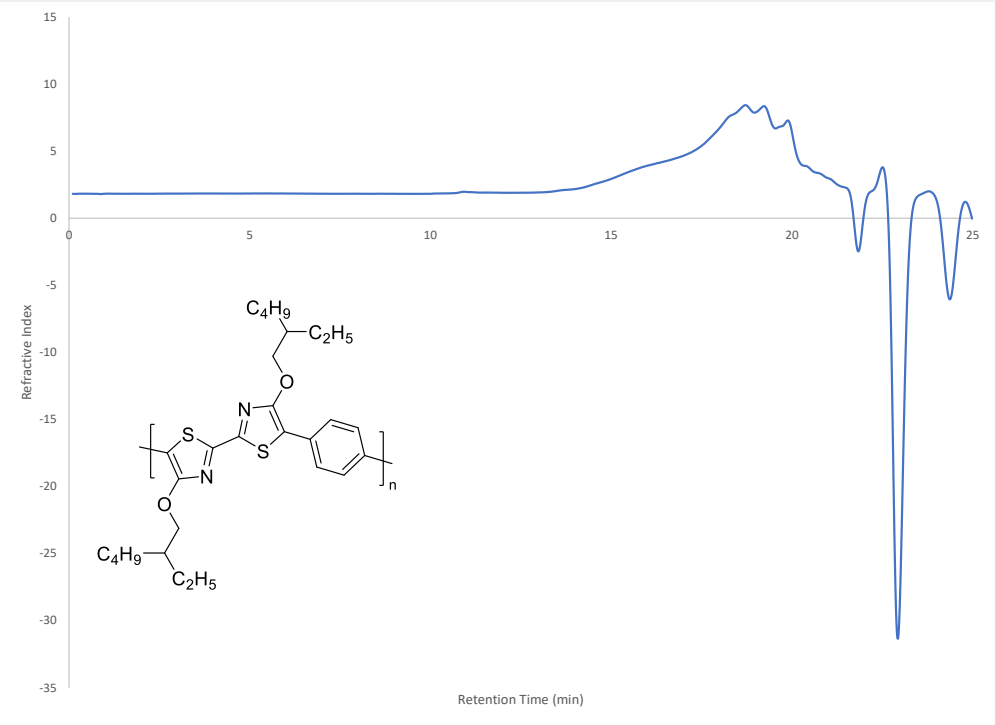
15
10
5
0
-5
-10
-15
-20
-25
-30
-35
0
5
10
15
20
25
Refractive Index
Retention Time (min)
C_4H_9
C_2H_5
O
N
S
S
N
O
C_4H_9
C_2H_5
n

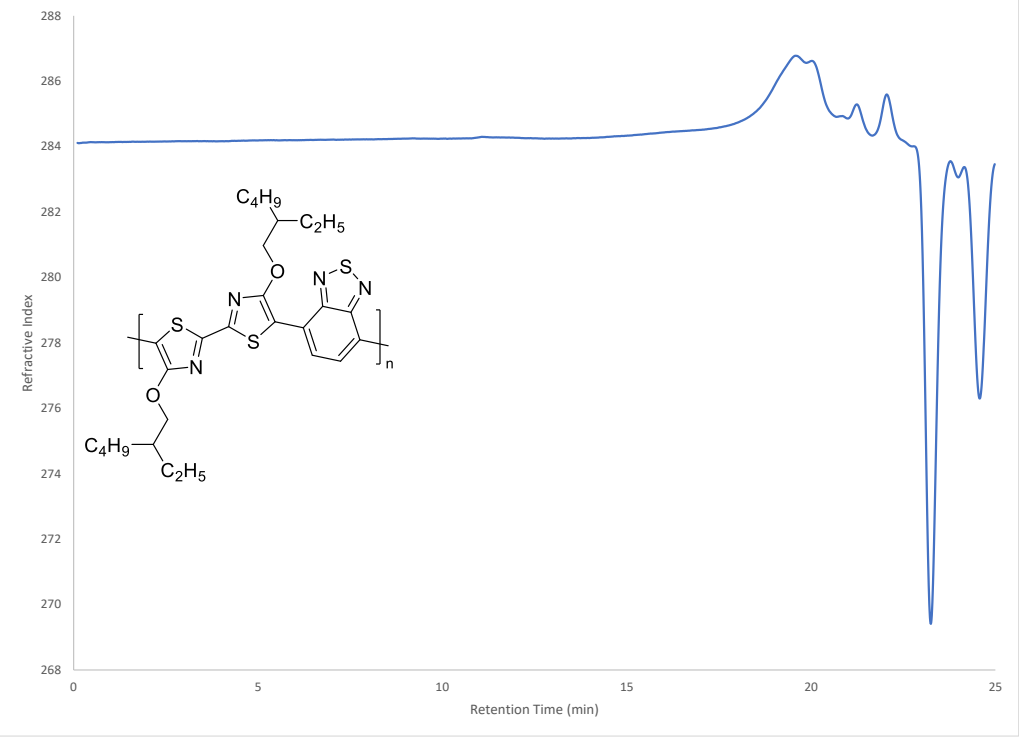
288
286
284
282
280
278
276
274
272
270
268
0
5
10
15
20
25
Refractive Index
Retention Time (min)
C_4H_9
C_2H_5
O
N
S
N
S
N
O
C_4H_9
C_2H_5
n

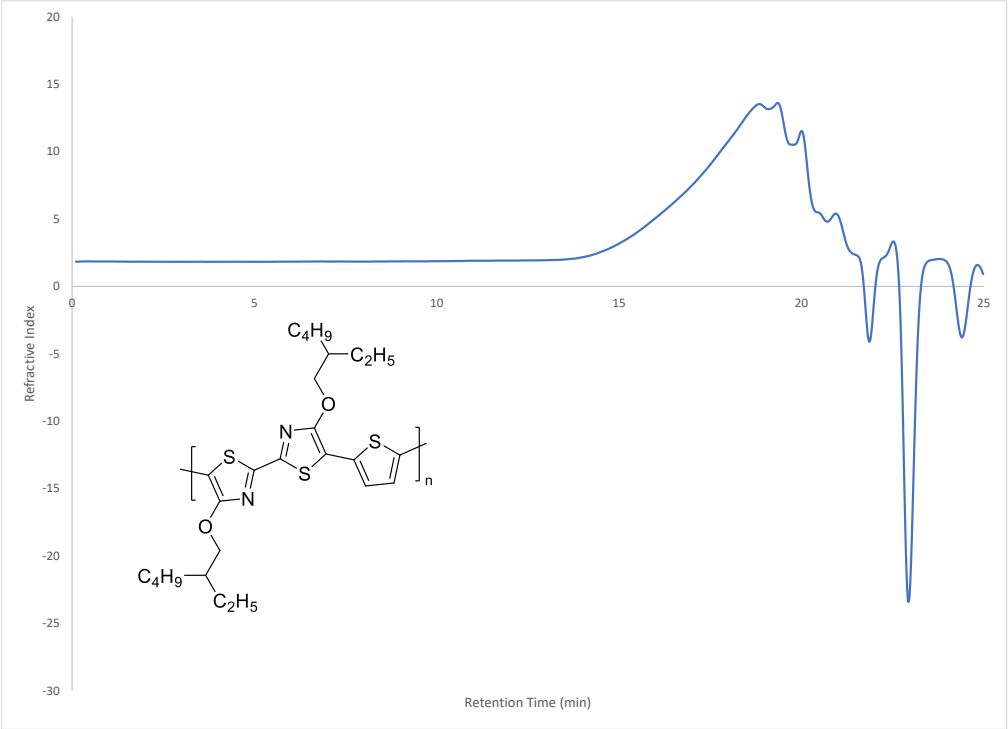
Refractive Index
Retention Time (min)
20
15
10
5
0
-5
-10
-15
-20
-25
-30
0
5
10
15
20
25
C_4H_9
C_2H_5
O
N
S
S
S
N
n
O
C_4H_9
C_2H_5

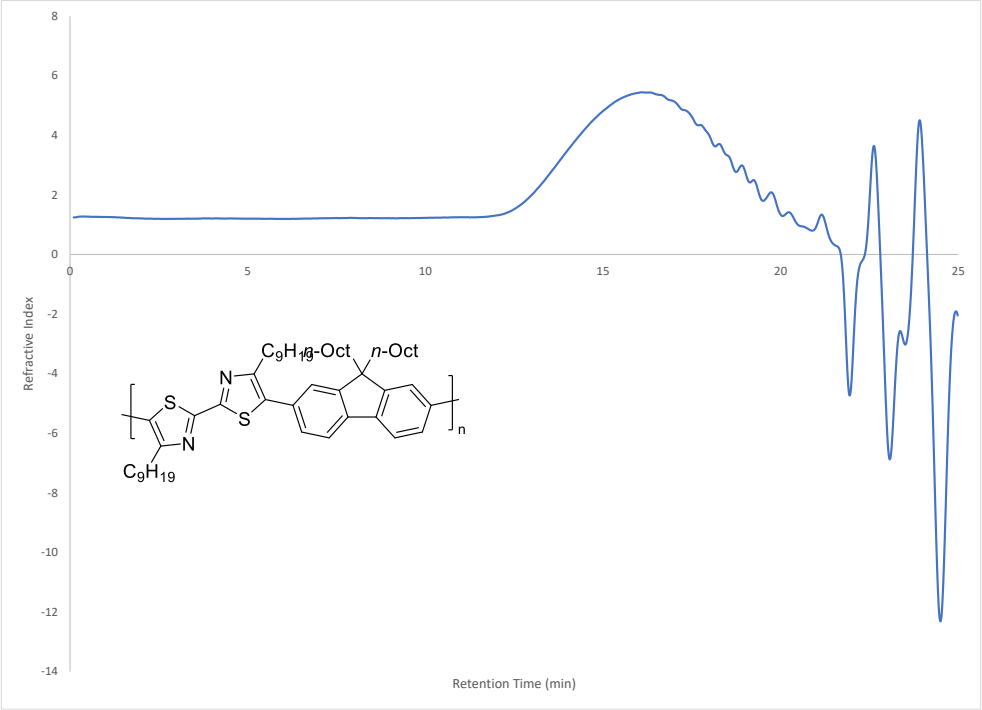
Refractive Index
Retention Time (min)
8
6
4
2
0
-2
-4
-6
-8
-10
-12
-14
0
5
10
15
20
25
C_9H_{19}
n-Oct
n-Oct
N
S
S
N
n
C_9H_{19}

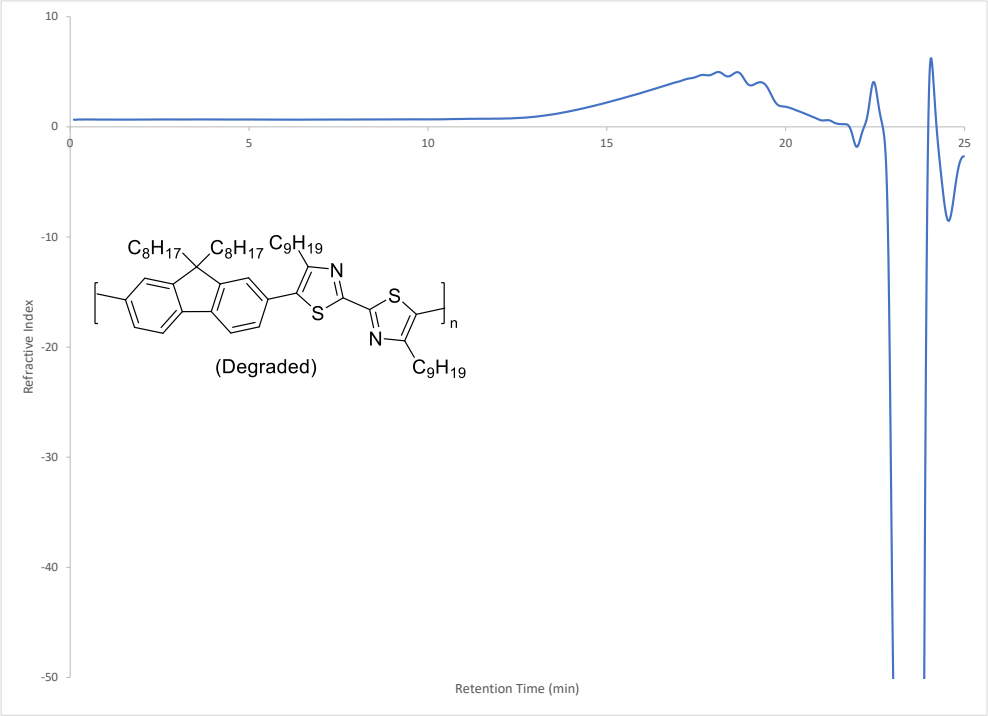
10
0
-10
-20
-30
-40
-50
0
5
10
15
20
25
Refractive Index
Retention Time (min)
C_8H_{17} C_8H_{17} C_9H_{19}
N
S
S
N
n
C_9H_{19}
(Degraded)

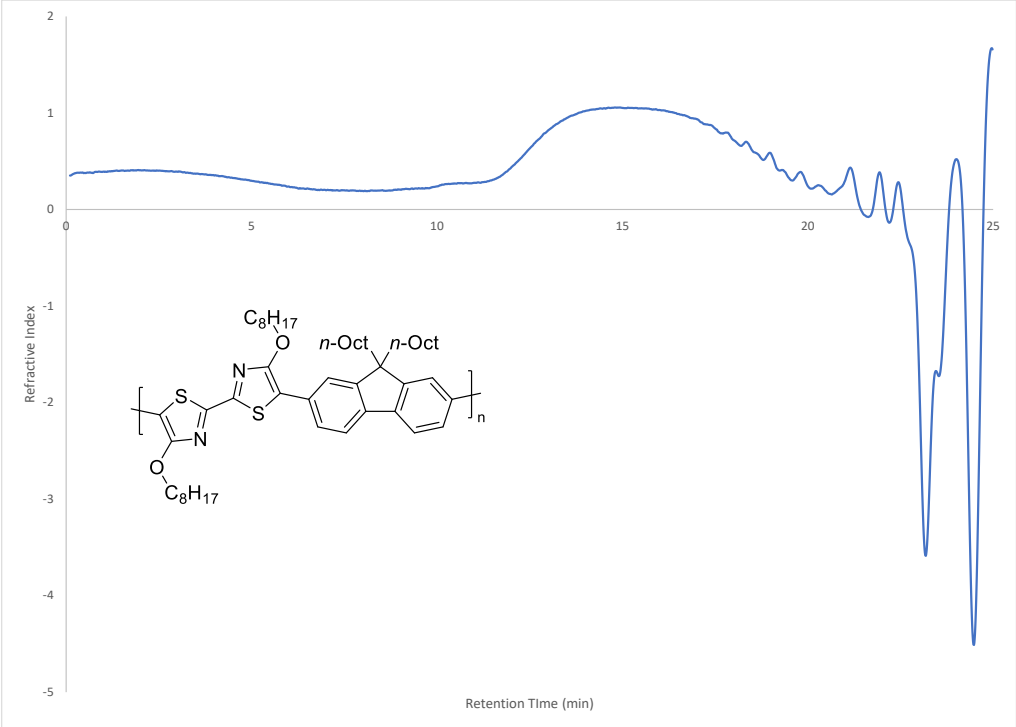
2
1
0
-1
-2
-3
-4
-5
0
5
10
15
20
25
Refractive Index
Retention TIme (min)
C_8H_{17}
O
n-Oct
n-Oct
N
S
S
N
O
C_8H_{17}
n

Ultraviolet-Visible Spectroscopy

All UV-vis spectra have been normalized.

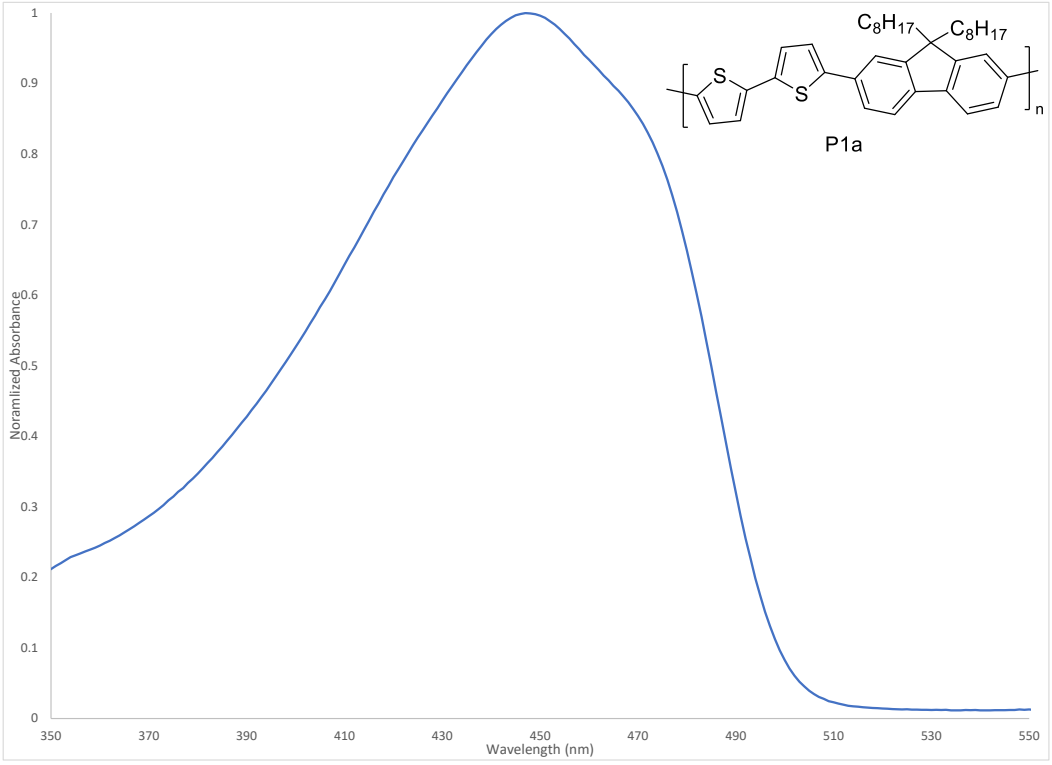

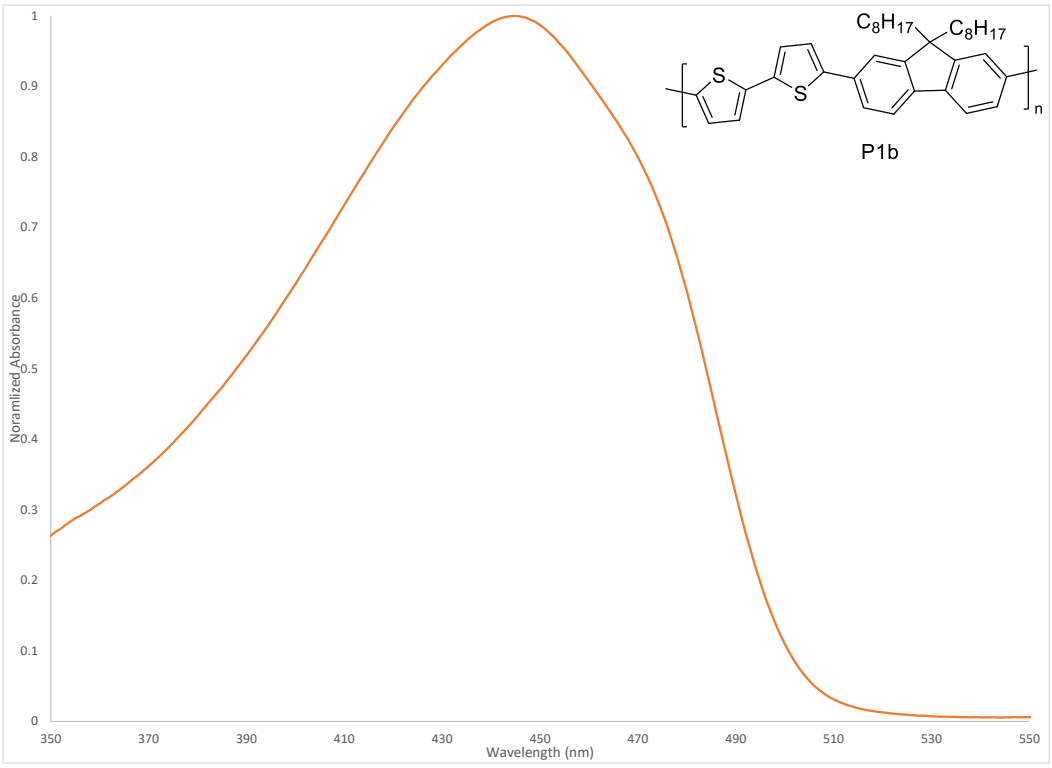

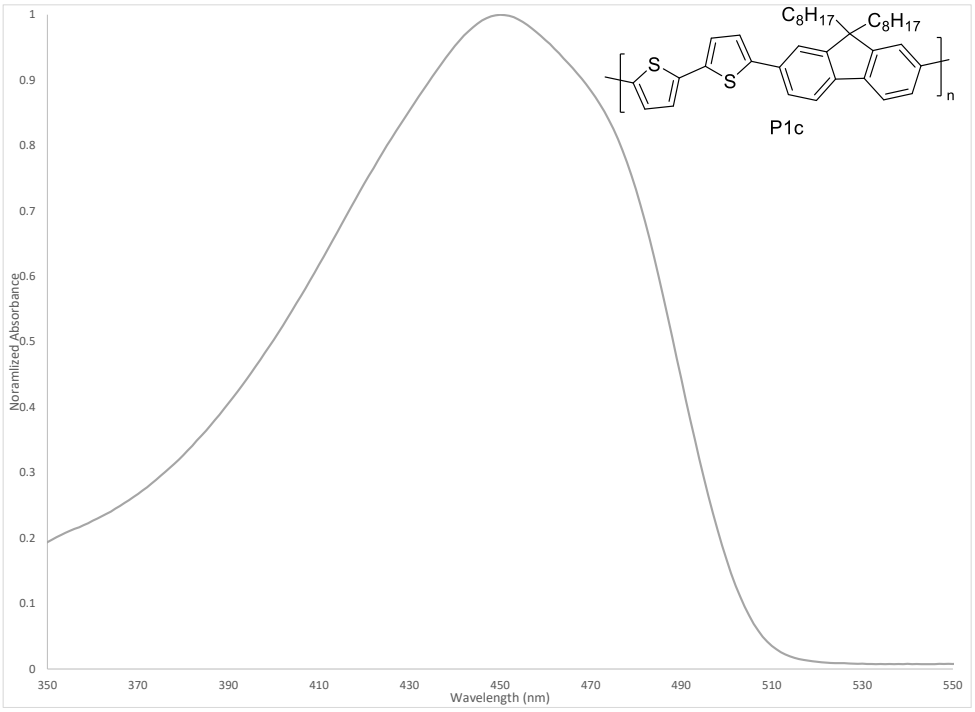
Noramlized Absorbance
Wavelength (nm)
P1c

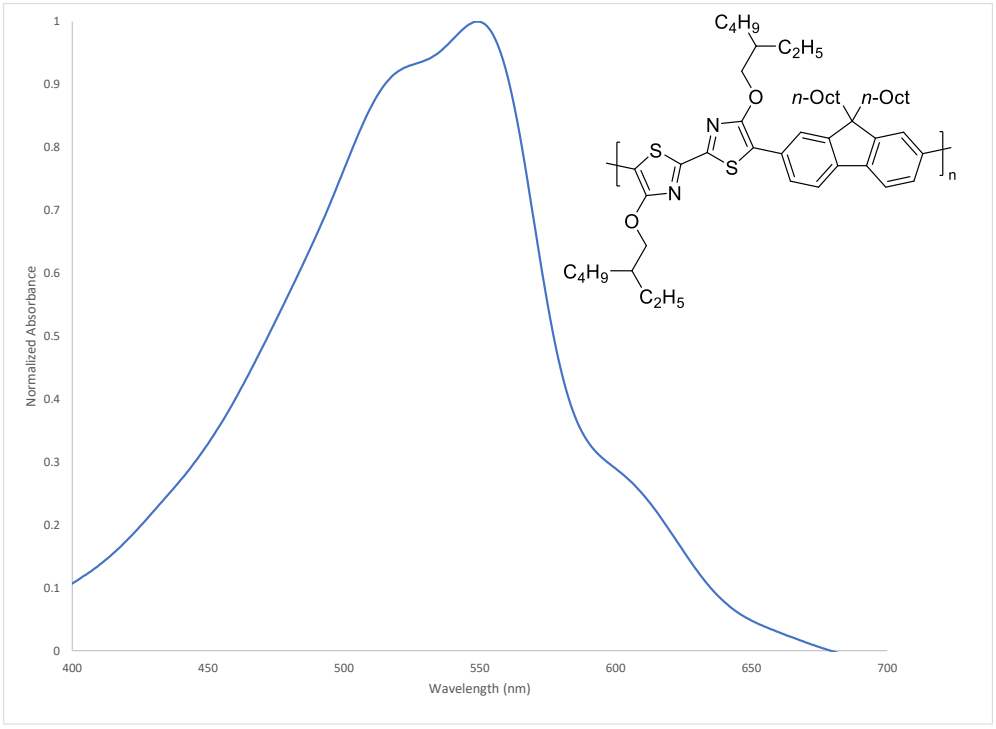
Normalized Absorbance
Wavelength (nm)

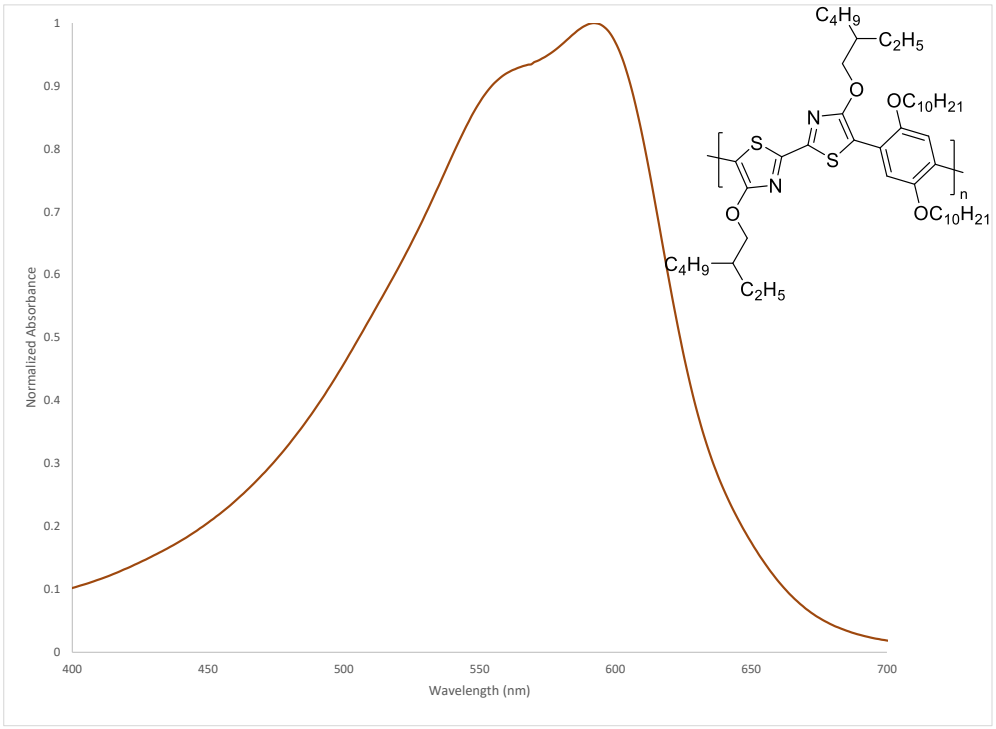
Normalized Absorbance
Wavelength (nm)
0
0.1
0.2
0.3
0.4
0.5
0.6
0.7
0.8
0.9
1
400
450
500
550
600
650
700
C4H9
C2H5
O
N
S
S
OC10H21
n
OC10H21
C4H9
C2H5

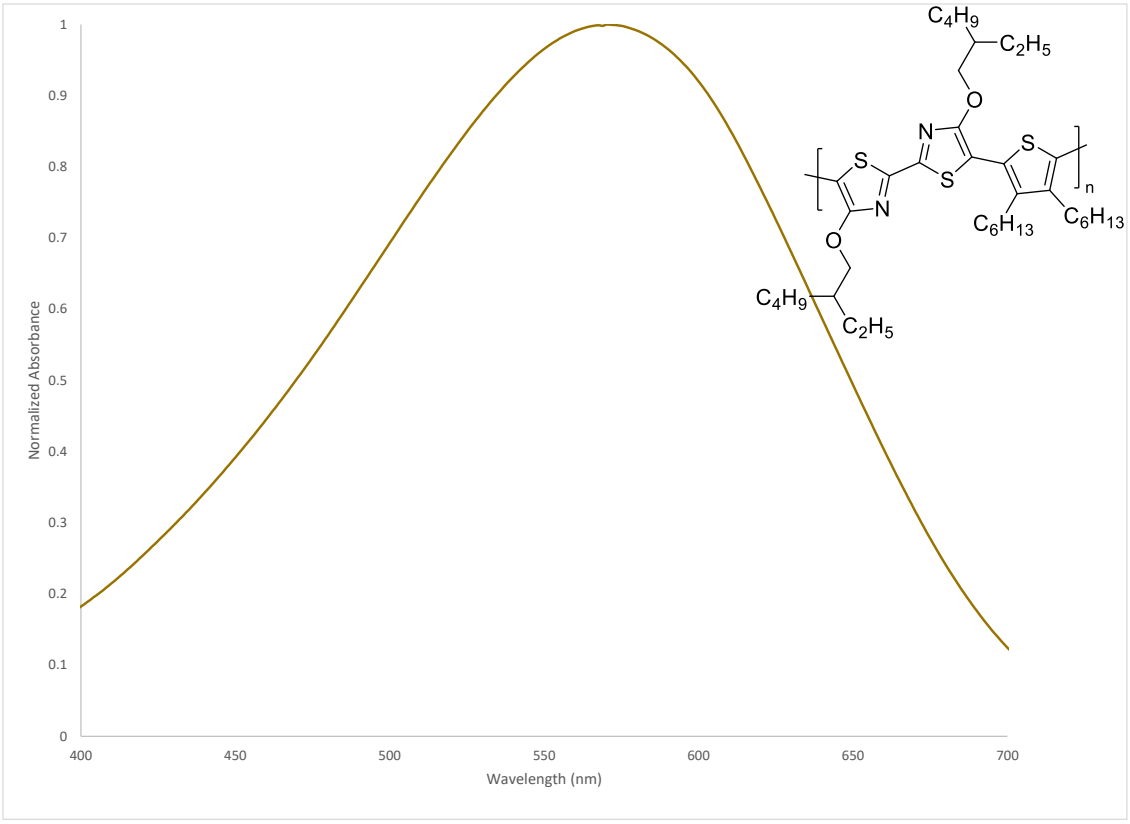
Normalized Absorbance
Wavelength (nm)
0
0.1
0.2
0.3
0.4
0.5
0.6
0.7
0.8
0.9
1
400
450
500
550
600
650
700
C4H9
C2H5
O
N
S
S
S
n
C6H13
C6H13
O
C4H9
C2H5

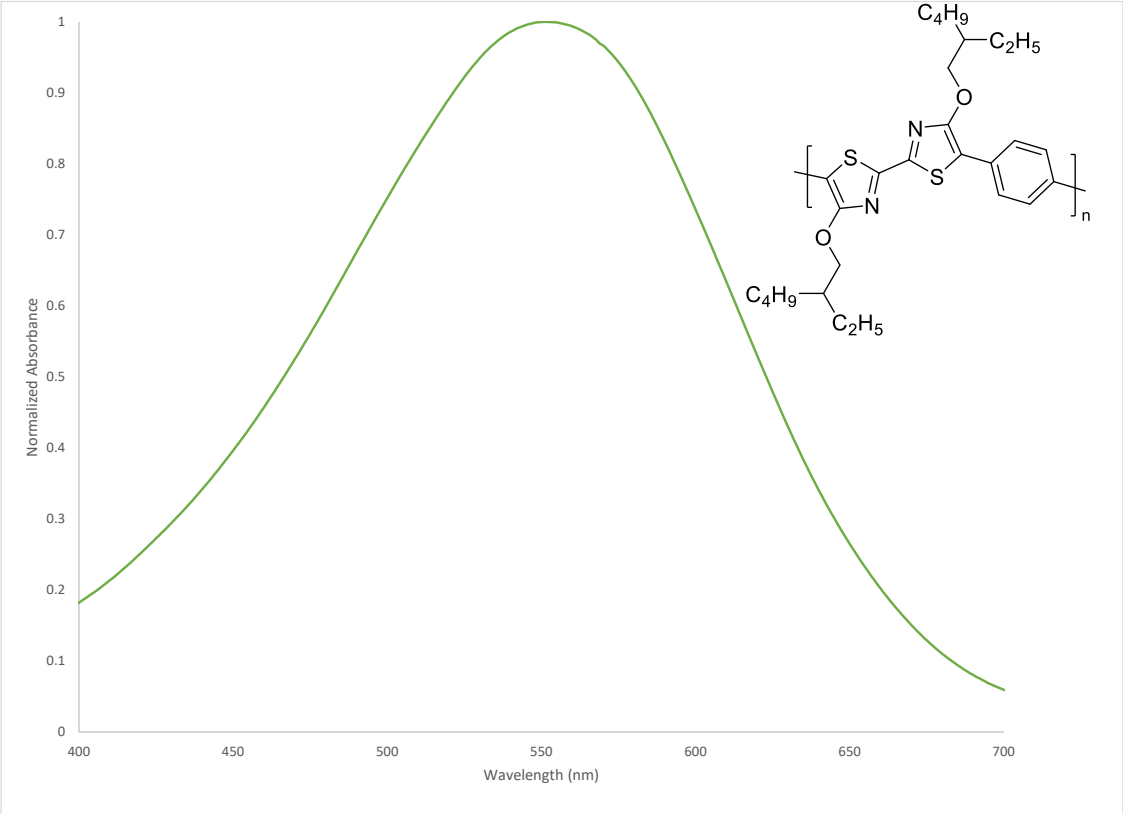
Normalized Absorbance
Wavelength (nm)
1
0.9
0.8
0.7
0.6
0.5
0.4
0.3
0.2
0.1
0
400
450
500
550
600
650
700
C_4H_9
C_2H_5
O
N
S
S
N
O
C_4H_9
C_2H_5
n

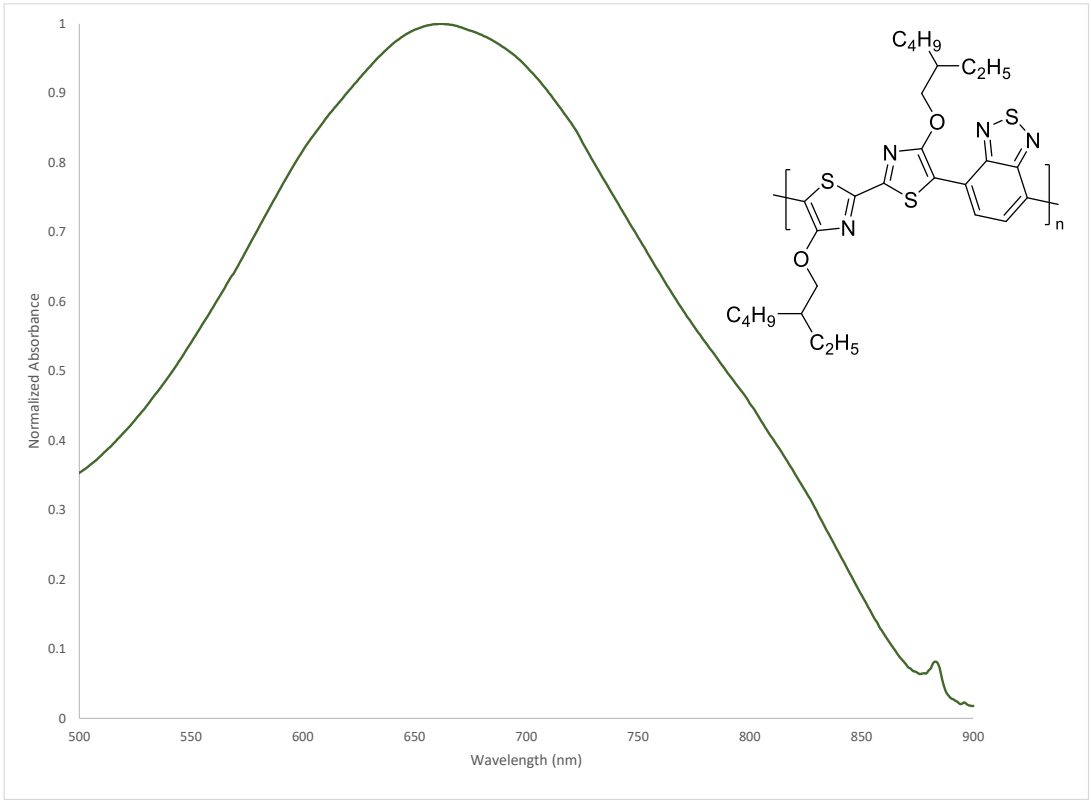
Normalized Absorbance
Wavelength (nm)
1
0.9
0.8
0.7
0.6
0.5
0.4
0.3
0.2
0.1
0
500
550
600
650
700
750
800
850
900
C_4H_9
C_2H_5
O
N
S
N
S
N
O
C_4H_9
C_2H_5
n

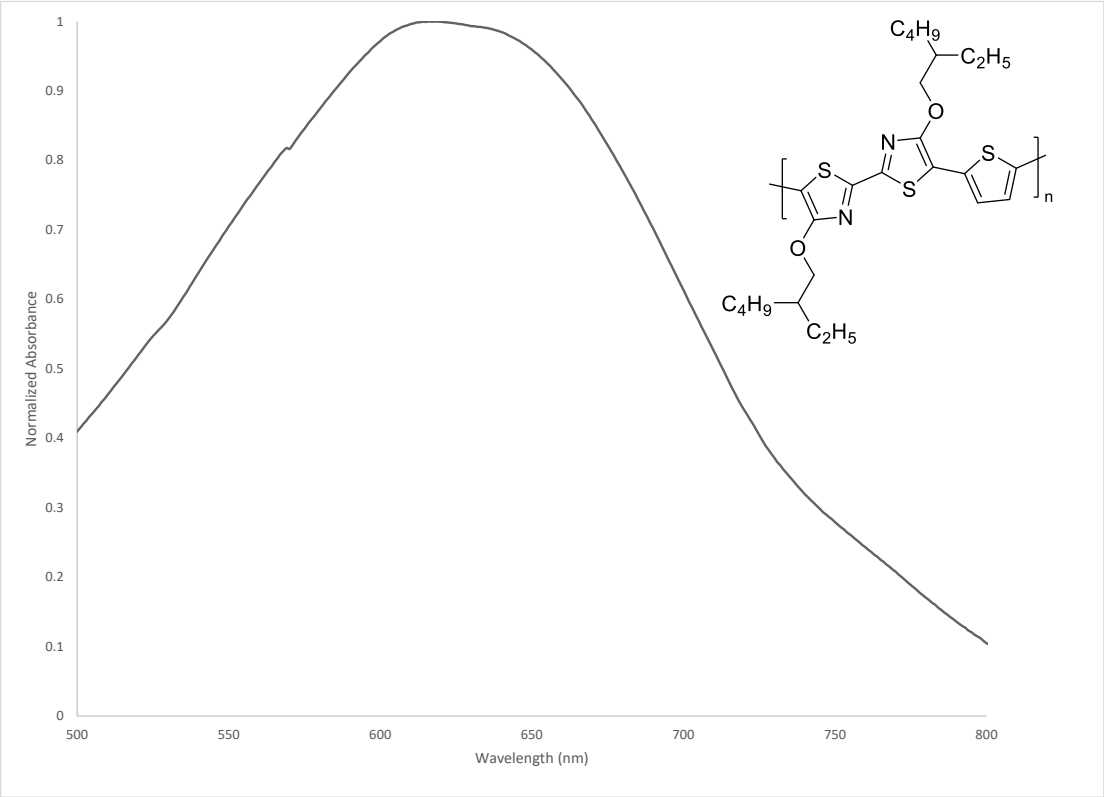
Normalized Absorbance
Wavelength (nm)
0
0.1
0.2
0.3
0.4
0.5
0.6
0.7
0.8
0.9
1
500
550
600
650
700
750
800
C4H9
C2H5
O
N
S
S
S
N
n
O
C4H9
C2H5

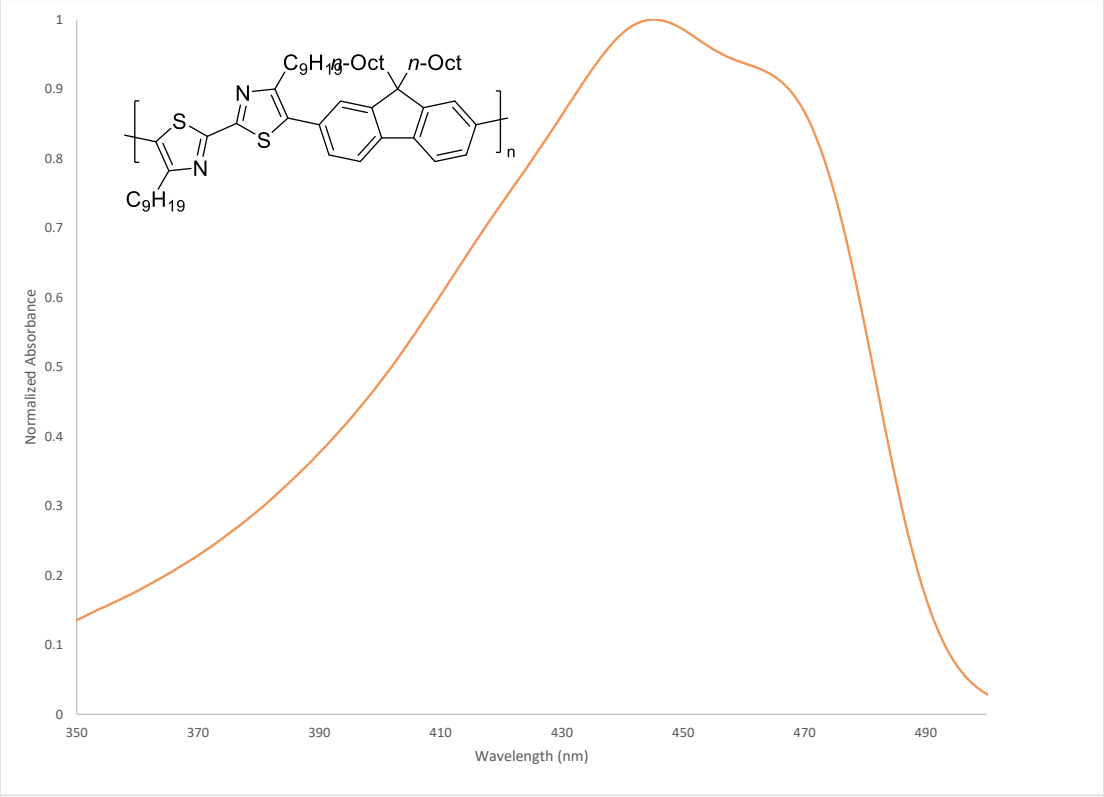
Normalized Absorbance
Wavelength (nm)
0
0.1
0.2
0.3
0.4
0.5
0.6
0.7
0.8
0.9
1
350
370
390
410
430
450
470
490
C9H19
n-Oct
n-Oct
N
S
S
N
n
C9H19

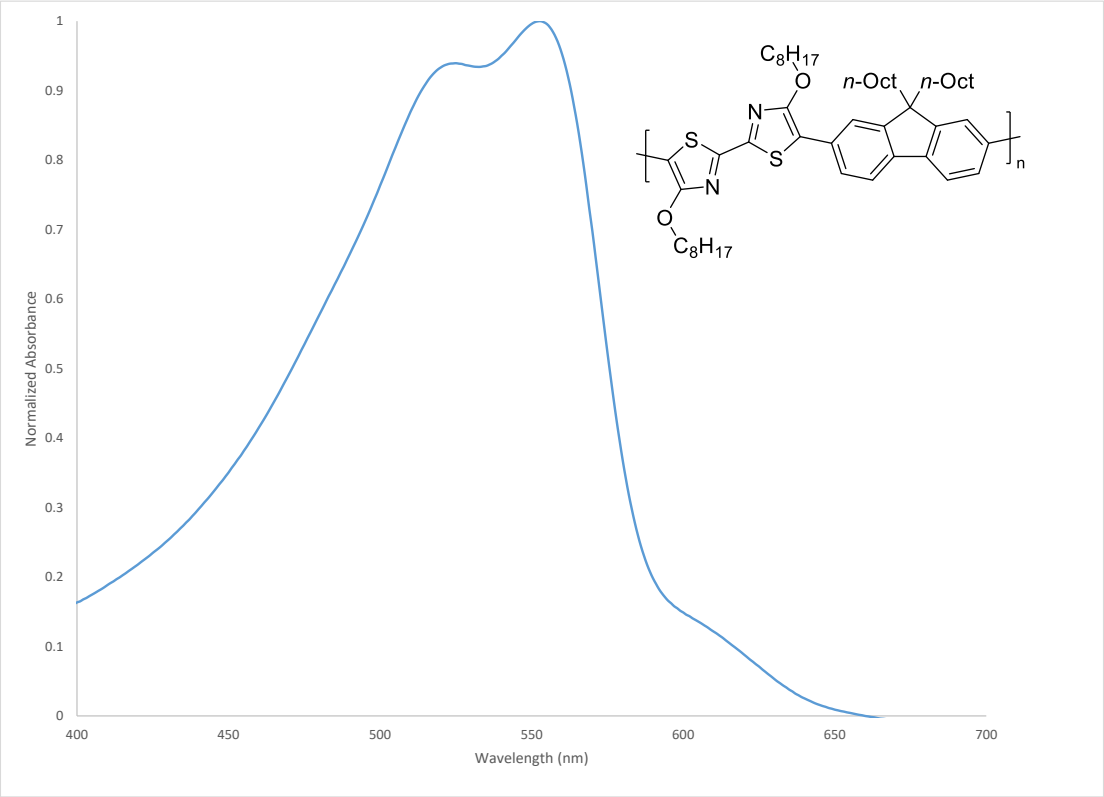
Normalized Absorbance
Wavelength (nm)
1
0.9
0.8
0.7
0.6
0.5
0.4
0.3
0.2
0.1
0
400
450
500
550
600
650
700
C8H17
O
n-Oct
n-Oct
N
S
S
N
O
C8H17
n

Cyclic Voltammetry

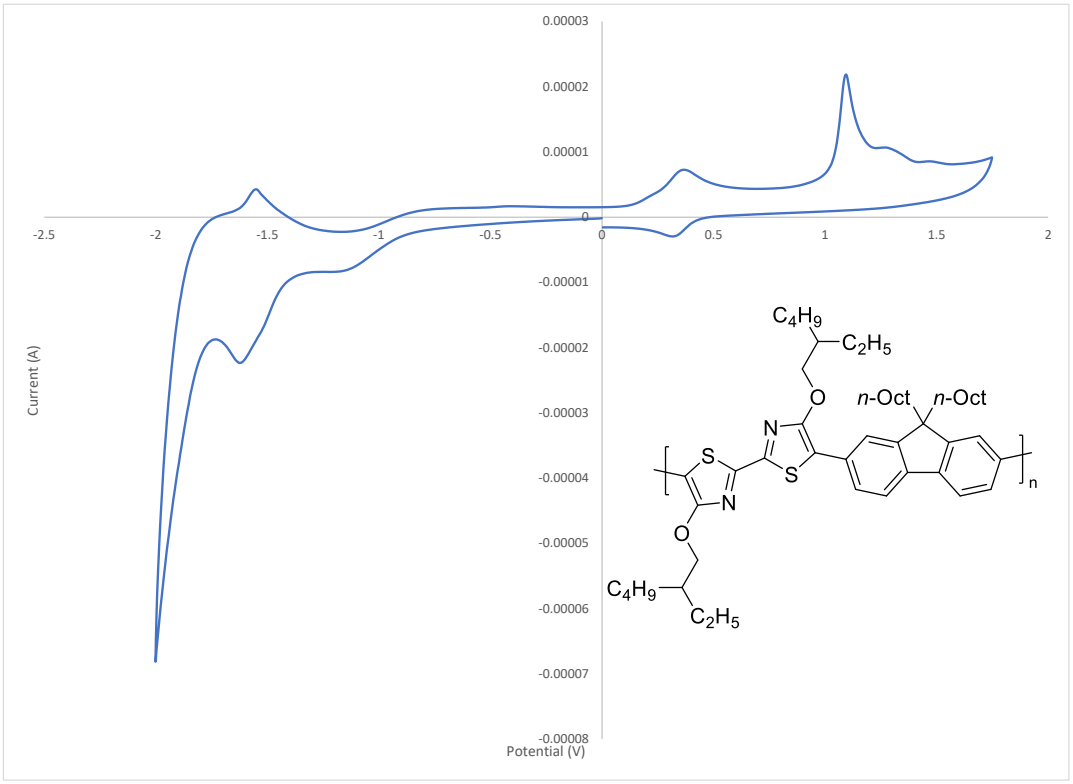

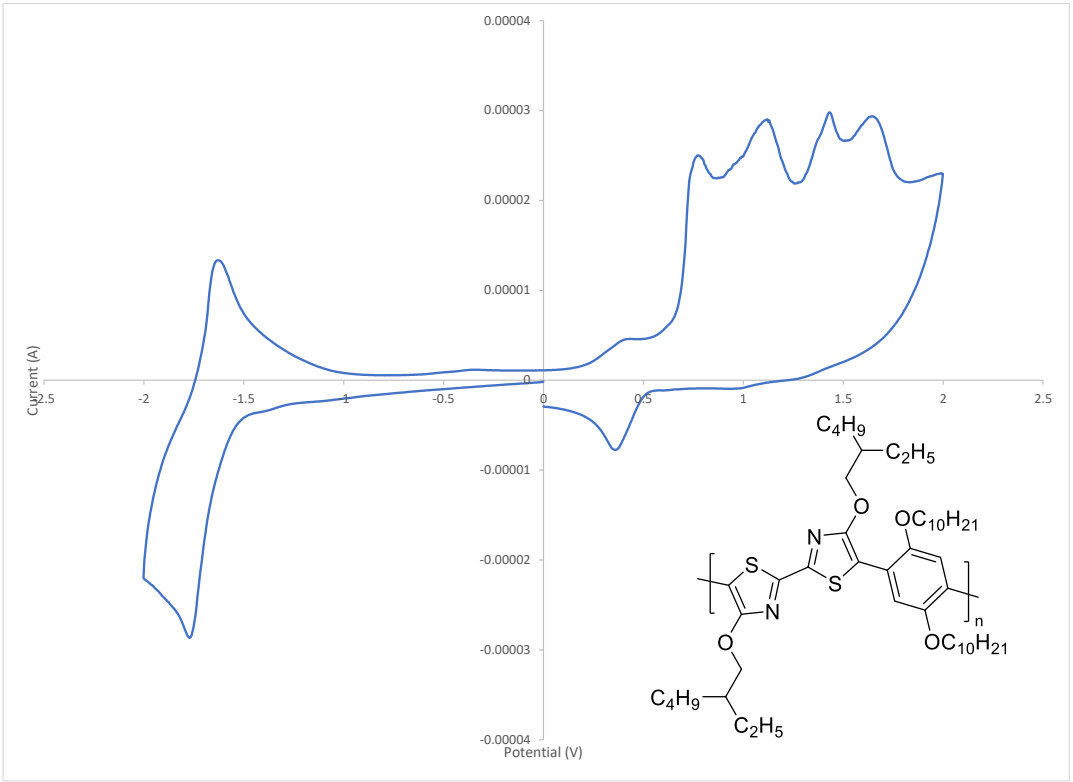

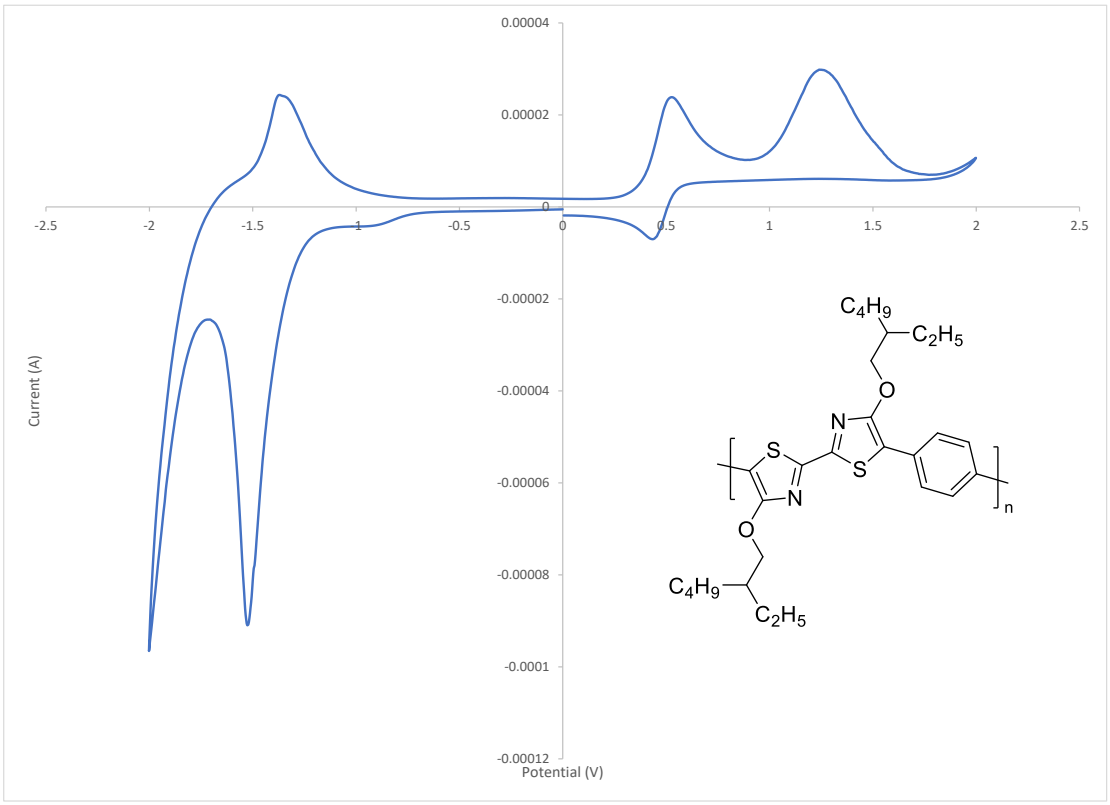
0.00004
0.00002
0
-0.00002
-0.00004
-0.00006
-0.00008
-0.0001
-0.00012
-2.5
-2
-1.5
-1
-0.5
0
0.5
1
1.5
2
2.5
Current (A)
Potential (V)
C_4H_9
C_2H_5
O
N
S
S
N
O
C_4H_9
C_2H_5
n

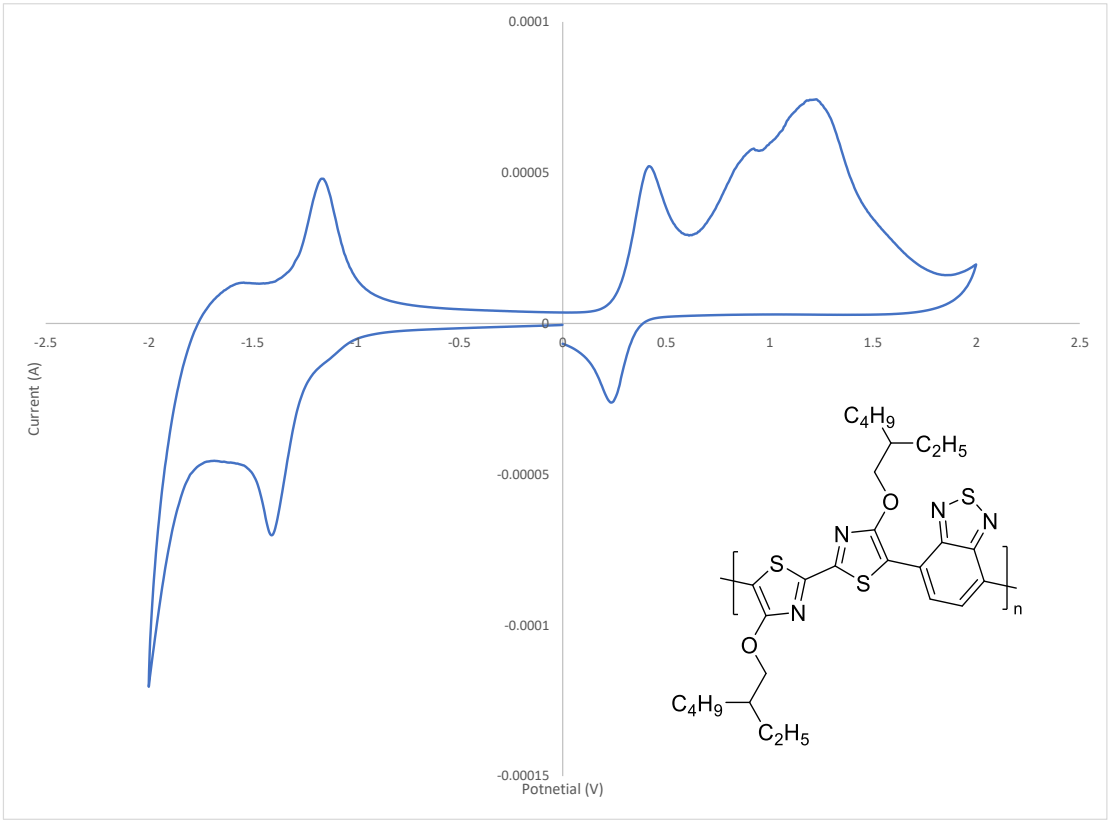
0.0001
0.00005
0
-0.00005
-0.0001
-0.00015
-2.5
-2
-1.5
-1
-0.5
0
0.5
1
1.5
2
2.5
Current (A)
Potnetial (V)
C_4H_9
C_2H_5
O
N
S
N
S
N
S
N
O
C_4H_9
C_2H_5
n

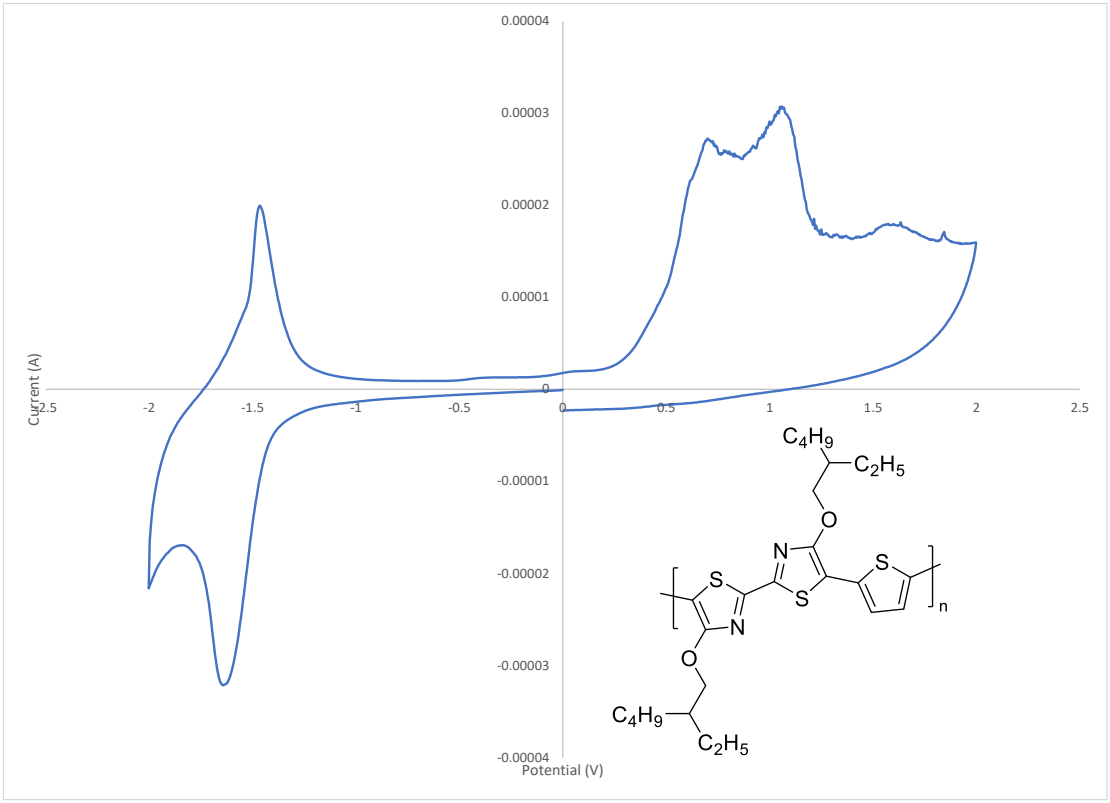
0.00004
0.00003
0.00002
0.00001
0
-0.00001
-0.00002
-0.00003
-0.00004
Current (A)
Potential (V)
-2.5
-2
-1.5
-1
-0.5
0
0.5
1
1.5
2
2.5
C4H9
C2H5
O
N
S
S
S
N
n
O
C4H9
C2H5

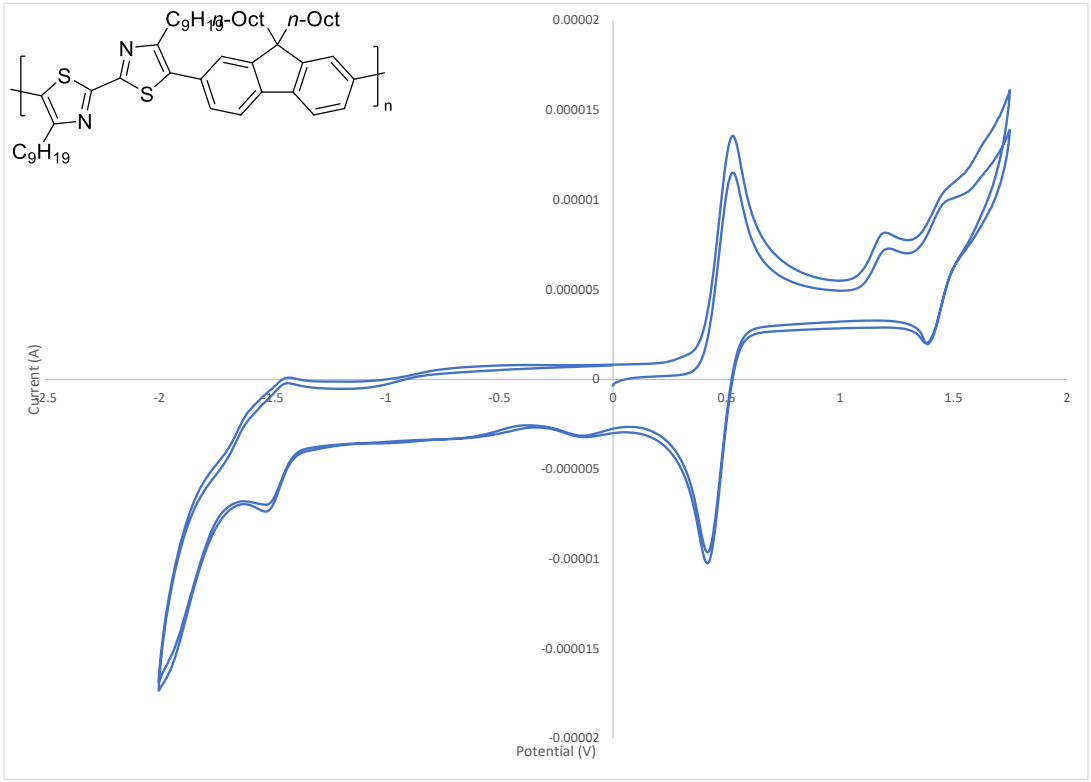
C9H19
n-Oct
n-Oct
S
N
S
N
n
C9H19
0.00002
0.000015
0.00001
0.000005
0
-0.000005
-0.00001
-0.000015
-0.00002
Current (A)
Potential (V)
-2.5
-2
-1.5
-1
-0.5
0
0.5
1
1.5
2

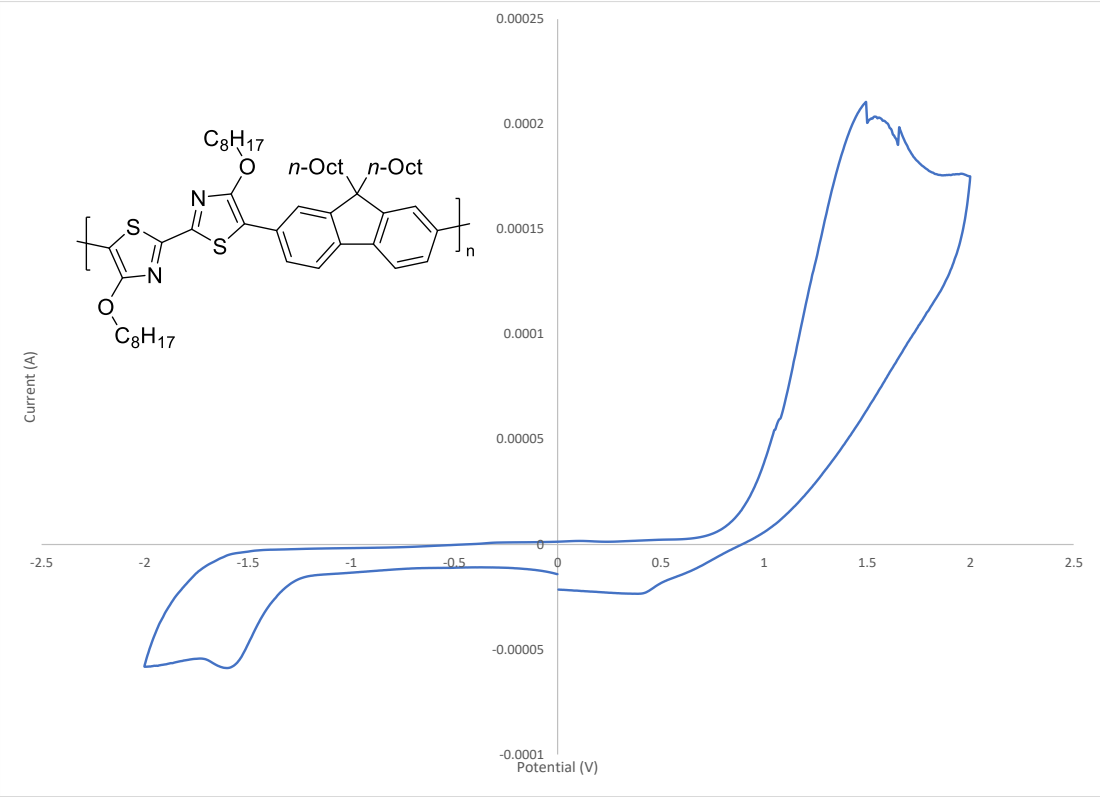
0.00025
0.0002
0.00015
0.0001
0.00005
0
-0.00005
-0.0001
Current (A)
Potential (V)
-2.5
-2
-1.5
-1
-0.5
0
0.5
1
1.5
2
2.5
C8H17
O
n-Oct
n-Oct
N
S
S
N
O
C8H17
n